A Precision Measurement of Parity Violation in Møller Scattering[*]

David R. Relyea

Stanford Linear Accelerator Center
Stanford University
Stanford, CA 94309

SLAC-Report-717

---

[*] Ph.D. thesis, Princeton University, Princeton, NJ 08544

A Precision Measurement of Parity Violation in Møller
Scattering

David R. Relyea

A Dissertation

Presented to the Faculty

of Princeton University

in Candidacy for the Degree

of Doctor of Philosophy

Recommended for Acceptance

by the Department of

Physics

November, 2003

Abstract

This thesis reports on E158, an experiment located in End Station A at the Stanford Linear Accelerator Center (SLAC). E158 has made the first observation of the parity violating right-left asymmetry (A_{PV}) in fixed-target low-Q^2 Møller scattering. At tree level, A_{PV} (expected to be around -150 ppb) is directly proportional to $\frac{1}{4} - \sin^2\theta_W$. A precision measurement of A_{PV} at low Q^2 allows the running of $\sin^2\theta_W$ to be compared to the Standard Model prediction. Disagreements between the two might provide evidence for new physics at the TeV scale.

This thesis presents the first physics data from E158, taken in the spring of 2002. The data were taken by scattering longitudinally polarized electrons at 45.0 and 48.3 GeV off a liquid hydrogen target at a Q^2 of 0.027 GeV^2. A 60 meter long spectrometer/collimator system and a copper-quartz calorimeter were used to detect the Møller signal electrons. Both devices will be described in detail.

The right-left parity violating asymmetry in Møller scattering has been measured to be $-152.3 \pm 29.0(stat) \pm 30.9(syst)$ ppb. The value of $\sin^2\theta_W$ derived from this measurement is $0.2370 \pm 0.0025(stat) \pm 0.0026(syst)$, in comparison with the Standard Model prediction of 0.2387 ± 0.0007.

Acknowledgements

all of the support necessary for me get started at SLAC, as well as providing much of the manpower and support necessary to build and maintain the experiment.

Of course, I wouldn't be anywhere without my parents, David and Rosie, and my brother Mark, who all supported me and enabled me to attain a Ph.D. And I must express my extreme gratitude to Jen Niedziela, whose wrists were a great source of typing for this thesis, and whose transition words prevented the word "thus" from appearing in this thesis more than eight hundred times.

Contents

List of Figures

List of Tables

Chapter 1

Introduction

For five decades, measurements of parity violation have played a fundamental role in exploring the bounds of the electroweak portion of what is now known as the Standard Model. This model, which has existed in more or less its current form since the 1970s, encompasses the theories of both the electroweak and the strong interactions of subatomic particles. In the fifties, the first evidence of parity violation in weak charged current interactions captured the interest of the entire physics community and forever eliminated the notion of parity conservation in weak interactions.[1, 2] Two decades later, in 1978, SLAC E122 first demonstrated parity violation in polarized electron scattering from deuterium.[3] Results from E122 were crucial in asserting the Glashow-Weinberg-Salaam SU(2)×U(1) gauge theory to be the "correct" model describing electroweak interactions. Furthermore, the methodology created for measuring the small parity violating asymmetry in E122 demonstrated the possibility of measuring extremely small parity violating asymmetries.

In recent years, experiments measuring interactions at the Z^0 pole have experienced phenomenal success in making precision measurements of electroweak parameters such as $\sin^2 \theta_W$.[4, 5] On the other hand, electroweak 1-loop corrections should cause the value

of $\sin^2 \theta_W$ to change by a few percent from $Q^2 = M_Z^2$ (at the Z^0 pole) to $Q^2 \simeq 0$. In order to constrain the running of $\sin^2 \theta_W$, precision measurements must be made at several different energy scales. Low Q^2 measurements of $\sin^2 \theta_W$ are therefore quite valuable, as values of $\sin^2 \theta_W$ inconsistent with theoretical predictions could be an indication of new physics beyond the Standard Model.

Within the past five years, three recent experiments have undertaken the measurement of the running of $\sin^2 \theta_W$ in low-Q^2, parity violating interactions. Two of these experiments, APV in Colorado and NuTeV at FNAL, have been published, yet both experiments have significant theoretical uncertainties in their results. The APV results rely on theoretical descriptions of the atomic wave function.[7] NuTeV, on the other hand, measured neutrino-nucleon deep inelastic scattering, and relies on nuclear calculations which are theoretically complicated.[6] A theoretically cleaner measurement of $\sin^2 \theta_W$ at low-Q^2 would be possible if one were to measure the parity violating asymmetry in electron-electron (Møller) scattering.[8] SLAC E158, the third experiment, plans to do exactly this, and to ultimately measure $\sin^2 \theta_W$ with a precision of 0.001. This paper will focus on the methodology of and results from the first six weeks of E158 physics data, which were taken in the spring of 2002.

Chapter 2

Theory and Method

Figure 2.1: The first order tree-level contributions to Møller scattering.

2.1 A_{PV} in Møller Scattering

If Møller scattering were only mediated by the electromagnetic force, then the polarization of the incident electron (assuming an unpolarized, fixed target electron) would not affect the cross-section[1]. However, Møller scattering can be mediated by the weak force as well. The interference between the four diagrams shown in figure 2.1 gives rise to a difference in the Møller scattering cross section depending on whether the incident electron is left-handed or right-handed. If the cross section for each state were measured perfectly, the interaction would be said to have a right-left asymmetry, given by

$$A_{PV} = \frac{\sigma_R - \sigma_L}{\sigma_R + \sigma_L}, \tag{2.1}$$

where σ_R and σ_L are the cross sections for right- and left-handed electrons incident on an unpolarized electron.

The formula for the asymmetry in the Møller scattering cross section is given by

$$A_{PV} = -\frac{m_e E G_F}{\sqrt{2}\pi\alpha} \cdot \frac{16\sin^2\theta_{CM}}{(4 - \sin^2\theta_{CM})^2} \cdot (\frac{1}{4} - \sin^2\theta_W), \tag{2.2}$$

where m_E is the electron mass, E is the incident electron energy, G_F is the Fermi coupling constant, θ_{CM} is the center of mass scattering angle, and θ_W is the weak mixing angle.[9] The simple functional form of this asymmetry suggests Møller scattering to be an excellent probe of $\sin^2\theta_W$ at low Q^2. However, there is one caveat. With a 50 GeV incident electron beam, even when this asymmetry is maximal (at $\theta_{CM} = \frac{\pi}{2}$, corresponding to a final-state energy of 24 GeV in the lab frame) and the beam is 100% polarized, A_{PV} is 320 parts per billion.[2] Furthermore, when the contributions from all first order diagrams are included, the expected asymmetry winds up smaller than the zeroth order tree level asymmetry.[10]

---

[1] Specifically, the cross-section integrated over the entire azimuth.

[2] Parts per billion will henceforth be known as ppb, and parts per million, ppm.

Loop diagrams, such as the ones given in figure 2.2 (γ-Z mixing and the W contribution to the anapole moment), reduce the overall asymmetry by nearly 40%. This brings the previous asymmetry down from 320 ppb to 190 ppb (and this is before spectrometer acceptance and beam polarization are taken into account).
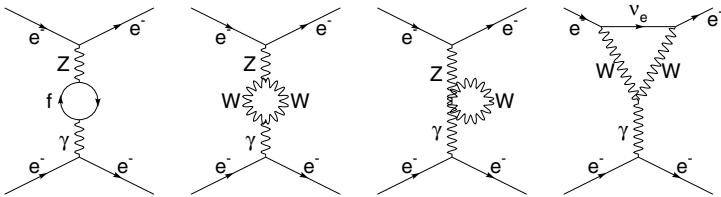
Figure 2.2: Loop diagrams which reduce the tree level A_{PV} in Møller scattering by nearly 40%.

To measure such a small asymmetry to a high degree of precision, a scattering medium with a high relative cross section and an electron beam with a high luminosity are required. In order to maximize the density of electrons relative to other potential scattering centers, liquid hydrogen will be used as the scattering medium. To calculate the amount of hydrogen needed, the amount of deliverable beam must first be considered. SLAC's accelerator can deliver up to $5\text{-}6 \cdot 10^{11} e^-$/spill at 120 Hz for the desired incident energy (45 or 48.3 GeV electrons)[3]. For unpolarized Møller scattering, the formula for the cross section is given by:

$$\frac{d\sigma}{d\Omega} = \frac{\alpha^2}{2m_e E} \frac{(4 - \sin^2\theta_{CM})^2}{\sin^4\theta_{CM}}, \tag{2.3}$$

where α is the fine structure constant, m_e is the mass of the electron, E is the incident electron's energy, and θ_{CM} is the scattering angle in the center of mass frame. For a 48.3

---

[3]SLAC can deliver up to $7 \cdot 10^{11} e^-$/$spill$, but beam jitter issues make it more prudent to run at the lower setting.

GeV incident electron beam (corresponding to a Q^2 of 0.027 GeV^2) and a spectrometer acceptance of 4.7 to 7.1 milliradians in the lab frame, the calculated cross section is 11.2 μbarn. Consequently, producing a statistical error of a few percent in a matter of months requires the target to be quite thick - in this case, 150 cm long.

2.2 New physics

E158 is sensitive to several varieties of new physics at the TeV scale, some of which are complementary to both e^+e^- and $p\overline{p}$ collider experiments.[8] Whereas those experiments are both sensitive to LL+RR interactions of the form $(\psi_L\gamma^\mu\psi_L)^2 + (\psi_R\gamma^\mu\psi_R)^2$, E158's sensitivity is primarily to LL−RR interactions of the form $(\psi_L\gamma^\mu\psi_L)^2 - (\psi_R\gamma^\mu\psi_R)^2$. Such complementarity is quite useful if high energy experiments happens to discover something outside the Standard Model, as the E158 results might help to discern which extensions to the Standard Model can be ruled out, and which seem more likely.

E158's sensitivity to new physics can be characterized in its most general form by a four point contact interaction. In general, the Lagrangian for the four point contact interaction is given by

$$\mathcal{L}_{ee} = \frac{4\pi}{2\Lambda_{ee}^2} \left[\eta_{LL}(\bar{\psi}_L\gamma_\mu\psi_L)^2 + \eta_{RR}(\bar{\psi}_R\gamma_\mu\psi_R)^2 + 2\eta_{LR}(\bar{\psi}_L\gamma_\mu\psi_L)(\bar{\psi}_R\gamma_\mu\psi_R) \right], \tag{2.4}$$

where Λ_{ee} is the compositeness scale for electron contact interactions. As this contact interaction is purely real, and the Z_0 amplitude at the pole is purely imaginary, the sensitivity of experiments on the Z-pole to contact interactions of this type is suppressed. Assuming there are parity violating terms in the interaction (take η_{LL} or η_{RR} to be ± 1), E158 will be capable of setting a 2σ limit on Λ_{ee} at 11.1 TeV, more than twice the energy limit set by LEP-II.

One specific type of contact interaction would be that mediated by a massive neutral Z' boson which does not couple strongly to the Z^0. If, like the Z^0, the Z' interacts with fermions via parity violating LL−RR couplings, E158 would measure a non-Standard Model contribution to the expected asymmetry. Conversely, if the E158 result for $\sin^2\theta_W$ is within 2σ from the predicted Standard Model value, a lower limit of 600 to 900 GeV could be set on the mass of the Z' (for certain theoretical models).[11]

2.3   Experimental Design

As was mentioned above, to achieve the desired statistical error on the asymmetry in Møller scattering, SLAC must run 48.3 GeV electrons at $5\text{-}6\cdot10^{11}\,e^-$/spill and at 120 Hz (making a 550 kW beam!) into a 150 cm LH2 target. A brief overview of the spectrometer design will be given here; more details can be found in chapter 4.

An important parameter in designing the spectrometer is the experimental figure of merit (f.o.m.), which quantifies the dependence of the statistical power of the experiment on the center-of-mass scattering angle. For E158, this f.o.m. is proportional to $(A_{PV})^2 \times \frac{d\sigma}{d\Omega}$, and its dependence on the center of mass scattering angle θ_{CM} goes as $\frac{1}{(3+\cos^2\theta_{CM})^2}$. A picture of this function (figure 2.3) shows that this f.o.m. is relatively flat from $\cos\theta_{CM}=0$ to $\cos\theta_{CM}=0.5$. Consequently, the experiment is tuned to accept particles in this range. However, $\theta_{CM}=0$ corresponds to electrons at around 24 GeV. To avoid double-counting Møller interactions, the spectrometer must be tuned to accept Møller electrons either above or below this energy. As the lower momentum Møller electrons scatter at a wider angle, it is easiest to choose them as the desired signal particles.

In addition to Møller scatters, a large number of electron-proton (ep, or Mott) scatters will happen in an LH2 target, so the spectrometer must be designed to remove this back-
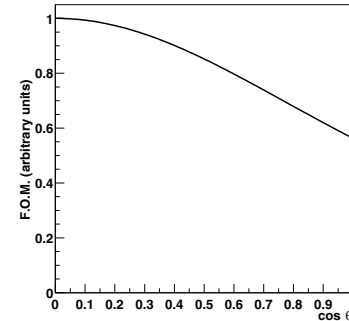
Figure 2.3: The dependence of the f.o.m. on the center of mass scattering angle.

ground. Finally, a large percentage of the beam energy (around 16%) will be converted into photons, so the spectrometer must also be able to block the fringes of this background (which could hit the detector) while allowing the majority of the flux to travel unimpeded to the beam dump.

The simplest method of blocking the photon background is through the use of a dipole chicane. Three dipoles can be used to bend all charged particles away from the beam axis, allowing the forward photons to be collimated. With an incident beam power of 550 kW, however, the power in the photon beam is around 85 kW! Blocking such a flux in the middle of the spectrometer is impossible. The photon collimators must therefore block only wide-angle photons, allowing the remainder of the photon beam through.

While passing through the chicane, the electron beam radiates quite a bit of synchrotron radiation in the horizontal plane. GEANT [12] simulations predict that this

synchrotron background, if unblocked, would place as much power on the Møller detector as the Møller signal flux. Consequently, this radiation must be blocked with collimators set in the horizontal plane.

Once the beam has been steered through the chicane, the ep scattered flux must be separated from the Møller flux. On average, the ep elastic scatters are at momenta very close to the beam momentum (48 GeV), whereas the desired Møller scatters are lower than 24 GeV. The easiest conceptual way to separate the two signals is to remove a radial slice from both distributions and then magnetically focus the lower momentum Møllers into that empty region. Therefore, immediately after the dipole chicane, there must be a radial collimator, followed by quadrupole focusing optics. Moreover, the Møller detector should be located as far from the target as possible so that the Møller/Mott radial separation at the detector is maximized.
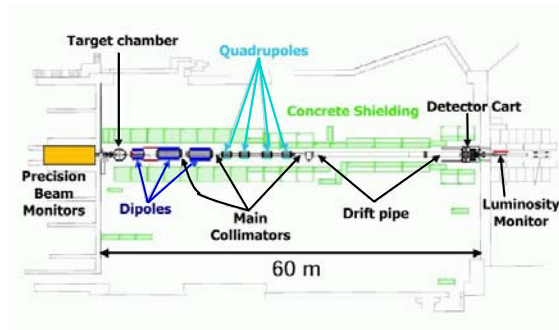
Figure 2.4: A diagram of the spectrometer. "Main Collimators" refers to the second photon collimator, the radial collimator, and the synchrotron collimator.

A conceptual image of the spectrometer can be seen in figure 2.4. This image is a plan view, and includes everything from the target all the way to the Møller detector.

2.4   Backgrounds

2.4.1   Electron-Proton Elastic and Inelastic Scattering

With a liquid hydrogen target, the largest contribution to the background at the Møller detector will come from ep scattering. The cross section and asymmetry for elastic ep scattering are both defined in [13]. The primary concern from this background is not only rate, but that the overall elastic ep parity violating asymmetry has approximately the same value as the asymmetry in Møller scattering (which will henceforth be called the "experimental asymmetry"). Although the spectrometer is optimized to separate Møller and ep scatters, there is still significant leakage of the ep flux into the Møller region, due to interactions in which the electron radiates before the initial scattering off the proton. These numbers have been calculated by a Monte Carlo simulation and will be presented later.

The more important contribution to the overall physics asymmetry comes from inelastic ep scatters. The cross section of this process, again detailed in [13], is quite small compared to the Møller scattering cross section, and contributes on the order of 2% of the flux in the Møller kinematic region. The parity violating asymmetry for this process, though, is much larger than the asymmetry in either the Møller or ep scatters. This asymmetry is not well known theoretically, primarily because calculation of the background involves both resonant and non-resonant processes, most of which have not been measured with any accuracy. As a result, the prediction for the magnitude of the inelastic asymmetry, $A_{PV} = 10^{-4}Q^2$, is an estimate based on the asymmetry of processes below

and at the Delta resonance. For a Q^2 of $0.027 GeV^2$, this asymmetry ends up at 3ppm, roughly 20 times larger than the experimental asymmetry. Any measurement of the experimental asymmetry will require, as a correction, an accurate estimate of the elastic and inelastic ep distribution in the Møller detector.

2.4.2 Pions

A secondary source of background for E158 comes from real and virtual photoproduction in the target, as well as DIS (deep inelastic scattering) processes. Real photon production creates pions with roughly the same overall asymmetry as the Møller scatters.[11] Pions created from virtual photoproduction have an even higher asymmetry. As [11] estimates, this asymmetry is somewhere between two and seven times higher than the asymmetry in the Møller scatters. However, the overall cross section for real photoproduction is on the order of 2 μbarns, so this background is unimportant. The scattering cross section is much higher for real photons (around 100 μbarns). However, the small spectrometer acceptance for said pions, combined with the small rate of pion interaction in the Møller detector, pushes the pion asymmetry contribution to the experimental asymmetry down to a level of around 1%.

More important is the contribution to the experimental asymmetry from DIS pions. These pions are produced in very small numbers: the overall scattering cross section is no more than 0.1 to 0.2 μbarns. The spectrometer acceptance for these pions should also be small, likely around 1%. However, the DIS asymmetry is, just like the inelastic asymmetry, calculated to be approximately $10^{-4}Q^2$. As pion flux can't be separated from the Møller flux, this would be a large background were it not for the minuscule cross section and acceptance. The Monte Carlo simulation predicts that the DIS pions should contribute to the experimental asymmetry at the level of 1%.

The overall uncertainty in the asymmetries and relative rates of all three pion processes stems from a lack of a precision pion measurement in this kinematic region (mainly because the signal is swamped by Møller electrons!). To estimate the pion contribution to the experimental asymmetry, these pions must be measured; in other words, E158 must contain a pion detector capable of distinguishing between pions and other charged flux.

2.4.3 Synchrotron Radiation

Another potential correction to the experimental asymmetry comes from synchrotron photons, because they can acquire an asymmetry if the beam has any vertical polarization component. The asymmetry of these photons is given by

$$A_{synch} = 2.84 \left(\frac{h\gamma^2}{2\pi m_e c\rho} \right)^2,$$

where γ is the relativistic term $\frac{E}{m_e}$, and ρ is the radius of curvature of the electron through the magnet.[14] Although the E158 beam should be polarized purely longitudinally, vertical magnets present in the beam line before the beam reaches the E158 spectrometer can impart some small amount of vertical polarization to the beam (through spin precession). This polarization can affect the measured beam asymmetry in one of two ways. First, synchrotron light emitted in the large bend (to be described later) before the E158 spectrometer can leave an overall asymmetry present in the beam which is uncorrelated with other beam parameters. A synchrotron light monitor has been placed upstream of the E158 spectrometer to measure this effect. Second, synchrotron light emitted in the E158 spectrometer chicane can strike the Møller detector. If this light carries a large asymmetry, it might contribute to the experimental asymmetry. As we will see, the spectrometer has been designed to suppress this synchrotron flux as much as possible.

2.4.4   Other Backgrounds

Aside from backgrounds with high asymmetries, the Møller detector is susceptible to neutral backgrounds from a variety of sources. These backgrounds will scale (dilute) the measured asymmetry by contributing to the denominator of A_{PV} (equation 2.1). When the electron beam passes through the target, approximately 16% of the beam energy converts to photons. Photons which scatter at wide angles need to be blocked, so as to prevent dilution of the experimental asymmetry. Fluctuations in this distribution could also ruin the statistical resolution of the overall detector[4]. A second source of neutral backgrounds is from showers occurring at the inner edges of of the momentum collimator and the photon collimators. These collimators, to be described later, block high-energy ep scatters as well as photons originating in the target. Although the collimators are made of tungsten, the magnitude of the incident flux on them leads to a sizable amount of photons emanating from the inner edges of the collimators, which would also dilute the experimental asymmetry. These photons might also contribute some asymmetry to the Møller detector, as wide-angle scattering from nuclei has not been studied very thoroughly, and the precise couplings are not well known. The third and final source of neutral backgrounds is neutral hadrons, which can originate from anywhere in the spectrometer, as well as from downstream sources such as the beam dump. This flux is expected to be quite small because of the small potential for interactions within the Møller detector.

---

[4]More qualitatively, this would add a lot of noise to the dithering and regression analyses, described later.

2.5   Experimental Requirements

With an incident beam of $5\text{-}6 \cdot 10^{11}$ electrons per spill, the overall flux on the Møller detector will be somewhere around $3 \cdot 10^7$ electrons per pulse[5]. Consequently, the expected statistical width of a pulse pair asymmetry will be around 130 ppm. The overall detector resolution needs to be much less than this number, and preferably on the order of 40 ppm. The detector must integrate the overall signal, as counting at this flux is prohibitively difficult. To achieve such a high precision, the target density must also be made as stable as possible (on a per-pulse basis), and fluctuations in the density should fall well under the level of 100 ppm.

In order to measure an asymmetry with the stated precision, the E158 beam must have the ability to rapidly change its longitudinal polarization state (on a pulse by pulse basis). Otherwise, slow drifts in any parameter would destroy the measurement. Also, the extremely small scattering angle acceptance of the experiment, combined with the strong dependence of the scattering cross section on the angle, causes the detector asymmetry to be very sensitive to helicity correlations ("right-left asymmetries", or just "asymmetries") in the beam parameters. Consequently, all pertinent beam parameters must be measured with very precise beam monitors. Assuming that the experimental asymmetry width is about 130 ppm, each monitor's resolution should be high enough such that, when asymmetries in the beam parameters are subtracted from the detector asymmetry, the overall contribution to the width of the final asymmetry from each monitor is no more than 30 ppm. Using a Monte Carlo simulation to estimate the beam contributions to the experimental asymmetry, this places limits on the monitor resolutions of 30 ppm for the intensity (which will also be called charge) and energy, about 1 μm for the position (in x

---

[5]The exact number depends on the spectrometer geometry.

and y), and about 100 nrad for the angle (in x and y).

In addition to having such precise beam monitors, E158 also needs a very stable beam. Beam jitter must be kept low enough to keep the beam contributions to the detector asymmetry small, preferably enough to limit the systematic error from any one contribution to 3 ppb. The expected jitter in and asymmetry of each of the four beam parameters described above is detailed in table 2.1.[11] Due to the large expected jitter in intensity and energy, having an intensity feedback at the laser source is necessary for suppressing the overall intensity and energy asymmetries. The experiment must also be able to minimize systematics through other means, such as making fixed sign changes of the beam asymmetry unrelated to the source electronics, and measuring the sensitivity of the detector to the beam asymmetries in real-time.

Beam Parameter	Jitter Per Pulse	Beam Asymmetry Without Feedback	Beam Asymmetry With Feedback (Goal)
Charge	0.5% (of Q)	350 ppb (of Q)	100 ppb (of Q)
Energy	0.04% (of E)	30 ppb (of E)	4 ppb (of E)
Position	0.1 mm	140 nm	140 nm
Angle	10 μrad	14 nrad	14 nrad

Table 2.1: The estimated jitter in every beam parameter, and (assuming 10^8 pulses in Run I) an estimate of the overall beam asymmetry (or, for the position and angle, the helicity correlated beam difference), with and without a laser intensity feedback.

Besides measuring corrections to the experimental asymmetry (which shift its value), E158 must also precisely measure all parameters used to normalize (scale) the experimental asymmetry. These parameters include the detector linearity, the beam polarization, and the analyzing power of the experiment (which is proportional to the spectrometer/detector

acceptance). As the measured asymmetry is directly proportional to each normalization (for the polarization, for instance, $A_{PV}^{measured} = Polarization \times A_{PV}$), the systematic error on the final result from each normalization is, as a percentage, equal to the percentage error on the normalization parameter. Consequently, keeping the error on each normalization parameter at the level of 1% is desirable.

Chapter 3

Polarized Electron Beam

3.1 Source

To achieve the proposed systematic error, E158 requires a stable beam with an intensity of $6 \cdot 10^{11}$ electrons per spill and with stringent demands on the beam position and charge asymmetries and the beam jitter. To produce such a stable beam, E158 uses a flashlamp-pumped titanium sapphire laser made by Big Sky Laser Technologies, which emits an 805 nm beam at a frequency of 120 Hz (the rate at which the accelerator delivers pulses).[15] The laser bunch length can be as long as 370 ns, which corresponds to an output intensity of 600 μJ. The laser pulse shape is controlled with a pair of crossed polarizers and a Pockels cell[1] driven with a high voltage pulser. This Pockels cell "slices" out a 130 ns pulse from the bunch at the point of the lowest intensity jitter. The intensity jitter in the laser is further reduced with a set of end mirrors on the laser cavity, and currently stands at 0.5% for nominal running.

---

[1] A Pockels cell is an optical device consisting of a stand-mounted crystal connected to a high voltage source. A large voltage will induce a birefringence in the crystal, allowing it to change the polarization of any incident laser light to any arbitrary elliptical polarization.

Circular polarization of the laser is accomplished by means of two Pockels cells, known as the CP and PS cells. The CP cell behaves like a quarter wave plate with an axis 45 degrees from the horizontal. This cell also allows pulse-by-pulse voltage control over the linear polarization of the beam. Even small amounts of linear beam polarization (arising from imperfections in source optics) can lead to large position and intensity asymmetries in the electron beam.[15] By controlling the helicity of the laser with the CP cell, systematics due to beam helicity correlations can be minimized. The PS cell is similar to the CP cell, but serves to eliminate linear polarization along the 45 degree axes of the laser.

Figure 3.1 depicts the entire source, from the laser to the photocathode.
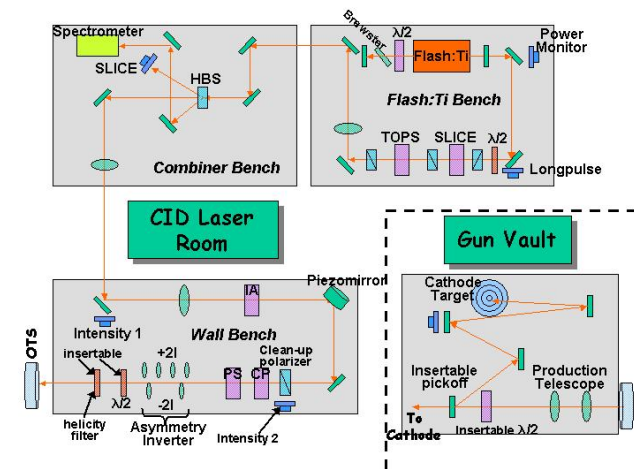
Figure 3.1: A schematic of the E158 source optics. The laser source area is sometimes referred to as CID, which stands for "Collider Injector Development".

3.1.1 Helicity sequence

The beam polarization is changed on a pulse-by-pulse basis, and consequently, it must follow some sequence. If the sequence of beam polarization states repeats at any specific frequency, there is a chance that systematic effects at that frequency could bias the experimental asymmetry. Accordingly, the polarization sequence is required to be random enough to negate this possibility. The beam polarization sequence is set by an electronics module located in a CAMAC crate at the laser source called PMON (Polarization MONitor). This module generates a pseudo-random helicity sequence for the beam using a 33-bit shift register algorithm which, at 120 Hz, would repeat approximately every two years.[16]

To measure an asymmetry, every pulse generated must have a complement. However, if each pulse is immediately followed by its complement, 60 Hz noise might systematically bias the measured asymmetry. Thus, a pulse quadruplet sequence is used for beam helicity: the first two beam pulses are members of the 33 bit sequence, and the next two are their complements (an "$AB\bar{A}\bar{B}$" pattern). This not only helps to remove systematics arising from the polarization sequence, but also it splits the experiment into "two" experiments at 60 Hz, allowing the measurement of any effects to the experiment from 60 Hz noise.

3.1.2 Asymmetry Inverters

One of the most powerful (and necessary!) tools for negating systematics in parity experiments is the ability to change the sign of the physics asymmetry independently of any other experimental parameter. By doing so in E158, the experimental asymmetry determined at one sign must be multiplied by -1 before it is averaged with the asymmetry determined at the other sign. As the asymmetry in each beam parameter (which will affect the experimental asymmetry: $A_{measured} = A_{M\o ller} + A_{beam}$) should be the same for

both signs, this sign-flip technique should suppress the overall contribution to the detector asymmetry from beam asymmetries, as well as any other potential sources of systematic bias.

E158 contains two such potential sign flips. The first is a simple halfwave plate, mounted at the laser source, immediately before the photocathode. This halfwave plate reverses the polarization of the laser beam while ideally leaving asymmetries in the beam position and intensity unchanged. In reality, the halfwave plate introduces some additional beam intensity asymmetry due to imperfections in the crystal (which introduce linear polarization into the laser beam).

The second method of inverting the experimental asymmetry uses g-2 spin precession to change the sign of the beam polarization. A large bend in the end of the accelerator (to be described in section 3.2) causes the beam to undergo multiple g-2 spin precessions before the beam enters the spectrometer. If the beam energy is raised from 45.0 GeV up to 48.3 GeV, the orientation of the beam polarization vector will change by 180 degrees at the target[2]. Consequently, the E158 data set for the spring run was taken at these two beam energies. The beam was run at each energy for approximately three weeks. If the two data sets from each energy are compared, the physics asymmetry should flip sign from one to the other. In practice, the Q^2 acceptance of the spectrometer is slightly different for the two energies, and this acceptance will have a small but measurable effect on the asymmetry.

One final device for changing experimental asymmetries is the "asymmetry inverter". This is a system of four lenses at the laser source, mounted in series and located immediately upstream of the halfwave plate described above. These lenses should perform exactly the opposite function as the halfwave plate: they invert the beam position and in-

---

[2]These energies are taken after synchrotron losses, which account for roughly 300 MeV of beam energy.

tensity asymmetries while leaving the experimental asymmetry unchanged.[15] By adding together two equal sets of data with opposite-sign beam asymmetries, systematic bias from beam asymmetries should be suppressed. Like the halfwave plate, the glass in the asymmetry inverter might introduce some small amount of additional beam intensity (and position) asymmetry.

3.1.3 Photocathode

After the laser light passes through the source optics, it strikes a strained Ga-As photocathode. To achieve the necessary luminosity ($6 \cdot 10^{11}$ electrons per spill), E158 uses a new kind of strained Ga-As photocathode that incorporates several more layers than standard Ga-As photocathodes.[11] Whereas prior photocathodes were limited to 2-$3 \cdot 10^{11}$ electrons in a single bunch, this new photocathode appears to have no charge limit, even at the level of $7 \cdot 10^{11}$ electrons per spill. Additionally, like prior photocathodes, this photocathode gives a very high ($\geq 80\%$) polarization, which was required for the proposed experimental running time (the measured asymmetry is directly proportional to the polarization).

3.2 Accelerator

Electrons exiting the source are sent into the accelerator, which consists of 30 sectors of klystron groups, each group containing eight klystrons. Each klystron consists of a copper cavity into which 65 megawatts of RF power is pulsed at a frequency of 2856 MHz. This RF power accelerates the electron beam by roughly 200 MeV per klystron. SLAC's 2 mile accelerator can achieve a theoretical maximum beam energy of 51 GeV. Each sector of the accelerator also contains steering magnets (one quadrupole and one dipole), necessary for keeping the E158 beam and the PEP beams (for BaBar) aligned.

At the end of the LINAC, the electron beam must bend 24.5 degrees to enter End Station A (henceforth called ESA), where E158's spectrometer and detectors are located. To create such a large bend in the beam, twelve dipole and twelve quadrupole magnets, collectively known as the "A-Line", are used to steer the beam. It is in this bend that the $g-2$ spin precession of the beam occurs, allowing the second method of inversion of the experimental asymmetry (described in section 3.1.2).

3.2.1 Beam Rate and Spills

For E158, the beam can be run at several rates, but for the majority of the experiment, the beam is run at either 30, 60, or 120 Hz. If PEP is running while E158 is running, PEP will request time to refill its positron and electron rings - typically once every hour for around five to ten minutes. During this period, E158 voluntarily drops its rate by a factor of two.

In the very beginning of the experiment, ten million pairs of data were taken at 60 Hz. For the remainder of the experiment, the beam was delivered at 120 Hz. These numbers are slightly higher than the actual delivered rate, due to two necessary sources of loss. First, while PEP is running, two hertz of beam pulses (in one 60 Hz timeslot) are constantly used to maintain proper steering of the PEP beams through the PEP rings (these pulses will henceforth be called "witness pulses"). Although these pulses wind up in the E158 spectrometer, they are unpolarized and cut from the data in the analysis. Second, 1 Hz of beam pulses (at 120 Hz; 0.5 Hz at 60 Hz) are pedestal pulses: they contain no electrons, and they are used for pedestal subtraction[3]. At 120 Hz running, each timeslot loses 0.5 Hz of beam to pedestals. Consequently, at "120 Hz" running, E158

---

[3]Electronic devices such as ADCs (analog to digital converters) typically put out non-zero values even with no input signals; these are known as "pedestals".

receives 117 Hz of beam, which falls to 59.5 Hz of beam during PEP fills (as the PEP witness pulses both occur in the timeslot used for the fill).

3.3   Beam monitoring

E158 requires very precise monitoring of all beam parameters, since quite a number of systematic errors from beam asymmetries could creep into the physics asymmetry. The four kinds of devices used to monitor the beam are toroids for charge, beam position monitors (BPMs) for position, a wire array for the second (and higher order) moments in beam shape, and a synchrotron light monitor for measuring beam energy fluctuations[4]. The placement of these monitoring devices both in the front end of the accelerator and immediately upstream of the hydrogen scattering chamber is shown in figure 3.2.
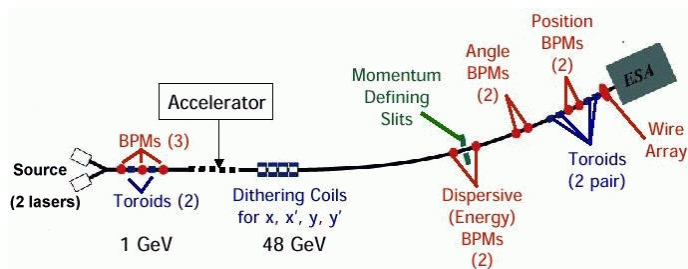
Figure 3.2: Placement of all of the E158 beam monitors.

---

[4]A fifth device, the polarimeter, will be discussed in the spectrometer section.

3.3.1   Beam Intensity

E158 measures the beam intensity with several toroids, each consisting of many turns of copper wire wound around an iron core. When the electron beam passes through the toroid, it induces a pulse on the windings. The ends of the windings are connected to a resistor/capacitor combination which converts the pulse to a ringing signal. This signal is then differentially run through two sets of amplifiers[5]. These amplifiers' gains are remotely controllable by switches located in the ESA Counting House (for the four ESA toroids) or in the ASSET[6] electronics shack (for the two ASSET toroids).

Once the toroid signal has been amplified, it is run across approximately one hundred feet of wire, depending on the location of the toroid, to an "absolute value" module. This module rectifies the ringing signal, allowing it to be measured with a standard integrating ADC (analog to digital converter). Once the toroid signal has been rectified, it is run into a custom-designed 16-bit ADC (described later).

By making the Q of the toroid RLC circuit as large as possible, the toroid signal can be integrated for more than 1 ms. This puts as much charge as possible onto the toroid ADC, allowing the best possible resolution in the measurement. The average resolution for the four ESA toroids is about 60 ppm per pulse. A plot of the resolution, determined from the agreement between two toroids' asymmetries, for a typical beam intensity is shown in figure 3.3. Charge asymmetry jitter is much higher than the toroid resolution, so resolution must be obtained from the agreement. The toroid linearity has also been measured with a calibrated charge pulse, and has been determined to be better than 99.9%.[17]

With such a large Q in the toroid RLC circuit, if nothing is done to damp out the

---

[5]The signal is amplified near the toroid to prevent noise pickup on any downstream electronics.
[6]ASSET stands for Accelerator Structure SETup, and refers to the 1 GeV region at the upstream end of the accelerator.

toroid charge, approximately one percent of the charge of one pulse will "leak" into the next pulse. This could both decrease the toroid resolution and create helicity systematics due to hysteresis[7]. As the signal must be damped, the initial ringing circuit contains a transistor (used as a relay) which can connect a large resistor to the overall circuit. Approximately 3 ms into the pulse (well after the integration is complete), this transistor is triggered, damping out the pulse and assuring that no charge leaks into the following pulse.
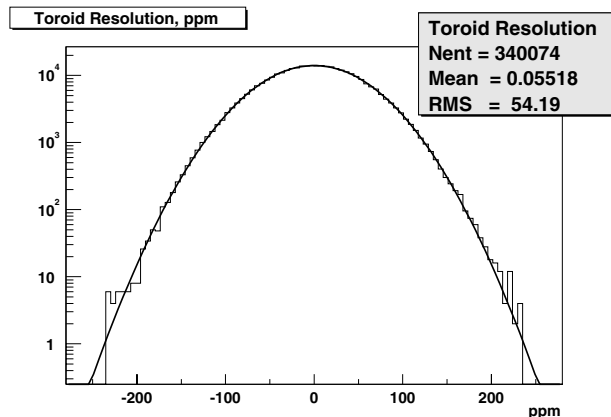
Figure 3.3: Typical toroid resolution. Plotted is the difference between two alcove toroids' asymmetries.

---

[7]If the toroid gain depends on the the size of the prior pulse, two events at different intensities but with identical intensity asymmetries could be measured as having very different intensity asymmetries.

3.3.2   Position

The second type of monitors used in E158 are RF cavity beam position monitors (BPMs).[18] These monitors consist of 3" copper boxes in which a charged beam can excite TEM 01 and 10 modes. An internal antenna then sees an induced pulse, which travels up approximately one hundred feet of cable and into BPM RF electronics. This pulse contains all frequencies found in the beam, so in the RF electronics, it is mixed (convolved) with a waveform from an oscillator running at the same frequency (2856 MHz) and phase as the beam. Assuming the difference between the oscillator phase ($\varphi_{oscillator}$) and the beam phase (φ_{beam}) varies slightly from pulse to pulse, the two outputs of the RF mixer end up proportional to $\cos(\varphi_{beam} - \varphi_{oscillator})$ and $\sin(\varphi_{beam} - \varphi_{oscillator})$[8]. Both signals are then run into a 16 bit BPM ADC, described later.

BPM linearity was measured by changing the attenuation on one BPM amd comparing its signal to the closest BPM (each BPM is adjacent to or very near another, for redundancy and crosschecks). If the attenuation on one BPM is decreased, its overall dynamic measurement range will be reduced (this increases the overall resolution by increasing the signal to beam position ratio). For the data taken in Run I, all BPMs were run with dynamic ranges large enough to keep the BPMs more than 99% linear for nominal beam positions. In the analysis section, a cut will be made to the data to eliminate instances in which the beam moved far enough off center to reduce any BPM's linearity below 99%. Typical resolution on the BPMs varied from 1 to 3 μm during the course of the run (they usually averaged around 2 μm or less), for such reasons as phase drifts, cavity shape degradation (one of the cavities has a dent), and dynamic range adjustments.

---

[8]These are sometimes referred to as the real and imaginary portions of the BPM signal.

3.3.3 Spot size

A tightly packed array of Cu-Be (drift chamber) wires is used to measure the beam spot size (and higher order moments).[19] This wire array consists of two planes of wires, one running horizontally and the other vertically. The wires in each plane are 7 mil in diameter and have been placed 14 mils apart from one another. An aluminum foil is located next to the wires, and is raised to a high enough voltage to allow the beam to induce 40 mV pulses on individual wires. This foil has a 1" hole so that the beam can pass through it. Each wire's signal is run up approximately one hundred feet of cable and into a standard CAMAC 2219W 11 bit ADC. The resolution of the array is slightly better than 13 μm in both axes. A typical output from the wire array is shown in figure 3.4.

The wire array is not designed to take the full power of the beam for several weeks, as radiation damage causes the wires to deform and snap. For Run I, the wire array was left in the beam full-time, causing it to become unusable after the first half of the run. For future runs, the wire array will be moved into the beam periodically to measure spot size effects and to make sure that the beam profile has not changed.
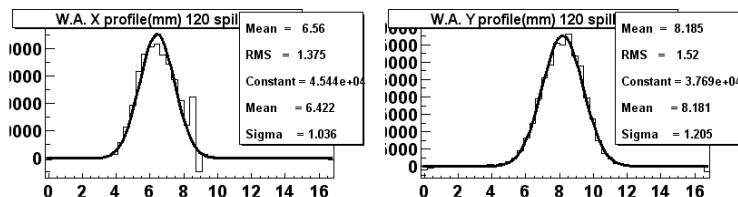
Figure 3.4: Typical output from the wire array, averaged over a one second period.

3.3.4 Energy

Two types of devices are used to measure the beam energy. The first, BPMs (two of them), are placed around the point of highest beam dispersion in the A-Line bend. These BPMs are read out in an identical manner as those described in section 3.3.2.

The second device which can measure the energy asymmetry is the A-Line synchrotron light monitor. This monitor measures synchrotron light emitted from the beam while it bends through the A-Line. The power of the synchrotron radiation is proportional to B^2E^2, where B is the magnetic field and E is the beam energy.[14] The measurement is therefore not linear in the energy, but is still useful as an independent measurement of the beam energy.

To detect the synchrotron light, a lead radiator and a quartz Cerenkov radiator are used to downgrade synchrotron light at 1 MeV into light in the visible spectrum.[20] The visible light is then run through a series of mirrors (see figure 3.5) into a lead housing (shielded to prevent background from soft-photon radiation) containing UDT PIN 10D photodiodes. Signals from (four of) the photodiode arrays are run up RG58 cables into a standard CAMAC 2219W 11 bit ADC.

3.4 Feedbacks

As was mentioned in section 2.5, feedbacks are essential for reducing the charge asymmetry to the point where its systematic corrections don't dominate the experimental asymmetry. With a 0.5% jitter in the beam charge, the charge asymmetry width for any given run is about 3500 ppm. If E158 were to take 10^8 pulses with no feedback, statistics would reduce the charge asymmetry systematic to 350 ppb, which would be large enough to inflate the systematic error on the experimental asymmetry.
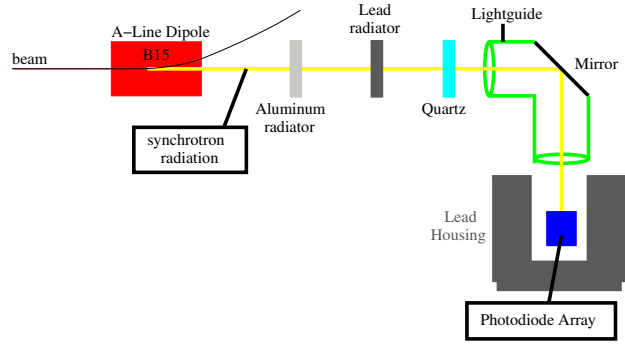
Figure 3.5: Schematic for the synchrotron light monitor.

Assume that the overall beam asymmetry is the linear sum of the statistically random beam asymmetry and an induced asymmetry[15],

$$A_{PV}^{beam} = A_{statistical} + A_{induced}. \tag{3.1}$$

This induced asymmetry is calculated from the average of every 1600 pulses[21], and is determined by the following formula,

$$A_{induced}^{n} = A_{induced}^{n-1} - gA_{beam}^{n-1}, \tag{3.2}$$

where n is the number of the current feedback cycle (henceforth known as a minirun) and g is the gain of the loop. Assuming that g is set to one, and that the beam asymmetry is

known perfectly, then the final asymmetry on the beam after n miniruns is

$$A_{beam}^{n} = A_{statistical}^{n} - A_{statistical}^{n-1}. \tag{3.3}$$

If the average of N miniruns is taken, algebra leads to

$$A_{average}^{beam} = \frac{1}{N}A_{statistical}^{n}. \tag{3.4}$$

In other words, the scaling for the asymmetry goes not as $\frac{1}{\sqrt{N}}$, but as $\frac{1}{N}$. This would be ideal, as it would reduce the 350 ppb charge asymmetry down to 0.35 ppb.

Several factors limit the effectiveness of the feedback, preventing $\frac{1}{N}$ scaling of the charge asymmetry. Most of these have to do with the fact that the accelerator is two miles long. Beam losses along the length of the accelerator can distort the correlation between the charge asymmetry at the source and the measured charge asymmetry immediately before the target. This distortion may not even be linear, and the efficacy of the feedback will suffer as a result. Accounting for the accelerator, the charge feedback should reduce the charge asymmetry to around 100 ppb.

The laser intensity asymmetry can be controlled with a Pockels cell immediately up-stream of the CP and PS cells.[15] This cell can be pulsed at 120 Hz with a helicity-correlated voltage, introducing a phase shift into the beam. The downstream CP Pockels cell then turns this phase shift into a helicity correlated intensity, negating any measured beam intensity asymmetry[9].

A second feedback negates position asymmetries in the laser beam. At one point, the laser reflects off a mirror mounted on several piezo-electric crystals. These crystals expand

---

[9]The monitors used to control the intensity asymmetry feedback will be described later.

or contract under high voltage, and can be pulsed at 120 Hz to translate the mirror up to 6 μm at any one point. This will change the position of the laser beam on the photocathode up to 50 μm, negating position asymmetries.[15] 50 μm is similar in magnitude to the beam angle jitter, and is not viewed as a large deviation.

3.5 Beam Dithering

At the beginning of the A-Line, there are several magnets which can be used for beam steering. These magnets have fast response times, and consequently are used for the beam dithering analysis. This analysis, described in appendix A, uses intentional beam motions to calculate the correlation between the experimental asymmetry and the asymmetries measured in each beam monitor. A total of eight such magnets are used to move the beam position: two redundant magnets each in X, Y, dX, and dY. To dither the beam energy, a klystron at the end of the accelerator has its phase dithered.

3.6 Results

The devices used for monitoring beam parameters are given in table 3.1. The beam asymmetries, averaged over all runs in Run I, are given in table 3.2. The error bars given for these quantities are not based upon the monitor resolution of the device described, but rather upon the jitter in the associated beam parameter. This error is more pertinent for systematics estimations, given later in chapter 7. In that chapter is also a list of cuts made to the data before these quantities were determined. Table 3.2 also gives the agreement (the difference in value) between redundant beam monitors for each beam parameter's asymmetry.

Beam Parameter	Device Used
Charge	Alcove Toroid 0
Energy	BPM24X
Target X	0.5*(BPM41X + BPM42X)
Target Y	0.5*(BPM41Y + BPM42Y)
Angle X	0.5*((BPM31X + BPM32X) - (BPM41X + BPM42X))
Angle Y	0.5*((BPM31Y + BPM32Y) - (BPM41Y + BPM42Y))

Table 3.1: A list of the beam monitoring devices. BPMs 41 and 42 (and the toroid) are a few meters upstream of the target. BPMs 31 and 32 are 40 m farther upstream. BPM24 is even farther upstream, at the point of highest dispersion in the A-Line.

Beam Parameter	Run I Asymmetry	Monitor Agreement
Charge	225 ± 320 ppb	-5.9 ± 5.5 ppb
Energy	-0.1 ± 1.4 keV	0.0 ± 0.2 keV
Target X	-16.9 ± 5.6 nm	-0.2 ± 0.3 nm
Target Y	-3.3 ± 4.0 nm	0.1 ± 0.5 nm
Angle X	0.41 ± 0.23 nrad	0.03 ± 0.02 nrad
Angle Y	0.12 ± 0.07 nrad	-0.01 ± 0.02 nrad

Table 3.2: A list of beam asymmetries, Run I. Also given are the agreements (differences) between redundant beam monitors' asymmetries for each measurement.

Chapter 4

Spectrometer

The E158 spectrometer was specifically designed for this experiment, and is tuned to accept very forward angle Møller scatters from a fixed target while suppressing backgrounds. The spectrometer runs the entire length of SLAC's End Station A (ESA), almost 60 meters. A plan-view image of the spectrometer is shown in figure 4.1. In this image, a single Møller scatter from the hydrogen target (yellow) passes through the collimators (orange and gray) in the dipole chicane (blue) and the quadrupoles (red) before traveling through the drift pipe (light gray) and onto the face of the detector (not pictured). The secondary Møller scatter is blocked by the radial momentum collimator. Not well-visible are the synchrotron collimators or the collimator masks (the lines sitting in the right half of the picture), mostly because of the scale of the image. The detector has been omitted, but would be sitting at the end of the spectrometer (its face would be at 5925 cm).

To summarize the geometry conventions: the spectrometer's beam axis is the z axis. The electrons initially bend to the north in the dipole chicane, or, if looking downstream at the detector, to the left. Thus the words "left" and "right" will refer to the north and south sides of the spectrometer, respectively.
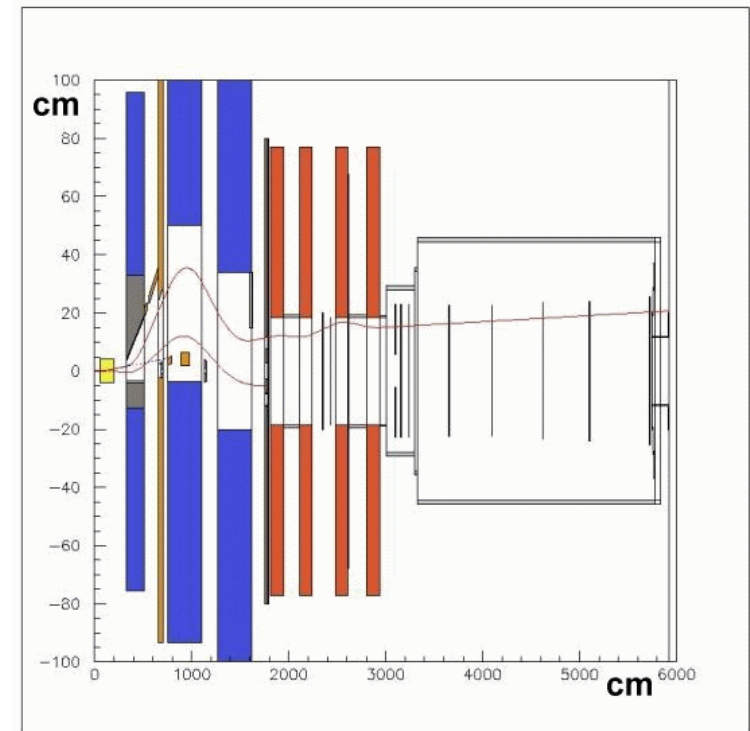
Figure 4.1: A plan-view image of the E158 spectrometer, showing a single Møller scatter from the hydrogen target. Note the discrepancy in the x and y scales. The outer edges of some collimators and magnets in the picture are not accurate. All collimator and magnet inner apertures are to-scale, however.

4.1   Iron

The most important feature of the E158 spectrometer is precisely what it lacks. The expected experimental asymmetry of around 150 ppb is almost eight orders of magnitude smaller than the asymmetry from polarized electron-polarized iron scattering! Thus, the chief constraint in designing the E158 spectrometer is that no component that might see incident particle flux (and then radiate scattered particles into the detector region), be it a collimator, a beam pipe, or anything else, can be made of iron. In the regions inside and between the magnets, this constraint is tightened to include stainless steel. Thus, almost all pieces of beampipe are made from aluminum, and all collimators have been fabricated either from copper, or from "non-magnetic" tungsten with a very low iron component.

4.2   Target

E158 uses a liquid hydrogen target as its source of target electrons. The target is insertable into and removable from the beam line, and must survive sustained power levels of 700 W and a lifetime radiation dosage approaching 100 MRad. The target has been published ([22]); the following is a brief overview.

The actual target is a 150 cm aluminum cylinder (which corresponds to 0.17 r.l. of LH_2), 3 inches in diameter, filled with liquid hydrogen at an operating temperature of around 17.5 K. The entire target assembly can be seen in figure 4.2. This cylinder is connected on one side to a heat exchanger and on the other side to a differential pump. The heat exchanger uses helium coolant to remove heat from the system. The differential pump moves the hydrogen through the system at a sustained flow rate of 10m/s. This high velocity is necessary to prevent hydrogen density fluctuations (due to beam heating) from artificially increasing the width of the experimental asymmetry.
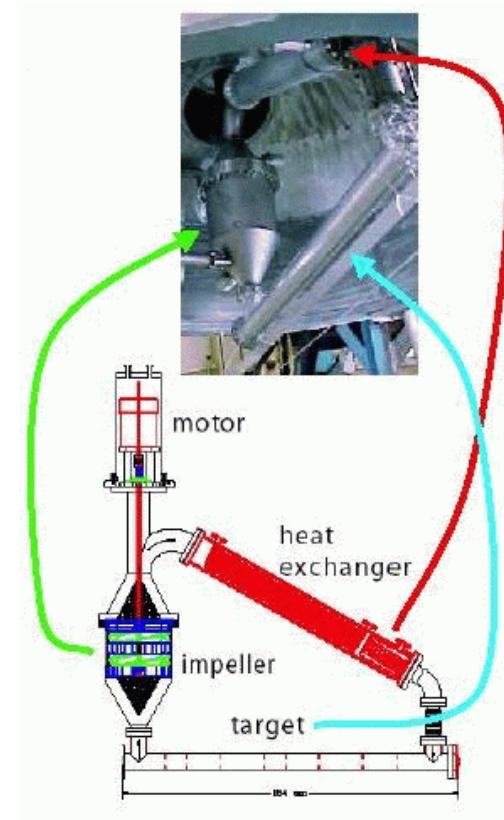
Figure 4.2: Schematic and photo of the LH2 target.

Inside the target cylinder are four sets of wire mesh partial-disks designed to increase transverse flow and generate turbulence within the liquid hydrogen. This turbulence should, in turn, reduce target density fluctuations below the 100 ppm level. For nominal running conditions, the density fluctuations were measured, and a limit of 65 ppm has been set.[23]

The entire target assembly is hung from a frame connected to motorized jacks, permitting the target to be moved into or out of the beam (the out position is 1.5 m from beam center) in about ten seconds. The entire assembly is located in a aluminum scattering chamber, kept at room temperature but evacuated to a pressure of roughly 10^{-8}-10^{-9} torr to prevent heat loss from convection.[24]

The hydrogen temperature and pressure is continuously monitored by SLAC's cryotechnical staff. LabView is used as a readout for all the various target sensors. In standard running, a computerized feedback loop keeps the target temperature stable to within 0.1 K, with small changes in coolant temperature by the cryotarget operator necessary from time to time. In the event of emergencies (or during target cooling or heating procedures), a manual control located in the ESA counting house is used to alter the heater setting.

Within the aluminum scattering chamber, there is also a table containing solid carbon targets used for spectrometer and detector checkout. This table is laterally insertable and removable so as to allow either itself or the LH_2 target to be placed in the beamline[1]. The carbon targets on the table range from 30 μm up to 8 cm thick, and are held in place with aluminum holders. Lateral adjustments of the table allow different targets to be moved into the beamline.

---

[1]A system of microswitches prevents the two targets from coming into contact during experimental running.

A second target assembly sits immediately upstream of the scattering chamber, and is used for polarimetry. This assembly contains supermendur[2] foils of varying thicknesses (30, 50, and 100 μm) mounted on rods which are connected to a remotely controllable motor. Each foil sits at a sixty degree angle to the beam axis to increase the scattering rate. Polarimetry measurements (which will be detailed in section 5.4) are typically performed with the 50 μm foil, though all three targets were used during the run. The polarization of the foil is controlled by 2 custom-designed Helmholtz coil magnets run at 6 amps (positive or negative), which together produce a field of roughly 92 gauss on the foil, which is too low to entirely saturate (and polarize) the supermendur. The power supply for the magnet and a readout of the foil position are both located in the counting house.

4.3 Chicane

Aside from ep scatters, the main potential detector background consists of soft (low momentum) particles created in the target. This flux contains photons, positrons, and electrons, including low momentum, low asymmetry Møllers. A standard approach for blocking low-momentum background is to place a dipole chicane downstream of the target. The requirements on the chicane are threefold: first, each magnet needs to have a large enough opening to accept the entire signal profile. Second, each of the dipoles needs to be strong enough to bend the primary beam several centimeters away from the beam axis (for photon collimation). Third, keeping the Møller signal profile azimuthally symmetric is desirable, so each chicane magnet should have a fairly uniform field.

SLAC's original 8 GeV spectrometer contained two copper-coil magnets, B81 and B82, which both meet all three requirements.[25] Consequently, these magnets are used as the

---

[2]Supermendur is an alloy of 50% iron and 50% cobalt.

second and third dipoles in the chicane. Whereas these dipoles see a wide particle flux, the first dipole sees a relatively confined distribution, owing to its proximity to the point of scattering. Consequently, the first dipole can be smaller and less uniform. Hence, the magnet chosen for the first dipole is an 18D72 magnet, normally used in the accelerator beam line. All three dipoles are connected to high voltage supplies located in a building adjacent to ESA, and all three are water cooled to dissipate heat from the high currents necessary to run the magnets at the desired strength.

To ensure the stability of the chicane, two independent measurements of the dipole fields were taken during the course of the experiment. First, the current from the dipole high voltage supplies was monitored (and logged) every several seconds, and was connected to software and hardware alarms in case of a large deviance. Second, NMR probes placed inside the dipoles and measured with an oscilloscope in the ESA counting house were used to confirm the fields once per shift (every eight hours). These NMR probes proved unsuitable for usage in such a high radiation environment, and stopped functioning halfway through the run.

The dipole field strengths are determined by geometry (stronger fields would send signal particles into the inner left wall of the second dipole) and by the desire to have zero net effect (integral BdL[3]) on the signal distribution once it has passed through the chicane. If the dipoles had a non-zero integral BdL, the distribution of the Møller flux after the dipoles would not be azimuthally symmetric, making it impossible for the momentum collimator to make a clean cut on the momentum of Møller scatters (which is directly proportional, assuming azimuthal symmetry, to their radii).

The placement of the dipoles is fixed by three constraints. First, the internal walls of

---

[3] "Integral BdL" is defined as the net amount of transverse magnetic field a charged particle sees while passing through a system of magnets.

every dipole need to be far as possible from from the high power (85 kW at maximum luminosity) photon beam created in the target. Otherwise, the magnets will take significant amounts of radiation damage. Second, the walls must not collimate any of the Møller flux which would strike the Møller detector. This limits the maximal beam bend angle in the chicane to 44 milliradians (to the right) in the second dipole (the bend angle of the lower-momentum Møllers is even greater), and half that (to the left) in each of the other two. The third constraint is that the three dipoles should together take as little room in z as possible, thereby allowing the quadrupoles to sit as far upstream as possible.

Due to its field strength, the first dipole bends all electrons with momenta up to five GeV into its inner left wall, and all positrons with momenta less than twenty-eight GeV into the inner right wall. The power in the two fluxes is quite high (2 kW in positrons and 1.5 kW in electrons at maximum luminosity), and would damage the magnet if it were unimpeded. Consequently, two pieces of water cooled copper, each three inches thick, run the length of the dipole on either side. Similar water cooled masks have been placed in the second and third dipoles to absorb power due to synchrotron radiation and mis-steered electrons.

The dipoles sit on large stands, designed so as not to interfere with the dipole fields. Each stand has jacks capable of aligning the dipole to within five mils. The dipole beam pipe is one quarter inch thick aluminum, specially designed to fit the dipole apertures and keep an unbroken vacuum throughout the length of the chicane.

4.3.1 Additional Dipole Protection

Blocking the low momentum electron flux does not stop at the end of the first dipole. To prevent contamination of the physics signal with low momentum electrons (and to protect the other dipoles), copper masks have been placed between the first and second dipoles to

block all electrons with momenta less than 9 GeV. The copper mask inside dipole one does not stop at the end of the dipole, but rather continues downstream for another 29 cm. A second copper mask starts a few more inches downstream of the end of this first mask, and runs downstream for 96 cm. A third piece of copper (located immediately downstream of the second and immediately upstream of dipole two) collimates all electrons with momenta less than 9 GeV [4]. Each of these copper pieces is water cooled, as each takes upward of a kilowatt of power. Since the electrons strike the third piece of copper head-on, it has been made forty radiation lengths (r.l.) thick to prevent punch-through.

4.3.2   Pole Face Rotations

Pole face rotations[5] of the electron beam passing through the dipoles generate a small quadrupole focusing component of the chicane.[25] This field is non-negligible, and if left uncorrected, would result in an approximately 5 mm difference between the horizontal and vertical size of the profile of Møller scatters at the detector face. The fourth quadrupole (described later) is used to correct for this amount, leaving the distribution of Møller scatters azimuthally symmetric at the detector.

4.3.3   Synchrotron losses

The primary beam's energy is left mostly unaffected by the hydrogen target; thus, primary beam electrons pass through the dipoles with momenta around 45 GeV. The signal Møllers, however, scatter from the target at energies from 11 to 24 GeV. If it weren't for synchrotron radiation, the chicane would be tuned to reduce the dispersion as much as possible in

---

[4]Some electrons between 9 and 13 are also collimated, due to their scattering angle; almost all particles under 11 GeV are collimated by the primary radial collimator described in Section 4.5.

[5]Pole face rotations refers to the bend angle of a charged particle passing through the fringes of a dipole field.

the primary beam or, in other words, to keep integral BdL as close to zero as possible. However, all charged particles undergo synchrotron losses in the chicane, with the amount of energy loss proportional to the square of the particle momentum. This effectively "boosts" the field strengths of downstream dipoles, as a lower momentum particle is bent more strongly than a higher momentum one. As a result of the different changes in the momenta of beam and signal electrons, the net magnetic force (or integral BdL) on the signal Møllers is slightly different than it is on the beam particles. If nothing is done to account for this loss, the Møller signal profile will be, on average (over the momenta of all signal Møllers), about three millimeters off-center (to the left) at the detector face. To keep the Møller signal profile horizontally centered on the detector face, the field of dipole three has been slightly decreased (by 0.07%).

4.4   Photon collimators

Once the primary beam has been deflected away from the beam axis by the chicane, target photons which have scattered at wide angles can be collimated. "Line of sight" photons traveling from the target to the Møller detector must be blocked to prevent fluctuations in Møller detector signals that would ruin the statistical resolution of the detector. To block line of sight photons, two cylindrical collimators have been placed on the beam axis. Tungsten is used for the collimators in order to create a "hard edge" to the collimation, minimizing the number of particles which might shower off the inner surface and travel downstream to the detector. To minimize "punch-through" leakage, each cylinder is 40 r.l. thick. The first cylinder absorbs much of the power in the fringe of the photon flux (approximately two kilowatts) and is located at the same point in z as the most downstream copper mask described in section 4.3.1. Both the collimator and the mask are part of one

solid assembly, known as 3DC2C. The second tungsten cylinder, called 3DC3 and located in the downstream end of dipole two, sets the exact radius of the photon distribution at the luminosity monitor. The inner opening of the second cylinder flares slightly (in the downstream direction) to account for beam spread. This prevents photons which are not blocked by the front of the collimator from coming into contact with the inner surface of the collimator, from which they might scatter or shower and hit the detector. A diagram of both cylinders (figure 4.4) shows the relative positions of both cylinders. Each cylinder has its own water cooling, though the first shares its cooling with the adjoining copper.

Both photon collimators are surrounded by copper, which provides a larger area to block line of sight photons from the target. This copper creates a problem, though, because wide angle ep scatters which would strike the ep detector on the right side instead strike the left side of the second photon collimator. It is an inescapable fact of the spectrometer design that blocking line of sight photons necessitates blocking these eps. To prevent punch-through leakage from these eps, the copper has also been made forty r.l. thick.

The effect on the overall ep signal is rather large - figure 4.3 shows the ep distribution at the detector face (as seen looking downstream). This effect will have a small impact on the analysis, as the loss in ep statistics on this side of the ep detector must be taken into account in the Monte Carlo simulation.

Even with both photon collimators, the entire line of sight between the target and the detector is not blocked - a small gap in coverage exists on the left side of the beam axis. Two pieces of copper have been placed in dipole two (figure 4.4) to block photons in this region. No electron flux of any kind should hit these copper pieces, because all wide angle ep scatters on the right side of the beam have already been collimated by 3DC2C. A small groove cut into both pieces prevents synchrotron radiation from striking (and melting) the uncooled copper.
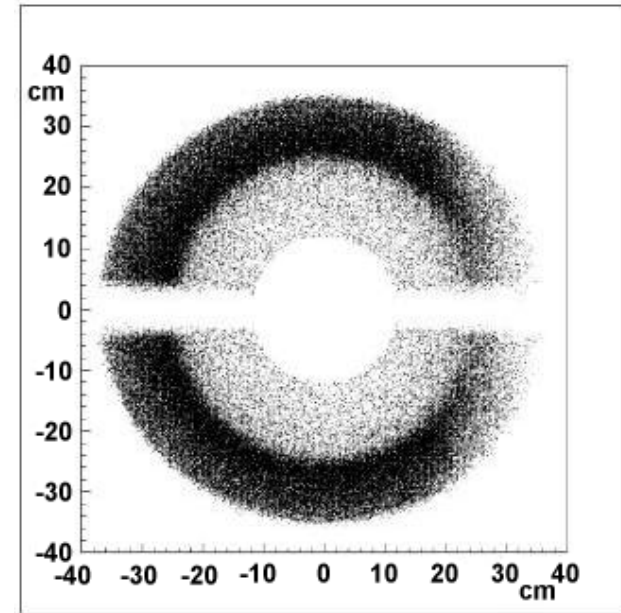
Figure 4.3: The ep distribution on the face of the detector (looking from upstream toward downstream). The loss of eps due to the photon collimator is visible on the right side.
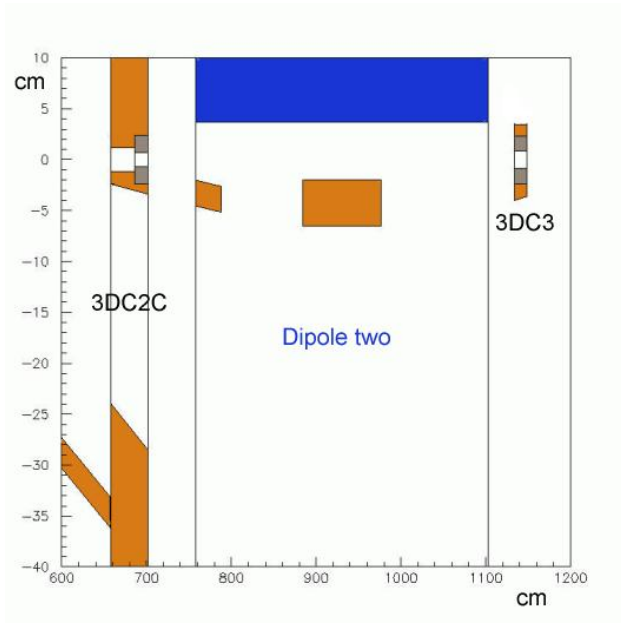
Figure 4.4: View (from underneath the spectrometer) of the photon collimators, as well as the copper in dipole two. Tungsten is gray, and copper is orange. Particles travel from the left to the right.

4.5 Radial collimator

The radial collimator (also known as the momentum collimator) sits immediately downstream of dipole three, and is used in tandem with the quadrupoles to separate the Møller scatters from the ep scatters. This collimator, also called 3QC1B, consists of two concentric cylinders, connected by two metal "spokes" (figure 4.5). The outer edge of the inner cylinder and the inner edge of the outer cylinder together create the radial slice through which the signal Møllers and the ep background pass. The placement of these edges was optimized (along with the positions and strengths of the quadrupoles) to maximize separation of the Møller and ep flux at the detector face while still allowing as many Møllers as possible to pass through for detection. All edges in this collimator flare radially inward or outward to prevent the same sort of "collimator wall scattering" as was described in the photon collimator section. Figures 4.6 and 4.7 show the phase space of the Møller and ep flux at the face of the Møller detector before and after this collimator has been inserted.
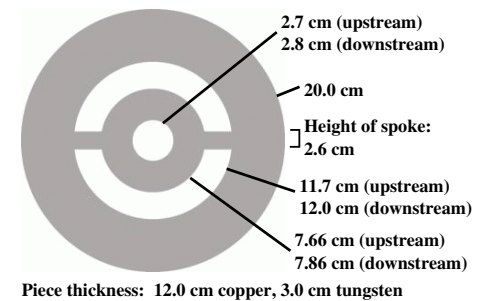
Figure 4.5: 3QC1B shape and dimensions. Upstream and downstream refer to the front and back side of the piece.
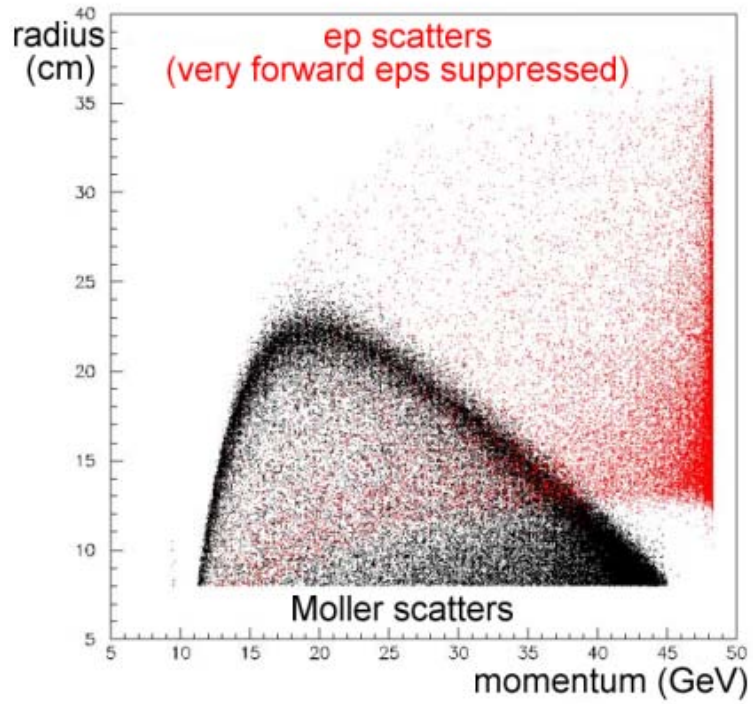
Figure 4.6: Møller and ep scatters, particle radius vs momentum at the face of the Møller detector, no radial collimator. Some very forward angle Møller and ep scatters have been suppressed for clarity.
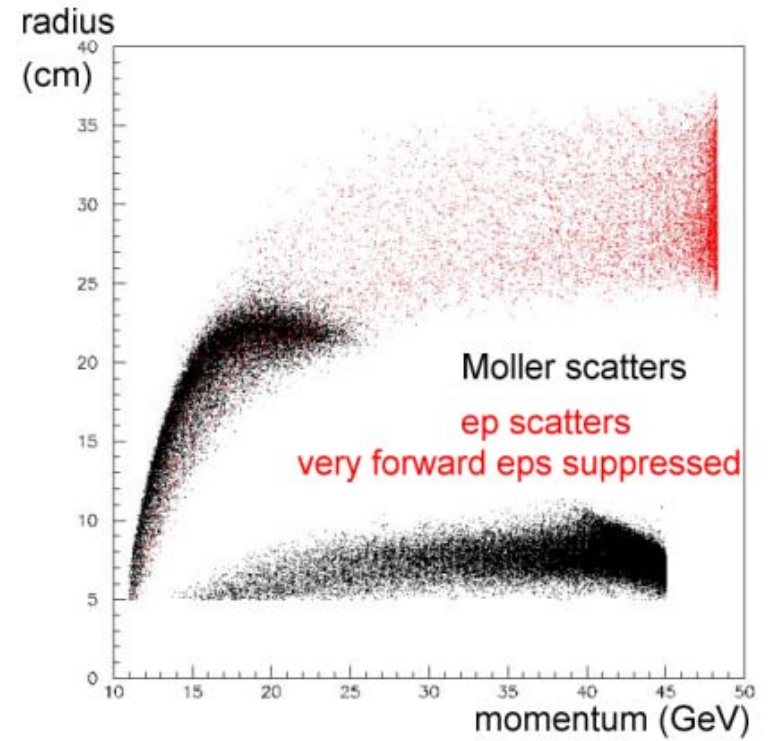
Figure 4.7: Møller and ep scatters, particle radius vs momentum at the face of the Møller detector, with the radial collimator. Some very forward angle Møller and ep scatters have been suppressed for clarity.

3QC1B actually consists of two pieces - an upstream copper collimator and a downstream tungsten collimator - which have been brazed together to create a single piece. The overall thickness of the piece is forty r.l. (roughly equally divided between tungsten and copper), again to prevent punch-through. The entire collimator is water cooled. The copper portion was placed upstream to facilitate the cooling.

The inner opening of 3QC1B is large enough to allow high energy eps and Møllers to strike the luminosity monitor without having them strike the very inner edge (or beampipe) of the Møller detector. Approximately one centimeter of clearance exists between the outer edge of this high energy flux and the inner edge of the Møller detector beam pipe, well within the tolerance of beam motions and collimator alignment. The outermost edge of QC1B was made large enough to block synchrotron radiation from striking the first quadrupole magnet[6].

4.6   Synchrotron Collimators

The inner and outer metal cylinders of QC1B must be connected by two sizable pieces of metal. These connectors, called "spokes", will collimate the physics flux, yet they perform a very useful function: collimation of the synchrotron radiation created in the chicane. Since the synchrotron light travels only in the horizontal plane, both of the 3QC1B spokes lie in the horizontal plane. Each spoke is 40 r.l. thick, which is more than enough to block synchrotron radiation, but which prevents punch-through from incident eps or Møllers from hitting the detector. The height of the spokes is a complex issue which is described below.

Figure 4.8 depicts the sources of synchrotron radiation and the phase space filled by

---

[6]This edge was also minimized as much as possible, as the cost of the piece was proportional to the square of the outer radius!

the radiation (in the horizontal plane). The spokes in 3QC1B cannot collimate all of the synchrotron radiation, since a sizable fraction of it travels through the center of the collimator. To block this background, two more sets of collimators have been placed at downstream locations. The first set is located immediately downstream of quadrupole four. These collimators are made of tungsten, water cooled, and each is twenty r.l. thick, enough to completely stop MeV photons. The inner edge of each collimator (the edge closest to the beamline) has been placed 5 mm from the high energy straightforward Møller and ep flux, enough to allow for beam motions. The second set of synchrotron collimators are bolted directly on to the detector face, and provide the final barrier for synchrotron radiation. Like the first set, these collimators are made of twenty radiation lengths of tungsten; unlike the first, these collimators require no water cooling, as they are in air, and only absorb around ten watts of synchrotron power.

For radiation protection purposes, a piece of copper connected to the water-cooled copper mask on the left side of dipole three blocks quite a substantial amount of synchrotron radiation. This radiation would not hit the detector if it were unblocked; it would hit the first quadrupole.

The height of each of the synchrotron collimators is determined by two factors. First, a Monte Carlo simulation suggests that the overall synchrotron flux should be cut down by a factor of one hundred before it strikes the Møller detector (to keep the synchrotron component of the measured asymmetry negligible). Second, none of these collimators should block any of the Møller signal flux. This requirement is impossible to fulfill for the 3QC1B spokes, which must block the Møller signal flux. Thus, the 3QC1B spokes are tall enough to provide an adequate "shadow" for the downstream synchrotron collimators, so that none of them are struck by Møllers or eps. The shadow is not perfect: the synchrotron collimator on the detector face is struck by a small number of signal Møllers. However,
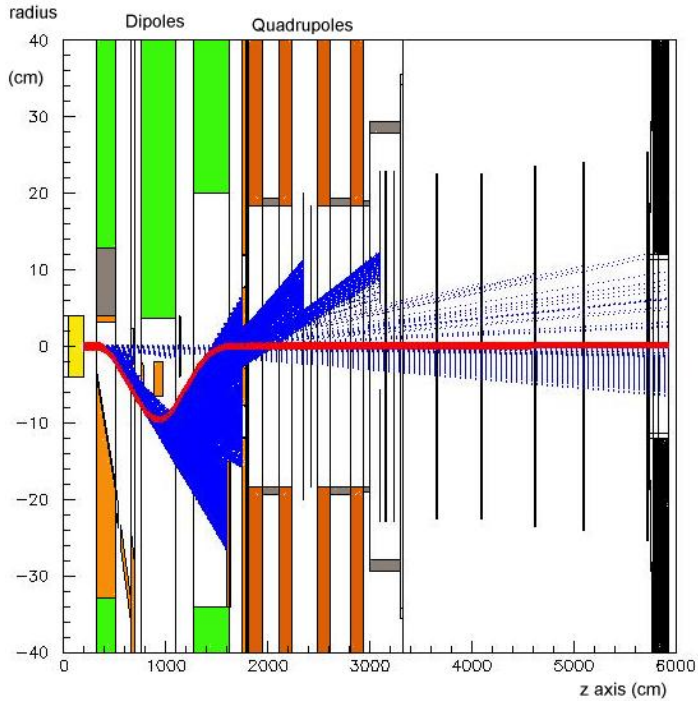
Figure 4.8: A simulation of the synchrotron backgrounds, looking up at the spectrometer from underneath. The dipoles have been colored green for clarity. The primary collimators blocking the synchrotron radiation are 3QC1B's spokes (at around 1750 cm), the spokes in the first collimator mask (to be described later; z is around 2350 cm), and the first synchrotron collimator (at around 3100 cm). The statistics are too low to show the flux which impacts the second synchrotron collimator near the Møller signal acceptance region.

as these Møllers are so close to the face of the Møller detector, there is no concern about smearing of the physics signal due to scatters from the collimator.

4.7 The "Holey" Collimator

Immediately in front of 3QC1B sits a movable collimator, 3QC1A, also called the "holey" collimator (figure 4.9). This piece is essentially a mirror image of 3QC1B, meaning it consists of two semi-circles designed to entirely cover the Møller signal acceptance region of 3QC1B[7]. On the other hand, four small holes (1 cm by 1 cm) have been cut into this collimator at various azimuthal angles and radii. These holes are all ninety degrees apart from one another[8], and they have been placed to allow a very precise measurement of the ep inelastic signal. When this collimator is inserted into the beamline, the holes create a very clean separation of the Møller and ep scatters at the detector face. Examination of the signal that falls between the two peaks will provide the best model of the ep inelastic flux in the Møller region under normal running conditions.

Two more holes have been cut into 3QC1A for the purposes of polarimetry. Measuring the beam polarimetry does not require a full azimuthal acceptance, but does require a smaller radial acceptance than afforded by 3QC1B. Therefore, these two holes are 2 cm high, 2.6 cm wide, and are centered on the vertical axis.

Since 3QC1A is only used for special studies, it has been placed on two metal tubes along which it can be inserted and retracted (via air cylinders). The motion is remotely controllable from the ESA Counting House.

---

[7] The piece would be one solid cylinder, but leaving out the horizontal plane (i.e. creating a "mirror" of the spokes) decreases the power on the piece to the point where it does not need to be water cooled.

[8] The top hole is offset 16 degrees from the vertical to the left, or counterclockwise if one is looking downstream.
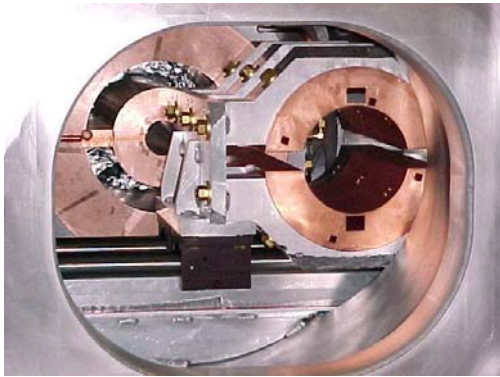
Figure 4.9: A photograph of 3QC1A and 3QC1B in their segment of beampipe.

4.8 Quadrupoles

Separating the Møller electrons from the ep background at the detector face requires the use of powerful focusing optics. Although two quadrupoles would be enough to focus the Møller signal profile, SLAC owns four incredibly uniform quadrupoles, originally used in the 8 and 20 GeV spectrometers. Each quadrupole has a field gradient that is uniform to 0.1% in the entire region where Møller electrons will travel (up to 18 cm from beam center)[26]. Using all four quadrupoles allows for a larger separation of the Møller and ep scatters at the detector face. A profile detector scan of the incident flux at the Møller detector with the quadrupoles turned off and on is given in figure 4.10. The profile detector will be described in the next chapter.

For maximal focusing, all four quadrupoles sit immediately downstream of the radial
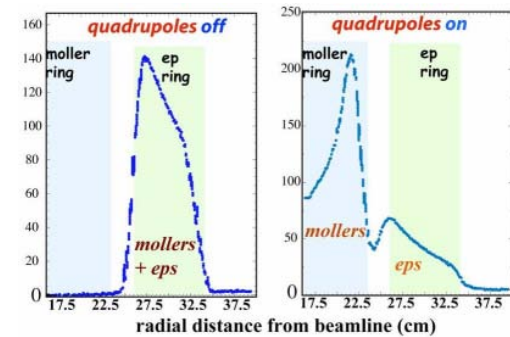
Figure 4.10: Data from the profile detector (to be described later) showing the distribution of the charged particles at the detector face with the quadrupoles turned off and on.

collimator. The position and strengths of the quadrupoles were optimized with three constraints: the distribution of the ep and Møller scatters at the detector face must remain azimuthally symmetric, they must be radially separated as far as possible, and the quadrupoles must take up as little room in z as possible. The latter constraint is imposed by the wide angle elastic ep flux, which would scatter off the inside of the fourth quadrupole were it located farther downstream[9]. After the field strengths were determined from these constraints, quadrupole four's field was altered to negate the quadrupole component of the chicane (see section 4.3.2).

Each of the quadrupoles has been placed upon precision jacks similar to those used for the dipoles. The four quadrupoles have been coaxially aligned with a precision of 5 mils,

---

[9]This flux is, in fact, incident upon the inner edge of the beam pipe in the end of quadrupole four, but the main concern would be polarized electron flux incident upon the iron poles of the magnets.

which ensures an azimuthal homogeneity of the Møller profile at the detector face with a tolerance better than one millimeter. The beam pipe passing through the quadrupoles is 1/4" thick, and is circular to within a millimeter at every angle (to prevent Møller electrons from scattering off the inner edge). Finally, like the dipoles, each quadrupole magnet is water cooled.

4.9 Beyond the Quadrupoles

4.9.1 Drift Pipe

To prevent signal degradation in air between quadrupole four and the detector face 30 meters away, a very large aluminum pipe is used to maintain a decent vacuum in the volume (figure 4.11). The synchrotron collimators downstream of quadrupole four are located in this pipe, as well as the collimator masks described below. An aluminum conical beam pipe connects this pipe with the detector beam pipe. This cone is 0.375" thick, which allows signal particles to pass through and onto the detector face without significant degradation.

4.9.2 Collimator Masks

The spectrometer as it existed for the engineering run of E158 (Feb-June, 2001) is described above. However, during that run, it was determined that a large amount of soft and hard photon background was coming from the edges of collimators, especially the inner edges of the second photon collimator and 3QC1B. Consequently, seven "collimator masks" were designed to block the line of sight between the inner edges of these collimators and the detector face (Figure 4.11).

These collimator masks consist of tungsten rings supported by horizontal tungsten
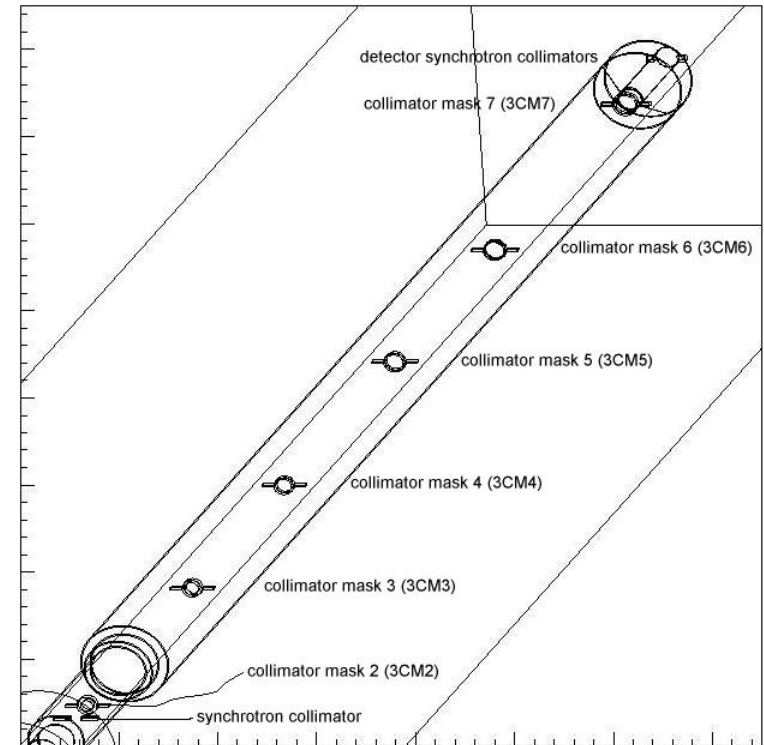
Figure 4.11: Schematic (from above and to the right) of the drift pipe, showing relative positions of the collimator masks as well as the synchrotron collimators.

bars thin enough vertically to sit in the same Møller electron "shadow" as the synchrotron collimators, yet thick enough in z to completely block any incident synchrotron radiation or collimator shower products. The inner edges of these rings obey the same constraint as that of the synchrotron spokes: namely, they should each be located at least five millimeters from the high energy Møller and ep flux. Only two of these rings, the first and the last, are water cooled, because only they receive substantial amounts of incident power[10].

The outer edges of these collimators are constrained by an imaginary line drawn between the inner (radial) edge of the Møller flux at the end of the fourth quadrupole, and the inner edge of the Møller detector. Although this line seems "safe", each piece nevertheless sees incident Møller and ep flux, since the quadrupoles over-focus a small fraction (a few percent) of the Møller electrons that pass through 3QC1B. Even so, if these particles shower off a collimator mask and into the detector, the overall detector resolution should not be affected, since fluctuations in these particles should be equivalent to fluctuations in the signal electrons.

The spokes supporting each of the collimator masks give some amount of redundant synchrotron protection. The very first collimator mask blocks quite a bit of synchrotron radiation (figure 4.8) which otherwise would have been blocked by the first synchrotron collimator. In addition, the supports for each of the other collimator masks end up blocking small amounts of synchrotron radiation that would have otherwise hit the inside of the detector beampipe.

---

[10]This power comes from synchrotron radiation.

Chapter 5

Detectors

The E158 detectors must measure a wide variety of signals, including electrons, pions, and photons whose energy ranges from 0 to 48.3 GeV. Consequently, several detectors are used for measurement of the physics signal and backgrounds. An overhead view of most of the detectors (which sit in a "cart" in the downstream end of ESA) can be seen in figure 5.1.

5.1   Møller Detector

The main detector for E158 is called the Møller detector. This detector uses quartz fibers packed between slabs of copper to measure incident particle energy flux, primarily from Møller electrons. A second detector, known as the ep detector, surrounds the Møller detector and is used to measure incident ep flux. The ep detector has the same basic design as the Møller detector; both will be discussed as a unit.

A photo of the Møller and ep detectors is shown in figure 5.2. The basic premise of the detector (figure 5.3) is simple - charged and uncharged particles hit the layers of copper in the detector and shower. The shower products which contact a quartz fiber scintillate,
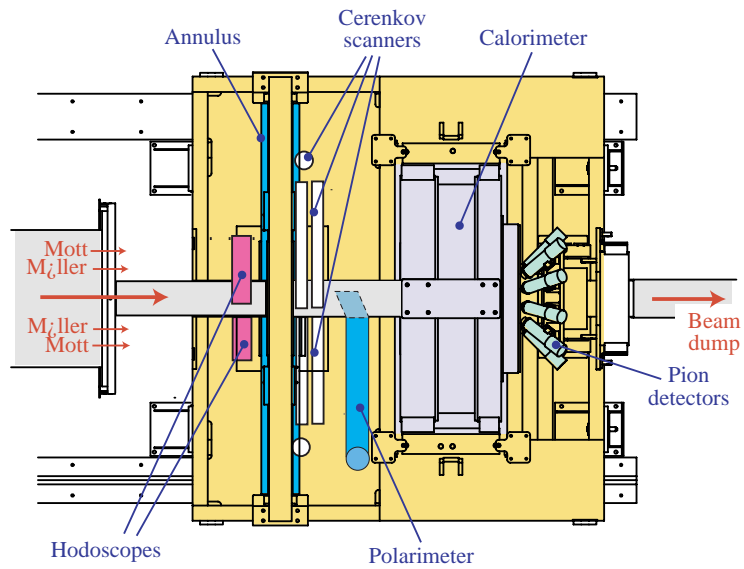
Figure 5.1: Overhead view of the Møller detector ("Calorimeter"), the pion detector, the profile detector ("Annulus" with "Cerenkov scanners") and the polarimeter.

Figure 5.2: Photo of the Møller detector during assembly. In this orientation, the beam would strike the detector from underneath. Visible are the copper slabs and the fibers, which lead upward to a point where the lightguide will be attached.

and the resulting light runs down the fiber, through a mirrored lightguide, and into a photomultiplier tube (henceforth called a PMT).
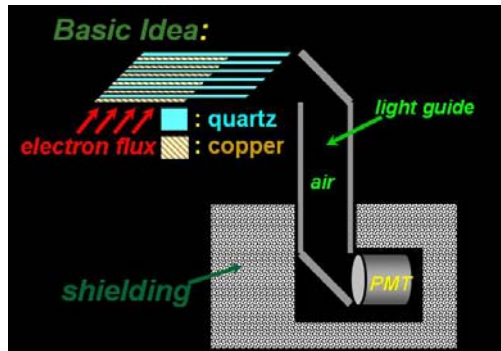
Figure 5.3: A schematic of the Møller detector.

The Møller detector should be azimuthally symmetric, and should be capable of measuring integrated flux at different radii and angles. Execution of this premise is complicated, and requires the use of a cylindrical slab geometry, which can be seen in figure 5.2 (also see [27]).

The Møller detector is approximately 15 r.l. thick, and is striated into a total of 20 azimuthal segments, each one containing three radial clusters of quartz fibers[27]. By bundling the quartz radially, the experimental asymmetry can be measured at different radii, useful for estimating contributions from radiative backgrounds. The quartz fibers are run across the copper, out the downstream side, and into bundles, which are then fed into highly reflective light guides. The ep detector is also 15 r.l. thick, and contains 10

azimuthal segments. The quartz for each segment is not radially clustered, so only one signal is read from each segment.

Once the photons have traveled through the light guides, they are detected by a Hamamatsu R2154 PMT. At the highest beam intensity, any individual PMT from the area of highest signal rate will receive up to twenty million photons per spill. This rate is high for a standard PMT, so to prevent cathode saturation (which would result in a sizable nonlinearity), a wire mesh rests on each PMT's cathode to allow charge to quickly redistribute over the cathode. Additionally, each PMT's gain is adjusted to give an output of 0.5 V off the anode, preventing anode nonlinearity. Even increasing the output by a factor of two on the bench changed the linearity by a few percentage points; thus, the PMT gain is fixed at this level.

The Møller detector is expected to receive a flux of roughly twenty million electrons per spill. From this flux, any one detector segment could receive up to one million electrons (due to the radial profile of the Møller electrons)[1]. The readout electronics for the Møller detector should therefore have a per-channel resolution better than 200 ppm (parts per million), an overall detector resolution better than 40 ppm, and should be linear to within 1%.

Initially, it was believed that the ADCs used for the BPMs and other detectors would be good enough to use for the Møller detector readout. That notion was quashed when the contribution to the resolution from pedestal noise was measured to be larger than 100 ppm, which is good enough for the BPMs, but not good enough (assuming all pedestal noise is common mode) for the Møller detector. The poor noise performance is due to fast noise in the MHz bandwidth originating on the ADC itself. Consequently, shifting the

---

[1] Each electron contributes approximately 10-25 photoelectrons, resulting in the number of photons given above.

phototube pulse from the MHz bandwidth into a lower frequency range to provide better S/N (the ratio of the signal to the noise) would be quite useful. Amplification of the 0.5 V phototube signals somewhere close to the Møller detector also seems desirable in order to avoid S/N degradation from losses along the cable run (200 ft into the integrating ADCs).

5.1.1 Møller Detector Electronics

The concept for the Møller detector electronics (also used for the ep detector) was devised when the initial electronics chain was being conceived. All of the Møller and ep detectors' PMTs' HV (high voltage) grounds are connected in a building called the electronics hut[2], approximately 200 ft from ESA. Since the HV ground and the signal ground are the same within each PMT, isolation transformers are connected to every single PMT's signal output to prevent massive ground loops. These transformers, if given enough windings, are nearly identical to the beam toroids![28] By adding a capacitor and a resistor to the transformer, the tube output is transformed into a ringing signal. This allows the toroid electronics to be adapted for use in the Møller detector electronics.

A diagram of the Møller detector electronics chain is given in figure 5.4. Initially, any PMT's output is run across a low-pass filter. This filter both prevents reflections and slows the pulse down, allowing it to deposit all of its energy in the isolation transformer, creating a large ringing signal[3]. After the filter, the pulse runs down a 40 foot cable and into the isolation transformer/RLC circuit. Once the ringing signal has been created, it is amplified in two successive gain stages (a 1/2/4/8 and a 10/100). The gain is remotely selectable; during the run, gains of 1 and 100 gave the best resolution overall. The RLC

---

[2]This building contains the ADC readout electronics from the Møller detector, the luminosity monitor, the pion detector, and the profile monitor, as well as the Møller detector electronics gain control module, and the HV supplies for the Møller detector and luminosity monitor.

[3]A faster pulse tends to travel "through" the transformer without depositing much energy, causing havoc when it hits the next stage of the electronics.
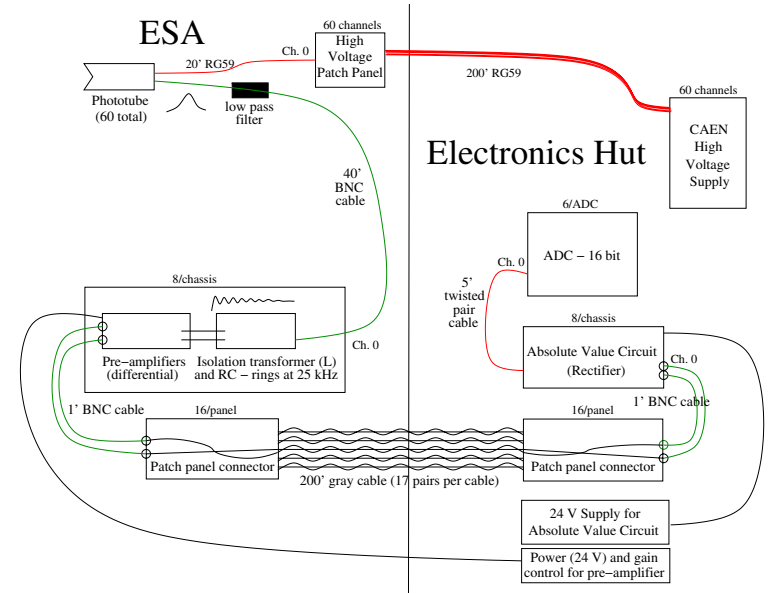
Figure 5.4: Diagram of the Møller detector electronics layout.

circuit and the amplifiers which follow are all located in a single chassis known as the "preamplifier" chassis; each chassis contains eight Møller detector channels. The overall circuit has been designed to make the ringing signal differential, giving a "free" factor of two in gain while further isolating the chances of noise from ground loops.

After the signal has been amplified, it travels down approximately 200 feet of twisted pair cable (to prevent crosstalk) and into an "absolute value" circuit (a rectifier) similar to the one used by the toroids. Again, eight such circuits are located a single chassis. Once the signal has been rectified, it is run into an ADC identical to the one used for the toroids (described in section 6.1).

The overall linearity of the Møller detector electronics (including the PMTs) was measured on the bench and in situ during the run; a conservative estimate places the linearity (with the entire electronics chain) at $99 \pm 1.1\%$.[17] However, at one percent of the input signal, the linearity of the circuit sits at 80% or worse. The reason for this nonlinearity is twofold: the isolation transformer has an iron core, which requires some threshold signal before it acts as a "pure" inductor. Small signals don't induce all of their energy into the ringing signal, producing a smaller output than expected. Furthermore, the rectifier's diodes are typical in that they tend to distort small voltages, further reducing linearity at the low-end.

To determine the resolution of the Møller detector electronics, the beam was run at several different current settings. The square of the width of the experimental asymmetry for each setting was then plotted against 1/N (N is the number of electrons per spill). A fit to this data will produce an offset which should be the square of the detector resolution. Figure 5.5 shows the results of the scan. Taking the offset from the graph, the detector resolution is $\sqrt{12060} = 110$ ppm. The width of the Moller detector asymmetry is typically around 190-200 ppm, so the detector electronics' contribution to this width is

non-negligible. Possible causes of the 110 ppm resolution include noise from the amplifiers in the first stage of the Møller detector electronics, as well as pedestal noise. Studies of this noise are ongoing.
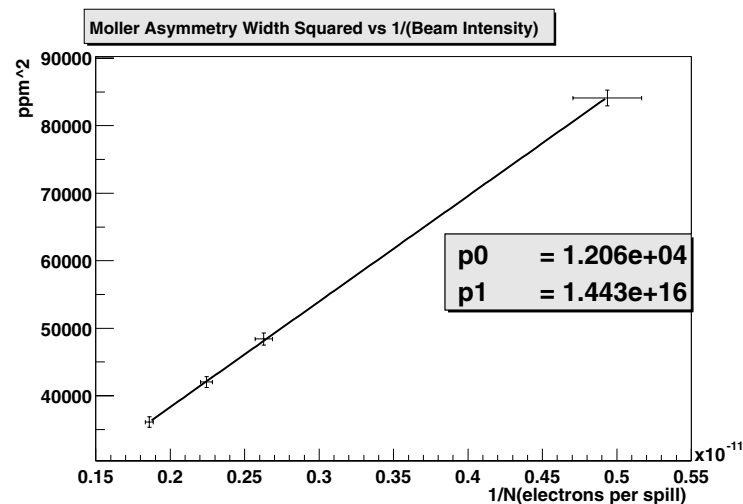
Figure 5.5: A plot of $\sigma^2_{M\o ller}$ vs 1/(beam intensity) for different beam intensities. The Møller detector resolution is $\sqrt{p0} = 110$ ppm.

5.2 Pion Detector

Immediately in back of the Møller detector sits the pion detector. This detector consists of ten Philips XP2232B PMTs, each of which receives Cerenkov light from an adjoining

quartz block.[29] The ten phototubes are equally spaced azimuthally around the beam pipe; each phototube/quartz assembly is placed at 45 degrees from the r and z axes (figure 5.6), and mounted to the main detector cart via an aluminum brace. This detector is sensitive to flux from electron and photon "backgrounds" (such as the Møller electrons). Nevertheless, the Møller detector copper and lead does an adequate job of shielding the pion detector from extraneous flux. Since the pion detector signals are expected to fluctuate on the order of 0.1%, the electronics for the detector are simple - each PMT signal is run down a BNC cable to the electronics hut and directly into a PMT ADC similar to those used for the BPMs (described in section 6.1). The resolution of the ADC is adequate for such a measurement.
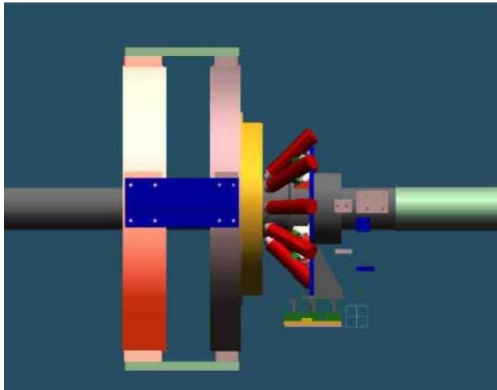
Figure 5.6: Schematic of the Møller and pion detectors. The pion PMTs are in red. The detector cart (upon which both detectors sit) is not pictured.

5.3 Profile Detector

Immediately in front of the Møller detector sits the profile detector. This detector consists of four quartz Cerenkov counters mounted on a large wheel capable of rotating 180 degrees (figure 5.7). Each counter consists of a piece of quartz, a lightguide, and a PMT to detect Cerenkov radiation. The counters are each mounted on an "arm" capable of moving the assembly radially inward (to 15 cm, the closest it can be to the beamline without striking the beampipe) and outward (to 55 cm, so that it doesn't block the Møller flux during normal running). The motion of the wheel and of each counter is controllable via LABVIEW software; the detector is primarily used to scan the profile of the Møller and ep flux.
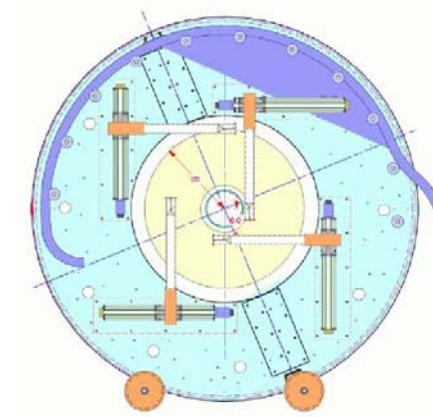
Figure 5.7: Rough schematic of the profile detector wheel, showing all four Cerenkov counters sitting on their movable drives.

Large amounts of soft background (photonic and charged) are present around the wheel[4]. Normal PMTs would be swamped by this radiation, so two of the counter assemblies contain features designed to minimize this background (figure 5.8). First, an insertable/removable tungsten preradiator can be placed in front of the quartz, blocking low momentum particles and giving high momentum particles a chance to shower before hitting the quartz. Furthermore, an insertable/removable shutter in the counter assembly can block all photons from the quartz, allowing a clean measurement of the signal originating within the PMT (since the PMT shielding doesn't entirely prevent particles from striking the tube). Both additions allow the profile detector to make a very accurate measurement of the Møller and ep flux. The preradiator and the shutter are both remotely controllable from the ESA counting house, allowing near-fully automatic scans of the signal profile. Each tube in the profile detector has its signal run outward on a BNC cable, down 200 feet to the electronics hut, and into a CAMAC 2219W 11 bit ADC.
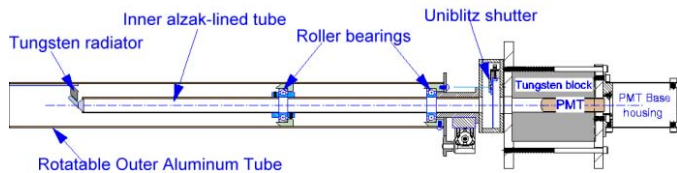
Figure 5.8: Diagram of a single Cerenkov counter.

---

[4]This background originates from the drift pipe and from the aluminum cone in front of the detector, both of which are hit by energetic electrons.

5.4 Polarimeter

To measure the polarization of the beam, E158 scatters the polarized electron beam off a longitudinally polarized supermendur iron foil target (described in the target section). The right-left asymmetry of Møller scatters from this foil is given by

$$A_{polarization} = P_z^{beam} \times P_z^{target} \times \frac{(7 + \cos^2 \theta_{CM}) \sin^2 \theta_{CM}}{(3 + \cos^2 \theta_{CM})^2}, \tag{5.1}$$

where P_z^{beam} is the longitudinal beam polarization, P_z^{target} is the longitudinal polarization of the iron foil electrons, and θ_{CM} is the center of mass scattering angle.[30] With typical values of $\theta_{CM} = 90°$ (to maximize the asymmetry), a beam polarization of around 80%, and a foil polarization of around 8%, the expected asymmetry is around 0.05. A very accurate measurement of the polarization is desirable, because the measured asymmetry is directly proportional to the polarization ($A_{PV}^{measured} = P_z^{beam} \times A_{PV}$), so the statistical error on A_{PV} from polarization is the fractional error on the beam polarization measurement.

To make the polarization measurement, a different setting is used for the spectrometer quadrupoles, and the holey collimator is inserted into the beamline. Both changes help separate the Møller scatters from the ep background. Statistics aren't a concern for the polarization measurement (the measurement typically takes 1/2 hour), so only the Møller flux that passes through the bottom hole of the holey collimator is used.

The detector used for polarimetry (the "polarimeter") sits between the profile detector and the Møller detector (figure 5.9). The polarimeter is a Cerenkov calorimeter made of alternating pieces of tungsten (7) and quartz (6) (the first two pieces particles encounter are both tungsten).[31] Each plate is tilted at a 30 degree angle from the vertical, and the sizes of the pieces have been optimized to measure Møller scatters which pass through the lower hole in 3QC1A while minimizing backgrounds (mainly ep scatters). The tungsten

plates contain reflective surfaces designed to maximize light collection. Light from the quartz is fed into a highly reflective light guide. The light runs horizontally through the guide, gets reflected off a mirror, and then travels vertically to the PMT. The mirror can be rotated to block all light from the tungsten/quartz assembly so that the amount of background directly hitting the PMT can be estimated. The light is detected by a a Hamamatsu R2154-02 PMT; the output from the PMT is run over 200' of BNC cable (into the electronics hut) and into a CAMAC 2219W 11 bit ADC. The entire lightguide/PMT assembly is shielded behind six inches of lead.

Since polarimetry uses the same spectrometer as physics running, the entire polarimeter assembly must be remotely insertable/removable. A small, remotely-controllable motor can lift (or drop) the entire assembly to 18 cm (from the beamline) during polarimetry, and out to 50 cm during physics analysis. The lead shielding is stationary and does not interfere with physics running.

5.5   Luminosity Monitor

The final detector used in the experiment is a luminosity monitor, sitting approximately seven meters downstream of the Møller detector. This monitor detects extremely forward-angle Møller and ep scatters with two goals in mind. First, no asymmetry is expected in the very forward-scattered Møller and Mott electrons, so the luminosity monitor should measure a null asymmetry (after having been normalized by the toroid charge), verifying the lack of a systematic asymmetry in the physics result. Second, this monitor can be used to measure the effect of target density fluctuations on the physics result, as such fluctuations would create a correlation between the Møller detector asymmetry and the luminosity monitor asymmetry.
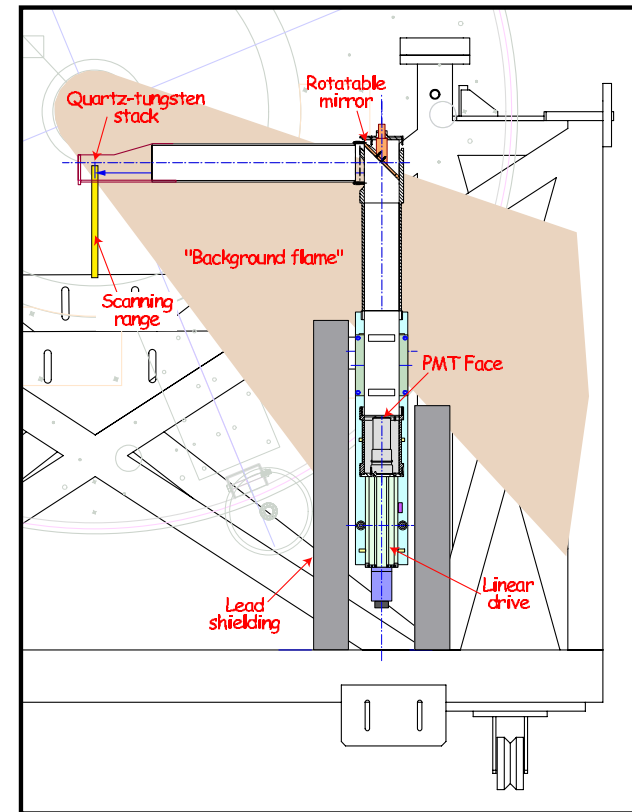
Figure 5.9: A diagram of the polarimeter. The lead shielding in front of the polarimeter is not visible.

The luminosity monitor consists of two separate detectors, each an aluminum "ring" extending 7 to 10 cm from the beam axis.[32] Each "ring" is made up of eight octants, each one a gas chamber proportional ion counter. Every chamber contains eleven parallel aluminum plates, alternately kept at either 100 or 0 V in order to maximize signal amplification without causing extraneous arcing in the chamber. Additionally, every chamber is filled with nitrogen to assure optimal operation (oxygen tends to prevent ionization, damping the observed signal). In front of each detector ring sits a ring of aluminum, used both as a preradiator and as a shield against synchrotron radiation. The two detectors are located only a few inches upstream/downstream from one another, giving a level of redundancy to the measurement.

Signals are read from the luminosity monitor plates in differential mode (on two separate BNC cables per octant) to avoid ground loops and other noise issues. From each detector, the signals are run over 200 feet of Foam 8 BNC cables into the electronics hut, where they are fed directly into an ADC similar to the standard BPM ADCs. Approximately one hundred million particles strike the luminosity monitor during every spill, so the requirements on its electronics are very tight - they should have no more than 20 ppm of common mode noise. In practice, the luminosity electronics contribute roughly 80 to 90 ppm of common mode noise.[33]

5.6   Good and Bad Spill monitors

Two ion chambers, one upstream of the target by a few meters and one located downstream of the target by a foot, are measured to determine the approximate level of backgrounds originating from the accelerator. These ion chambers are respectively known as the bad and good spill monitors. Both ion chambers are several inches away from the beamline,

outside the beam pipe, and are not consequential to spectrometer operation. The good spill monitor measures wide-angle scattered flux from the target, whereas the bad spill monitor provides a rough measure of the amount of beam halo particles. This halo could be quite problematic, as the spectrometer acceptance is very open to scatters from upstream in the accelerator. Consequently, the bad spill monitor is used to tune the accelerator in such a way as to minimize the beam halo. Each spill monitor's signal is run up around 100' of BNC cable into the ESA counting house, where it is split and run into both an oscilloscope and into a CAMAC 2219W 11 bit ADC.

Chapter 6

Data Acquisition System

In this chapter, the system of electronics for measuring and recording signals for all detectors will be described. First, the E158 analog-to-digital converters (ADCs) will be described in detail, as these modules measure the signals from almost all detectors and monitors, including the Møller detector. After other components of the hardware have been described, the geometric and electronic layout of the hardware will be given. Finally, the online and offline data-collection and monitoring software will be summarized.

6.1 ADCs

The ADCs used for most of the detectors are SLAC custom-built 16 bit VME ADCs, with six channels per board[34]. The channels can be run in either single-ended or differential mode: differential mode halves the maximum possible input signal, but allows for integration of positive and negative signals. Each channel contains a gain stage, an integrator, and a digital sampling chip. The integrator gain, the timing of the integration, and several other parameters described below are all remotely programmable (through the

VME backplane). Each ADC receives its triggers from a master board[1][35], which in turn receives triggers from the main data acquisition system.
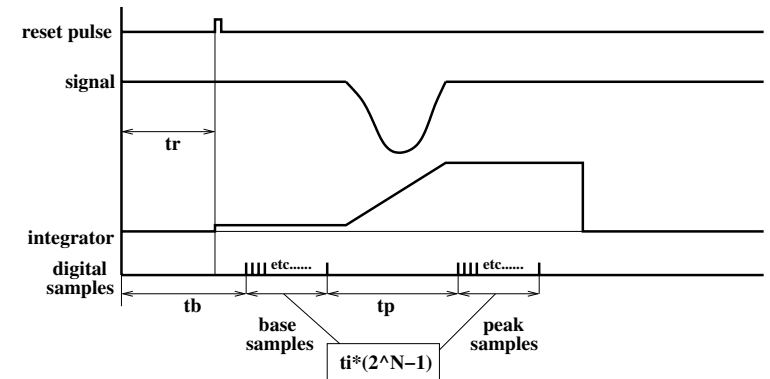
Figure 6.1: Pictorial view of the timing on an ADC channel.

Measurement of the integrated signal happens in several steps.[34] The timing of each step can be remotely set via the VME backplane. For reference, a diagram of every typical step in a signal integration is given in figure 6.1. Initially, all ADC boards in one VME crate receive a trigger signal from the master board in that VME crate. For any individual ADC, some period of time (in roughly integral numbers of μs^2) later, called t_r, the integrator opens (via a relay); prior to this, it has been shorted (so that the initial charge on the integrator should be zero). The process of opening the relay induces a small

---

[1]The master boards will not be described in this document, save that they allow each VME crate to couple to others solely through fiber optics, preventing ground loops over copper wires.

[2]The master board sends a timing signal to clock everything on each ADC board; this clock is quantized at around the 1.1 μs level - the exact value depends on the clock being used to drive the master board.

amount of charge onto the integrator; this is depicted in the diagram. Another period of time after the initial trigger, called t_b (which does not have to occur after t_r), the ADC on the board begins measuring (sampling) the current integrator value. This value can be measured once, or up to sixteen times (the number must be a power of two). The individual measurements, called "baseline samples", occur on the picosecond timescale, though each successive sample must (due to the internal clock) occur at nearly integral units of μs after the prior measurement. The space between any two samples can be set via the parameter t_i (which determines the number of "μs"); for practical reasons, t_i is almost always set to one. The timing should be set so that the signal pulse enters the integrator a few μs after the last of the baseline samples has been taken. Once the signal has been integrated, at some time t_p after the last baseline sample, the ADC chip takes as many measurements (called "peak samples") of the integrator as it took for the baseline measurement. The peak samples are taken in an identical fashion as the baseline samples. The board then takes the average of all peak samples, the average of all baseline samples, and stores the difference in an I/O buffer, readable through the VME back plane.

The same ADC design is used for BPM ADCs, pion detector ADCs, luminosity monitor ADCs, and toroid/Møller detector ADCs. The differences between these boards are few; for instance, different boards have different integration capacitors (to deal with the difference between the one millisecond long toroid signal and the 250 nanosecond BPM or luminosity monitor signals). Each type of board has a different gain on its initial amplification stage, as well. Finally, to optimize resolution (due to a problem with fast noise on the ADC), the toroid/Møller detector ADC boards are typically set to take sixteen baseline and peak samples, while the PMT, BPM, and luminosity monitor ADC boards (with a 2-4 μs integration gate) are typically set to use four samples.

6.2 Polarization Information

As was mentioned in section 3.1.1, a CAMAC module located at the laser source (called PMON) controls the helicity sequence of the beam.[36] This module has a few possible operating modes, including all left pulses, all right pulses, a toggle state (LRLRLR...), and E158's pseudo-random helicity sequence. This module sends polarization information to the rest of the experiment. To prevent signals from this module from creating artificial helicity correlations in the rest of the experiment's electronics, the helicity information for each pulse is delayed by one pulse before being sent to the data acquisition system.

PMON receiver modules exist in two areas: ASSET and the counting house. The source PMON module transmits polarization information through SLAC's SLCNET (an RF network used to transmit accelerator machine instructions).[36] The ASSET PMON receiver is located in (and read out through) a VME crate. The counting house contains two PMON receivers, one located in a CAMAC crate, and one located in a VME crate.

6.3 Feedback

As was explained in the beam analysis, preventing large beam asymmetries is necessary for making the E158 physics measurement. Consequently, beam asymmetries must be nullified as much as possible using a realtime feedback on appropriate beam monitors. For feedback purposes, E158 can nullify the asymmetry measured at either the beam monitors at ASSET or the monitors immediately upstream of the hydrogen target. Higher order effects in the accelerator can make feeding back on downstream monitor asymmetries impossible, as the relation between those asymmetries and source asymmetries may be highly nonlinear. Consequently, the feedback for most of Run I was set up to nullify the charge and position asymmetries from the ASSET beam monitors.

All optics used to make the asymmetry feedbacks are located at the source (described in section 3.1). Although an ideal feedback system could remove all measured beam asymmetries, it is not possible for the source optics to remove any beam energy asymmetry. However, the beam energy asymmetry is mostly proportional to the beam charge asymmetry, so the charge feedback should take care of the energy asymmetry.

The realtime software that implements the feedback is known as FbAnal, and it keeps track of every beam pulse that is used for feedback. Since the data acquisition systems at ASSET and in ESA (both the counting house and electronics hut systems) are independently triggered and independently recorded, FbAnal must synchronize both data streams in realtime, perform cuts on the data set to determine which spills to use for feedback, and then send signals through the data acquisition system up to the source (and into the tape logging system for recording) to change the voltages on the source Pockels cells or piezomirror.

The results of the feedback are very evident from the beam asymmetries given in table 3.2. However, these asymmetries are not what would be expected with perfect 1/N scaling, as a good feedback should give. There are several reasons for this discrepancy. First, as was just mentioned, the effects of the accelerator on the beam asymmetry are complicated, so small beam asymmetries in the ASSET region might be magnified by the time the beam reaches ESA. Second, the data cuts FbAnal used during Run I did not include all of the cuts used in the physics analysis, so the perfect scaling was suppressed by the altered set of events. Finally, FbAnal weighted each event equally for feedback purposes. However, the analysis weighs the results of runs by the error on the experimental asymmetry. Consequently, the overall value of the beam asymmetry will shift by a non-negligible amount. Even with all of these discrepancies, the feedback succeeded in reducing the beam asymmetries to acceptable levels.

6.4 Data Acquisition

The data acquisition system is run at 120 Hz, and collects approximately 2 kB per spill. An overall flowchart of the entire system is complicated; the picture described here will be rather simple.

The data acquisition system consists of several distinct geographical locations. The central area, the ESA counting house, contains VME crates which receive data from the downstream BPMs, toroids, and the synchrotron light monitors. The wire array signals are run into CAMAC ADCs here, and so are the good and bad spill monitors' signals. The dithering recognition pulses are also sent here into a VSAM (essentially a very slow ADC, good for slow monitoring of signals). Both of the PMON receivers described in section 6.2 are located here. Finally, an I/O module is used to determine beam trigger identification bits, such as "no beam" (pedestal) or "witness" (a BaBar pulse). The counting house also contains computers which serve as the hubs for incoming data from all other areas. The overall network will be described in the next section.

Outside ESA on the detector end sits the electronics hut (which is also known as Building 420), in which signals from the Møller, ep, pion, and luminosity detectors are read into VME ADCs. Signals from the polarimeter and the profile monitors are also sent here, into CAMAC ADCs.

At the upstream end of the detector, the CID area contains a VSAM (in a VME crate) which both monitors and sends voltages to the source Pockels cells and piezomirror. An I/O module in this crate also reads beam trigger identification bits and the state of the source halfwave plate and asymmetry inverter. CID also contains the master PMON controller.

A short distance downstream of the source is the ASSET area, which contains VME

ADCs for the ASSET BPMs and toroids. ASSET also contains a VME PMON receiver. Finally, ASSET also contains an I/O module used to read beam trigger identification bits.

Triggers are generated in SLAC's electronics, and are sent to two different locations. At ASSET, triggers are read into NIM electronics, and doled out to both the main VME crate and the toroid electronics (for damping purposes). In the ESA counting house, a second trigger is also run into several sets of NIM electronics and used by many modules, such as the main VME crate, the CAMAC ADCs (for gate purposes), the toroid electronics, etc.

6.4.1 Data collection

The overall data collection system can be viewed (to first order) as a linear chain of various modules. In the ESA counting house, the main VME crate contains a module which collects all data from the ESA counting house and the electronics hut and streams the data (via a program called LDATSERV) to the central processing computer, ESASUN1. This VME crate is connected to all other VME crates in the ESA counting house and the electronics hut via fiber optic connections[3], which eliminate sources of noise and pickup such as ground loops. Through these connections, all VME modules (ADCs, VSAMs, etc.) can be read out of one virtual VME backplane. All CAMAC modules are read through VME CAMAC interface modules. These modules exist in crates in the ESA counting house and the electronics hut.

Meanwhile, a similar chain exists in the front end of the accelerator. The main VME module is located in a crate at ASSET, and receives data both from ASSET and CID VME modules. Since the amount of data collected in this system is small (less than one kilobyte per spill) and since packet loss over SLAC's ethernet is a possibility, the data are

---

[3]Two different types of modules can act as fiber optic "extender" boards: a commercial module, and the "master" ADC controller.

bunched up in groups of 30 spills and sent over ethernet to ESASUN1.

A "slow" monitoring system also exists to record such items as spectrometer magnet currents, accelerator magnet settings, and profile detectors' angles and radii (this list is by no means complete). This system, a hodgepodge of various modules and systems, collects bunches of data at varying rates and sends them all to ESASUN1.

Data storage to tape is controlled by a program known as DAQCntrl, which is also used to start and stop runs. All the data are backed up in mstore, a tape system located in SLAC's computing center. For reference, the entire spring dataset is approximately 450 Gb. To copy the data to mstore, DAQCntrl communicates with ESASUN1 via ethernet and simple communications protocols. All the data collected on ESASUN1 are stored on its hard drive until they are confirmed as having been written to mstore. ESASUN1 can store roughly a day's worth of data. ESASUN1 also feeds data (through a process called NETSERV) to another computer, ESACON1, so online analyses can read most of the data without disturbing data flow to tape or to FbAnal. As FbAnal needs to receive 100% of the data, it cannot afford to compete with online monitoring processes to receive data. Therefore, FbAnal connects directly to ESASUN1 in order to receive data.

6.4.2 Online monitoring

Several of the experiment's detectors are monitored in realtime on stripcharts and in various other formats. The realtime monitoring analyses connect to ESACON1 to receive data, and use ROOT[4] macros to plot the data. A realtime alarm system also exists for ROOT, though DAQCntrl contains almost all the alarms necessary to assure smooth running.

For typical running, a few charts are continuously monitored. One ROOT macro plots

---

[4]ROOT is CERNLIB's data analysis software package.

all Møller detector and luminosity monitor channels, so that quick action can be taken if a detector PMT dies. A second ROOT macro plots all ESA BPM and toroid signals on stripcharts, which update once per second. This stripchart, although it plots only a small fraction of the actual data, is invaluable for maintaining proper beam position through the spectrometer. A third process monitors the output of the wire array, both as a check on the BPM readout and as a spot size monitor.

6.4.3   Data Processing

The data are stored to tape in a similar condensed format as was used in previous SLAC ESA experiments (such as E154 and E155). For data analysis, a program called "anal" is used to decode the condensed format. "anal" has been wrapped in a larger piece of code, known collectively as "the framework". This code runs through the data several times for processing. In the first pass, the ASSET and ESA data streams are synchronized and merged into a single data stream. Events failing synchronization are cut from the physics analysis. In the next data pass, pedestals are calculated for all channels. The details of this pedestal subtraction, as well as all of the following steps, are described in the next chapter. In the third pass, the pedestal-subtracted data are written to a ROOT tree. Dithering slopes are also determined in this pass. In the fourth pass, regression slopes are calculated and asymmetries for all channels pertinent to physics analysis are written to a second tree. This pass also contains zeroth-order analysis, such as the calculation of a covariance matrix for the Møller detector, and the calculation of weights for the physics analysis (to be described in section 7.4, below).

Once all of these passes have been completed, analysis of the physics data can begin.

Chapter 7

Analysis

For the spring 2002 run, E158 collected over 250M spills, corresponding to around 450 Gb of data. To extract the physics asymmetry from this data, corrections must be made to the experimental asymmetry for random fluctuations that inflate the size of the statistical error bar and for beam helicity correlations that shift the value of the asymmetry. Contributions from parity-violating backgrounds must also be measured and then subtracted from the experimental asymmetry. Finally, the appropriate normalization factors from the beam polarization and dilution factors from various backgrounds must be applied to the measured asymmetry.

7.1   Raw Channel Asymmetry

The Møller detector data consists of ADC counts from 50 detector channels, each with its own relative gain and noise properties. Before any detector channel asymmetries can be calculated, every channel (monitor and detector) in the experiment must undergo pedestal subtraction. To calculate pedestals for every channel, a first pass is made through the data

which keeps a running average of every ten pedestals in each timeslot[1] for each channel. Ten pedestals are used to keep pedestal noise down to acceptable levels. Once this pass is finished, a second pass is made which takes each channel and subtracts the averaged pedestal calculated for that event. All asymmetries are also calculated in this second pass.

To find the asymmetry of any one tube, we could take its pedestal-subtracted signal, S_i, and form the tube asymmetry[2]

$$A_i = \frac{S_{iR} - S_{iL}}{S_{iR} + S_{iL}}. \tag{7.1}$$

From the formula, it is clear that the tube asymmetry is not affected by the tube's gain, so the relative gains between different detector channels do not matter[3].

Although tube asymmetries are independent of tube gains, they depend very strongly on charge fluctuations. Charge asymmetry dominates the channel asymmetry, so the very first correction to the raw asymmetry must account for charge. This correction can be made in either of two fashions. First, since the individual tube signals are proportional to the beam charge ($S_i \propto Q$), the tube signal can be normalized by the beam charge before the asymmetry is calculated:

$$A_i = \frac{\frac{S_{iR}}{Q_R} - \frac{S_{iL}}{Q_L}}{\frac{S_{iR}}{Q_R} + \frac{S_{iL}}{Q_L}}. \tag{7.2}$$

On the other hand, it is possible to take the tube asymmetry, A_i, and find its correlation to the charge asymmetry, $(m_Q)_i$. If this is done, the contribution from the charge asymmetry

---

[1] Timeslot refers to the phase on the 60 Hz waveform where the 120 Hz signal arrives. Since $120/60 = 2$, there are two different timeslots.

[2] "i" will henceforth refer to any individual detector channel; later, tensor notation will be used to take sums over channels and events.

[3] This is not entirely true: detector gains affect channel linearity, but this effect is negligible for the range of gains in which the PMTs were typically run.

---

can then be subtracted:

$$A_i' = A_i - (m_Q)_i \cdot A_Q \tag{7.3}$$

In practice, both the normalization and the correlation removal are used, but the correlation removal is only needed for PMTs which detect electrons on the outer (radial) edge of the Møller signal distribution.

7.2 Beam effects

For now, assume that the individual tube asymmetry is given as formula 7.2. A representative histogram of this asymmetry for one run for channel mid04 (the fifth PMT in the middle ring of the Møller detector) is shown in figure 7.1. Each PMT in the middle ring detects roughly 10^7 electrons per spill (at an incident luminosity of $5 \cdot 10^{11}$ electrons). Statistics noise should therefore be at a level of $\frac{1}{\sqrt{10^7}} = 3 \cdot 10^{-4}$. Why is this distribution so wide?

The statistical width of a single PMT's asymmetry is so small that correlations between tube asymmetries and beam parameter asymmetries can both induce large deviations in the value of and greatly increase the width of the PMT's asymmetry. For instance, a plot of one PMT's asymmetry against a sample beam monitor's "asymmetry"[4] (figure 7.2) shows large correlations.

Since monitor asymmetries can significantly affect detector channel asymmetries, methods must be devised to account for and remove the correlations between the two. The two

---

[4] The reason asymmetry is in quotes above is because BPMs are measured with a bipolar ADC, and typically put out very small signals (zero counts corresponds to the center of the monitor). As a result, taking an asymmetry of the monitor output would be misleading, as the denominator might be arbitrarily small. For the analysis, we instead choose to measure the difference in position, $BPM_R - BPM_L$, between right and left helicity states. For the rest of this discussion, BPM differences will be referred to as asymmetries for simplicity.
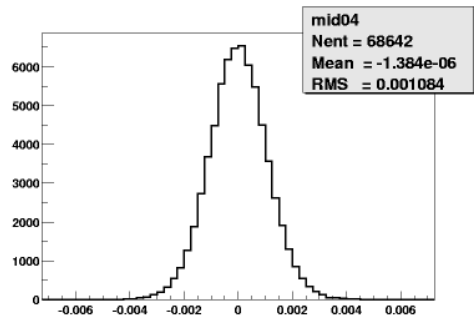
Figure 7.1: A_{PV} for mid04, run 5606.

methods used for the analysis are known as regression and dithering. The regression will be used to compute the physics asymmetry. The dithering serves as a cross-check, and will be described in appendix A.

7.3 Regression

Regression, as its name would suggest, removes detector dependence on beam asymmetries by subtracting a linear component of all monitor asymmetries from each detector PMT's asymmetry. To do this, each PMT's asymmetry is plotted against all pertinent monitor asymmetries at once (multi-dimensionally), and a single linear fit is made to the data. The beam jitter must be small for the regression to produce an accurate fit, as large jitter would create a wide distribution, obscuring the correlations between PMT asymmetries and beam asymmetries. As the slopes obtained from regression can change over time,
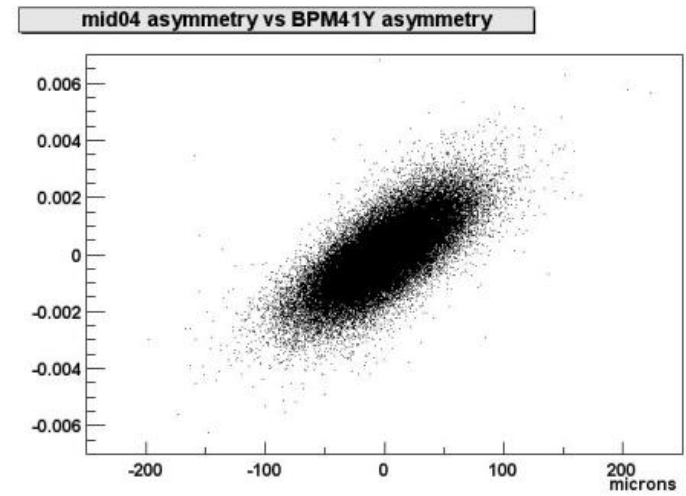
Figure 7.2: A_{PV} for mid04 vs A_{PV} for BPM41Y, run 5606.

slopes are calculated for approximately every ten thousand events (called a regression cycle)[5]. Using around ten thousand points tends to minimize any statistical errors in the fitting. The resulting slope for any one beam monitor describes the relative correlation between the PMT asymmetry and that monitor asymmetry. From all the slopes, one can obtain the regressed tube asymmetry,

$$A_i^{regressed} = A_i - m_{ij}b^j, \tag{7.4}$$

where m_{ij} is the regression slope for PMT i and beam monitor j, and b^j is the monitor asymmetry.

Before the multidimensional fit is taken, a set of beam monitors should be selected so that each one measures a mostly orthogonal beam parameter. The reasoning behind this is straightforward: regressing against two redundant beam monitors would produce semi-arbitrary slopes for each one. In the case that one monitor, even if less sensitive to the beam parameter, has a narrower signal, the regression would account for monitor noise rather than actual beam fluctuations. Furthermore, if two monitors were equally sensitive (and/or equally noisy), the slopes would vary from regression cycle to regression cycle. Of course, if two monitors work equally well and measure exactly the same parameter, their average (assuming they are calibrated to one another) should be used. The set of independent (sums of) monitors used for the regression is given in table 7.1.

---

[5]The exact algorithm used was to take every 10000 pairs, and to split the data up by timeslot. This results in roughly 10000 events falling in each timeslot.

Parameter	description	Monitor(s)
Q	charge	toroid 0 + toroid 1
E	energy	BPM24X
X	X position at target	BPM41X + BPM42X
Y	Y position at target	BPM41Y + BPM42Y
dX	X angle at target	$\frac{(BPM31X+BPM32X)-(BPM41X+BPM42X)}{40}$
dY	Y angle at target	$\frac{(BPM31Y+BPM32Y)-(BPM41Y+BPM42Y)}{40}$

Table 7.1: List of monitors used for the regression analysis.

7.4 Weights

Now that the formula for the beam-helicity corrected channel asymmetries has been determined, the overall detector asymmetry must be calculated. This simplest formula for the total asymmetry is the sum of the asymmetries of every channel:

$$A_{detector} = \sum_{i=0}^{49} A_i = A_i^i. \tag{7.5}$$

This formula is somewhat naive, though, as different tubes detect different numbers of incident particles. To account for statistical variations, individual channels can be weighted by their overall width, σ_i (calculated on a per-run basis), to give the detector asymmetry:

$$w_i = \frac{1}{\sigma_i^2} \tag{7.6}$$

$$A_{detector} = \frac{A_i w^i}{w_i^i}.^6 \tag{7.7}$$

---

[6]This is standard tensor notation; sums over the numerator and denominator are taken separately.

The differences between the two formulae are significant: equation 7.5 produces a detector width of anywhere from 220 to more than 500 ppm (depending on which run is used), whereas the equation 7.7 brings the detector asymmetry down to approximately 190-200 ppm.

Although this second weighting scheme removes most of the statistical error, it does not account for variations in detector channel electronics noise. To minimize the overall detector width, first the covariance matrix of the detector is calculated:

$$M_{ij} = M_{ji} = \frac{1}{N_{events}}(\sum_{events} A_i A_j) - \frac{1}{N_{events}^2}(\sum_{events} A_i \sum_{events} A_j).$$ (7.8)

To calculate the weight w_i for each channel i, the sum $w_i w_j M^{ij}$ is minimized:[7]

$$\min[w_i w_j M^{ij}] \Rightarrow w_i$$ (7.9)

This minimization could be the last step in determining the per-channel weights. However, it turns out that each ring of the Møller detector manifested a large dipole (a sinusoidal azimuthal dependence) in its physics asymmetry throughout the run (figure 7.3). The cause of these dipoles will be discussed later; for now, it is necessary to discuss their effects on the overall physics asymmetry. If the channels in each ring are statistically weighted, a portion of this dipole will end up added to the experimental asymmetry. In fact, if statistical weights (based on the widths of each tube's distribution) are used to calculate the experimental asymmetry, the dipole in the asymmetry ends up contribut-

---

[7]This algorithm must also constrain each channel's weight to be positive; otherwise, "common mode" effects in the overall detector asymmetry could be completely obscured.

ing 5 ppb to the experimental asymmetry[8]. The best weighting algorithm should both minimize the overall detector width and nullify the asymmetry dipole contribution to the average asymmetry.

To minimize the asymmetry dipole contribution, first the average amplitude of the asymmetry dipole for each ring for all runs in a particular energy state (either 48 GeV or 45 GeV) must be determined. Call this height (for the x asymmetry dipole) $A_{(x)dip_i}$ (i still refers to a channel, but $A_{(x)dip_i}$ is the same for all channels in any given ring). Now the formula to determine the weights takes the following form:[9]

$$\min[\frac{\sum_{i,j} w_i w_j M_{ij}}{10^8} - (\sum_i A_{(x)dip_i} w_i \ \sin(\frac{2\pi i}{N_{ring}}))^2 - (\sum_i A_{(y)dip_i} w_i \ \cos(\frac{2\pi i}{N_{ring}}))^2] \Rightarrow w_i,$$ (7.11)

where N_{ring} is the number of channels in the ring. The first term in this formula minimizes the overall statistical error (10^8 is the approximate number of events taken during the entire run), while the second and third terms minimize the overall systematic shift to the mean from the dipole. The w_is derived from this formula will be used as the "standard" weights for the channels, and will be referred to as such for the rest of the analysis.

7.5 Run I Asymmetry Equation

Now that $A_{detector}$ has been defined for one event, it can be defined over an entire run and over several runs. For one run, the value of $A_{detector}$ is given as the mean of $A_{detector}$

---

[8]This contribution was calculated with the following formula:

$$A_{dipolecontribution} = \frac{\sum_i A_i \cdot \cos(\theta_i) \cdot w_i}{(w_i^i) \sum_i \cos^2(\theta_i)}$$ (7.10)

[9]Here there is an implicit assumption that the sums begin with the channel in the upward direction. Otherwise, there is a phase inside the sin and cos terms.

Moller Asymmetry vs Channel (Azimuth)
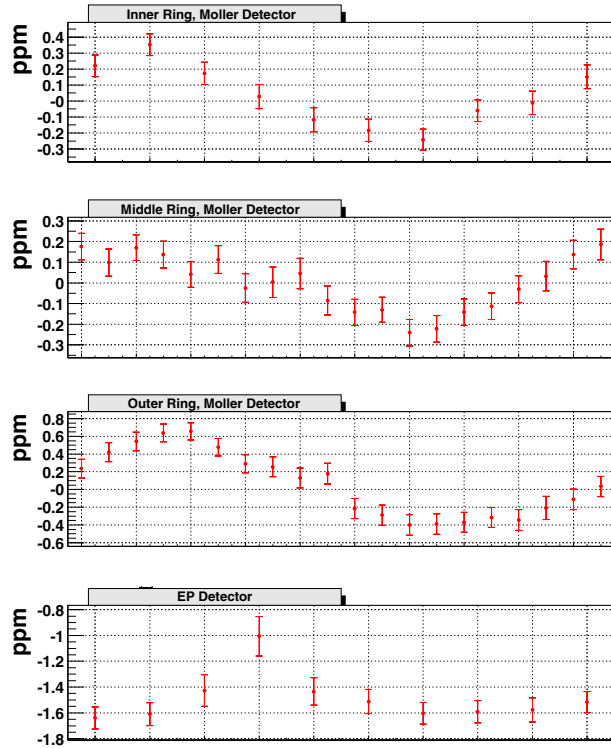
Figure 7.3: Asymmetry for each tube plotted vs azimuthal angle, Run I (all data)

over all events. The regression slopes change every 10000 events, though, so the overall formula for the detector asymmetry for a single run is given as

$$A_{run}^{detector} = \frac{\sum_e A_e^{detector}}{N_{events}} = \frac{1}{N_{events}}\sum_e \frac{A_{ie}w^i - m_{ije}b_e^j w^i}{w_i^i}, \quad (7.12)$$

where A_{ie} is the per-event asymmetry of a detector channel, w^i is the weight for that channel, m_{ije} is the regression slope between channel i and beam monitor j for that particular event, and b_e^j is the value of beam monitor j for that event.

To find the asymmetry over a number of runs, the average of $A_{run}^{detector}$ could be taken without any statistical weighting. However, since the beam luminosity was different for different energies, and since the detector electronics noise varied over long timescales, the decision was made to weight each run's asymmetry by the error on the asymmetry:

$$w_r = \frac{1}{(\sigma_{regression}^2)_r}, \quad (7.13)$$

where r is the run index and $(\sigma_{regression})_r$ is the error on the regressed asymmetry for run r. Consequently, the formula for the experimental asymmetry, averaged over all runs, is

$$A_{tot} = \frac{A_r w^r}{w_r^r}. \quad (7.14)$$

7.5.1 Blinding

The total detector asymmetry, if averaged over the entire experiment, should (perhaps!) give an asymmetry close to the theoretical prediction of around -150 ppb. If no steps are taken to hide the actual value of the asymmetry, an immediate analysis of the physics asymmetry would likely yield a value no more than 30 to 40 ppb from the final experimental

result. Knowledge of this asymmetry might cause the people performing the analysis, particularly in systematics studies, to bias the result toward or away from the predicted standard model value.

To prevent human bias of the physics result, a simple blinding algorithm is used to hide the true value of the physics asymmetry. This bias shifts the raw asymmetry of each Møller detector channel by a fixed amount A':

$$A_i \rightarrow A_i + A' \tag{7.15}$$

A' is constant across all Møller detector channels and across all events. The magnitude of A' falls somewhere between $+200$ ppb and -200 ppb. Only the Møller detector results are blinded; all other detectors' data are unblinded. Until the final physics asymmetry is calculated, every experimental asymmetry presented from here on will be a blinded value.

7.6 Cuts

Once the detector asymmetry has been defined, a reasonable set of cuts need to be implemented to remove all "unwanted" data. These cuts should remove as few events as possible, and should not introduce any bias to the overall asymmetry. Two types of cuts are made to the data. "Baseline" cuts must be made before any physics analysis can occur, as these cuts eliminate hardware failures and other conditions in which the data are meaningless. All other cuts are geared to remove systematics from the measured asymmetry. To ensure that no biases are introduced by these cuts, all cuts will be turned on and off in the physics analysis, and the asymmetries from both analyses will be compared. Lack of a systematic shift between the values is a good indicator that the cuts are unbiased.

7.6.1 Baseline Cuts

A set of eight cuts are initially made to the data before any others; these cuts would typically be described as a "first pass", except that standard first pass cuts are done in hardware, whereas these cuts are done in software and applied to data already stored to tape. The first cut is a beam level cut: all events in which the toroids measured less than $1 \cdot 10^{11}$ (these are not pedestals, but rather events in which the accelerator was unable to deliver us any electrons) or more than $7 \cdot 10^{11}$ electrons per spill are removed. A second cut removes all BaBar witness pulses and pedestal pulses from the physics data (the pedestals are only used for pedestal subtraction, of course). The third baseline cut forces the timeslots of each member of a pulse pair to be identical, removing 60 Hz noise.

The fourth cut is made on a variable called diffTrigger, which measures the time between a pulse and the preceding beam pulse, whether or not that pulse was used in the analysis (witness pulses are included in the diffTrigger calculation). The diffTrigger cut requires that diffTrigger be the same for both members of a pulse pair. It turns out that the gain of the toroid electronics is weakly influenced by the time elapsed since a pulse (of any size) passed through the toroid. Without the diffTrigger cut, these gain effects will make otherwise identical events with different diffTriggers appear to have slightly different beam luminosities. Due to the incredibly small charge asymmetries being measured, events with these false luminosity differences would appear to have (relatively) massive charge asymmetries. The diffTrigger cut completely removes this problem. Even without the diffTrigger cut, charge hysteresis (the magnitude of the charge in a prior pulse affecting the measurement of the charge in the current pulse) is very small, and is not a problem.

The fifth baseline cut removes all dithering data (data taken during accelerator dithering) from the physics analysis. Although this data is used to determine dithering slopes, the regression analysis, which produces different slopes than the dithering analysis, cannot

correct for the massive deviations induced in the beam.

The sixth baseline cut made on the data removes events in which the DAQ suffered a "mixed-up spill". In such an occurrence, the DAQ begins reading data from some (but not all) ADCs with a delay of one event, scrambling the physics data. These events are easily diagnosed, since pedestals pulses and real pulses become scrambled for affected channels. Whenever this occurred, the DAQ alerted the shift takers to end the current run, so events like these are only expected in the ends of runs. When an event with a mixed-up spill is detected, the cut is extended backward in time by two hundred events.

The seventh baseline cut removes all data in which the source CP and PS Pockels cell voltages were not above 2000 V (or below −2000 V), thereby leaving the beam polarization in an undetermined state. This data is useless for the asymmetry analysis.

The eighth baseline cut made to the data removes all events in which the ADC signal from any Møller detector channel was above 50000 counts, or below −100 counts. Neither situation can occur unless the channel is dead or unless there is an electronics glitch. If an ADC channel has died, the data from it is useless. Additionally, if one ADC channel has died, there is no reason to trust the ADC module (which reads six detector channels), so the entire event is cut.

The reason no channels could have reached 50000 ADC counts during the experiment is because the PMTs were typically run at gains which caused the ADCs to read around 20000 to 30000 counts. This was done intentionally, because the Møller detector (and toroid) ADCs begin to saturate and go nonlinear above 50000 counts (the exact level each channel saturates varies from board to board), and if they become extremely saturated, the ADC puts out large negative numbers. Tubes reaching 50000 counts likely did so because of temporary glitches in the Møller detector electronics.

The eighth baseline cut also removes all data in which any Møller detector channel

recorded an asymmetry above 0.9. Such an asymmetry cannot physically occur, and is the result of a DAQ failure, most likely a failure to read an ADC board.

7.6.2   Other Cuts

Once the baseline cuts have been made, we can begin to study the affects of other cuts on the data set. As it will turn out, the final set of cuts made to the data leaves the physics result virtually unchanged. Nevertheless, bias to the experimental asymmetry could still be introduced if cuts were made at specific beam monitor levels. With this in mind, several of the cuts are "stretched" in time via a simple algorithm which finds events failing the cut and removes several hundred or thousand points before and after these events. This decreases the chances of systematic bias affecting the data set.

The first cut deals with the specifics of the regression algorithm. To find data for regression, the algorithm takes every 10000 pairs, breaks the data into two pieces based on timeslot, and then calculates the regression slopes. One problem with this algorithm is that occasionally there will only be a handful of events for one of the two timeslots (the actual cut is on any cycle with less than 100 pairs in one timeslot). When this occurs, the slopes calculated by the regression have large enough error bars to render them useless. As this happens rarely enough, it seems prudent to cut all data in the timeslot without statistically significant regression slopes.

The second cut is a general beam cut designed to remove all sorts of odd beam occurrences. For this document, I will explain what this cut does qualitatively; quantitative details of this cut can be found in [37]. First, outliers at a several sigma level (the precise level depends on the particular monitor) are removed. Second, periods in which the beam centroid wandered by significant amounts are removed from the data, since such motions could induce systematic errors in the beam helicity measurements. Finally, periods in

which the beam jitter was very high are also removed. Each of these cuts are stretched in time by 50 pairs before and after the offending events so as to prevent systematic bias and to assure beam stability outside the cut region.

The third cut requires that two of the alcove toroids measure the same asymmetry to within 100 ppm. If the toroids disagree by more than this amount, neither can be trusted, and the event should be disregarded.

The fourth cut made requires that the alcove toroids measure at least 90% of the levels measured in the ASSET toroids. These toroids have both been calibrated with the same calibrator, so they should both give identical readings for 100% beam transmission through the accelerator[10]. A loss of more than 10% of the beam in the accelerator is unacceptable because it could introduce helicity correlations unrelated to any of the standard "measured" beam parameters. This cut is also stretched (for 2 pulses before and 4 pulses after the bad event).

The fifth cut removes all klystron cycles[11] from the beam, as well as events with extremely aberrant energies. During such periods, beam correlations and detector regression slopes could behave in a fundamentally different way from normal running, due to the rapid change in beam energy. This could affect systematics calculations in unforeseen ways, so this data is removed from the physics analysis. This cut is stretched by 50 pairs in either direction from the offending event, which should be wide enough in time to capture a klystron cycle.

The sixth cut removes all events with large variations in the BPM Q-cavity phases[12]. Large phase variations measured in the Q cavity could indicate that large phase variations

---

[10]Due to differences in cable lengths between the two toroids, the actual agreement is probably good to within a few percent.
[11]A klystron cycle is a period of time in which one of the accelerator klystrons decides to turn off, causing another klystron in the accelerator to be rapidly turned on to keep the beam energy constant.
[12]The x and y cavity phases will move around more due to beam motions in the cavities.

---

are occurring in the X and Y cavities, which would then affect the measured position. Consequently, all such events are removed. This cut is stretched in time 5 pairs before and 50 pairs after the offending pulse, since the signature of a phase jump typically had a very fast risetime followed by a slow "decay" back to the original phase.

The seventh cut made to the data removes all points in which the beam was far enough off center to reduce the BPM linearity below 99%. The quantity of data removed by this cut is small, justifying the rather conservative cut. This cut is also stretched to make the point at which physics data can be taken in the monitors less rigidly "fixed" on the 1% level, suppressing any potential systematic bias to the experimental asymmetry.

The eighth cut made to the data is only made over a subset of data taken in the end of April (close to the beginning of the run). During this period, work was being done on the toroid electronics to diagnose the problem that eventually led to the discovery of the necessity of the diffTrigger cut. However, during this period, changes were made to the toroids which exacerbated this problem to the point where only data taken at 120 Hz or data taken at 60 Hz in the second timeslot[13] were useful. Data taken at other rates had spurious toroid readings, as did 60 Hz data taken in the first timeslot (which had to contend with witness pulses). Consequently, all data not meeting the above conditions is cut for all events before the run (4840) in which the toroid electronics were fixed.

Table 7.2 gives all nine cuts and a summary of their cumulative acceptance levels. As we can see, none of the cuts remove a large fraction of the data, aside from the necessary baseline cuts. Figure 7.4 depicts the blinded experimental asymmetry for each of the cuts (made cumulatively). None of the cuts has a significant impact on the data, either to the mean or the width of the asymmetry. Therefore, no systematic error due to cuts is assigned to the experimental asymmetry, and all of the cuts are used for the physics

---

[13]While running at 120 Hz, SLAC can rate limit the experiment to 60 Hz in either timeslot.

Baseline Cuts	19.7 ± 21.2
Previous Cut + Regression Slopes	20.3 ± 21.2
Previous Cut + General Beam	20.9 ± 21.5
Previous Cut + Toroid Agreement	20.9 ± 21.5
Previous Cut + Transmission	20.5 ± 21.6
Previous Cut + Klystron Cycles	18.9 ± 21.7
Previous Cut + BPM Phases	21.6 ± 21.9
Previous Cut + BPM Linearity	21.0 ± 21.9
Previous Cut + Beam Rate	21.1 ± 21.9
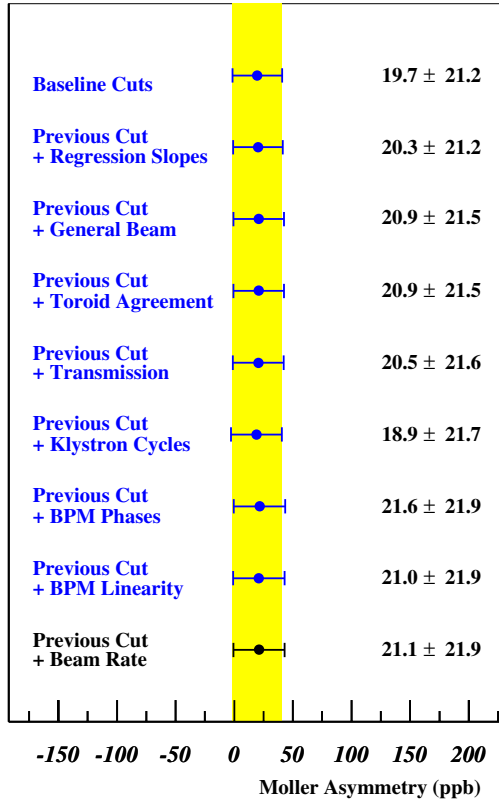
Figure 7.4: Møller Detector Asymmetry (blinded) plotted versus (cumulative) cut. The asymmetry is very stable with respect to all cuts.

Cut	Acceptance Percentage	Number of Events (Mpairs)
None	100%	107.80
Baseline	86.32%	93.06
Previous + Regression Slopes	86.32%	93.05
Previous + General Beam	82.75%	89.21
Previous + Toroid Agreement	82.75%	89.21
Previous + Transmission	82.69%	89.14
Previous + Klystron Cycles	81.81%	88.19
Previous + BPM Phases	80.48%	86.76
Previous + BPM Linearity	80.21%	86.48
Previous + Beam Rate	79.65%	85.86

Table 7.2: All cuts and their cumulative acceptance levels. Cuts are defined in the text.

analysis.

7.7 Møller Detector Results

7.7.1 Pull plots

The first method to ascertain whether or not the data are systematically clean on a run by run basis is to look at the asymmetry distribution for all runs during the experiment (figure 7.5). A simple linear fit to the data reveals a χ^2/NDF very close to 1, and no obvious outliers. On the other hand, the χ^2/NDF may only be representative over this timescale, due to statistical noise. Consequently, a second plot (figure 7.6, made over each "slug"[14]), reveals the experimental asymmetry to be stable over much longer timescales.

In both plots, the shape of the distribution around the mean is still unclear. To discern

---

[14] A slug is henceforth defined as a particular configuration of source and energy conditions. Any changes in the state of the halfwave plate, the asymmetry inverter, the beam energy, or deliberate, non-feedback changes to the Pockels cell voltages will each constitute the start of a new slug.
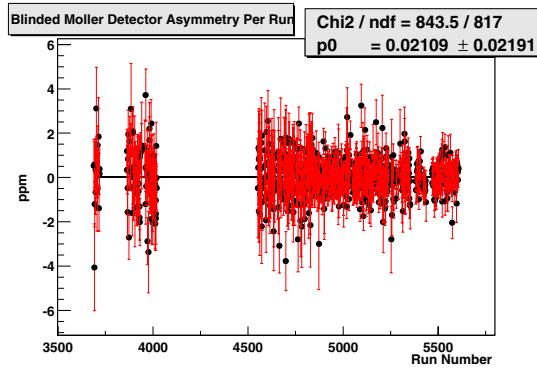
Figure 7.5: Møller Detector Asymmetry (blinded) for every run
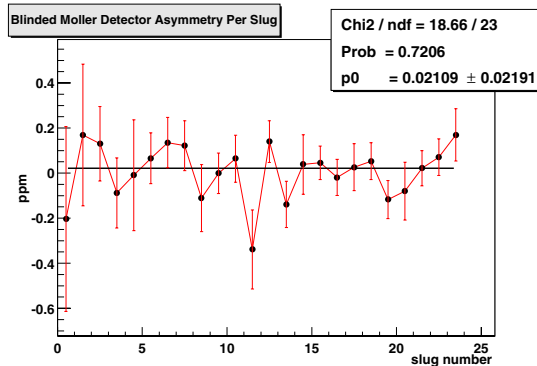
Figure 7.6: Møller Detector Asymmetry (blinded) for every slug

this shape, one can use a pull plot, which takes the average value of the Møller detector asymmetry, $< A >$, and its error, σ_A, and histograms the value of χ, $\frac{A_r - <A>}{\sigma_A}$ for all runs. For the Møller detector, this plot (figure 7.7) shows no significant outliers and has a gaussian shape. From these two plots, it seems evident that no large systematics are affecting the data.

7.7.2 Asymmetry Flips and Other Comparisons

As was noted in the methodology, E158 periodically changed either the state of the source halfwave plate or the energy of the beam in order to introduce sign flips in the experimental asymmetry. As systematic contributions to the asymmetry should remain constant across all states, these sign changes should suppress the overall magnitude of systematic errors. Furthermore, the spread of the data (when plotted on a per-slug basis) should give a handle on the magnitude of the systematic error for any particular state.

To compare all of the sign flips, it is necessary to take the experimental asymmetry for each of the four potential sign-flip states (such as 45 GeV, halfwave plate in) and compare it to the overall experimental asymmetry. Figure 7.8 shows all four asymmetries (with the sign renormalized already) and the overall physics asymmetry. None of the sign flips change the absolute value of the asymmetry by a significant amount. This and the prior per-slug plots appear to bound the overall systematic error to at least the level of the statistical error.

Other comparisons can be done in addition to sign flips. For instance, since the asymmetry is not expected to vary much between individual rings in the detector, the rings' asymmetries should all agree. Figure 7.9 shows each ring's asymmetry as compared to the Møller detector asymmetry. All the rings are in good agreement, as expected (there will be systematic corrections to the rings from the ep flux, described later).

Moller Detector Pull, All Runs

Moller Pull

Nent = 818

Mean = 0.00489

RMS   = 1.02

Chi2 / ndf = 20.9 / 14

Prob = 0.1043

Constant =   128 ± 5.691

Mean   = 0.01049 ± 0.03551

Sigma   = 0.9948 ± 0.02699
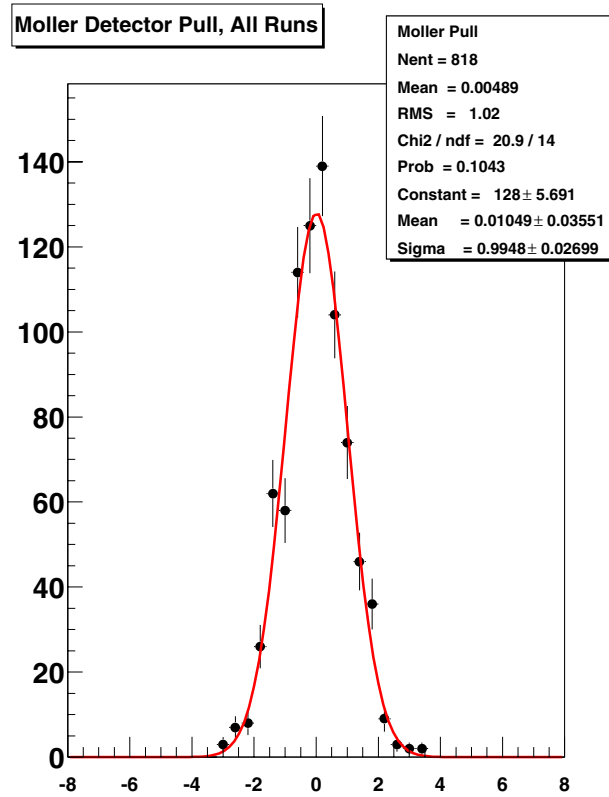
Figure 7.7: Møller Detector Asymmetry (blinded) Pull Plot

Moller Asymmetry, BLINDED

48 GeV HWP IN	62.9 ± 51.5
48 GeV HWP OUT	-5.8 ± 47.5
45 GeV HWP IN	12.1 ± 37.7
45 GeV HWP OUT	25.6 ± 42.3
Average	21.1 ± 21.9
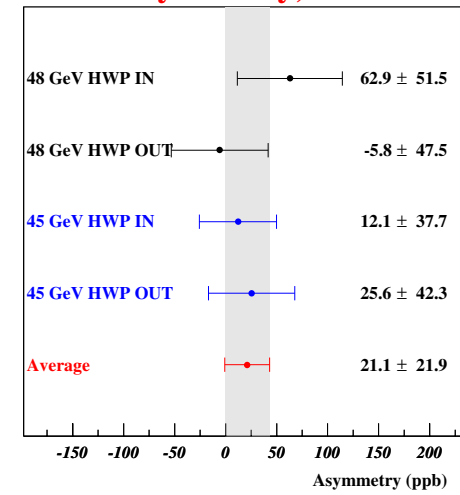
Asymmetry (ppb)

Figure 7.8: Møller Detector Asymmetry (blinded), Different g−2 and source states. The asymmetries have already been corrected for the sign of the state. HWP stands for halfwave plate.
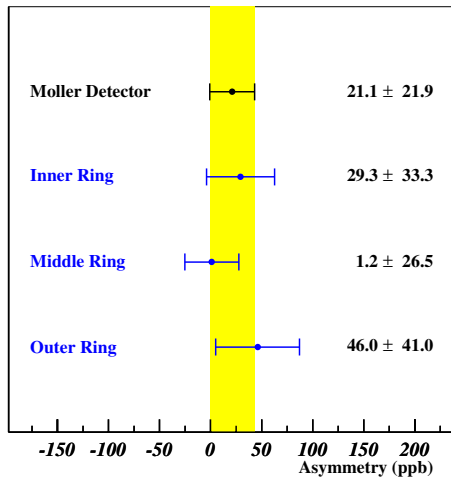
A third comparison can be made between data taken in timeslot 0 and data taken in timeslot 1. Figure 7.10 expands upon the ring plot to give each ring's asymmetry as a function of timeslot. Unlike other asymmetries in this analysis, every asymmetry in this plot was weighted by the error on its own value on a run-by-run basis. This was necessary because each timeslot has different statistics, so weighting them by the same value would not make sense. The results for either timeslot agree very well with the overall asymmetry, with the exception of the mids, which are 2.2 σ from each other. As all of the other rings agree so well, this is likely a statistical fluctuation. The overall agreement points to a lack of any systematic error stemming from timeslot effects.

7.7.3   Beam Systematics, Part One

As it can be seen from the right hand side of equation 7.12, the overall regressed asymmetry may be heavily dependent on beam corrections, especially if the product $m_{ij}b^j$ is large. The feedbacks used for the experiment were intended to keep the corrections from each beam monitor as small as possible. Since this is the case, the total contribution to the experimental asymmetry from beam corrections should be small (assuming a reasonable dependence between the experimental asymmetry and any single monitor's asymmetry). The second column in table 7.3 gives the overall integrated asymmetry for every monitor for the entire run, using the cuts outlined above.

The regression corrections, which can be seen as the very right hand term in the right hand side of equation 7.12, are given in column three. To calculate the errors on the corrections for a set of runs, each correction is first calculated for an individual run in exactly the same way the experimental asymmetry is calculated. The total correction is

Figure 7.9: Asymmetry (blinded), Each Møller Detector Ring
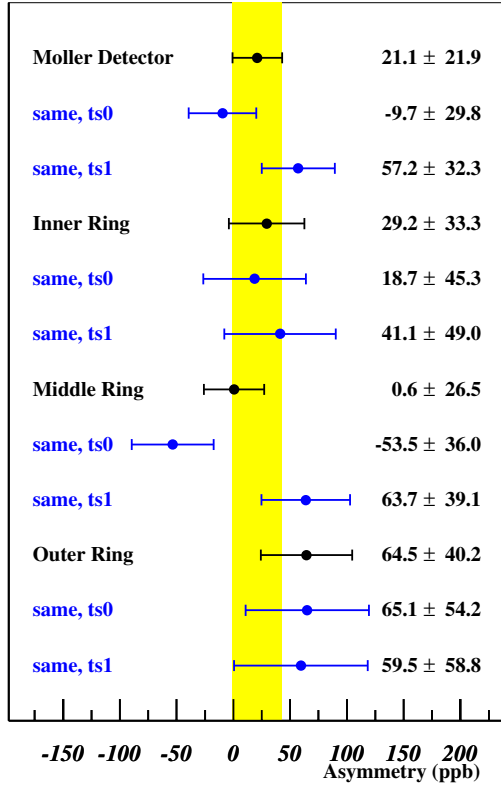
Figure 7.10: Asymmetry (blinded), Each Møller Detector Ring with Each Timeslot

Parameter	Run I Asymmetry	Regression Correction (ppb)
Q	225 ± 320 ppb	-8.4 ± 5.2
E	-0.1 ± 1.4 keV	4.6 ± 13.2
X	$-16.9 \pm 5.6 \mu$m	-36.2 ± 11.3
Y	$-3.3 \pm 4.0 \mu$m	-3.5 ± 3.2
dX	0.41 ± 0.23 nrad	-3.4 ± 9.7
dY	0.12 ± 0.07 nrad	7.5 ± 3.8
total	(undefined)	-39.4 ± 18.2

Table 7.3: Beam asymmetries and corrections to the experimental asymmetry.

the weighted sum of all the individual run correction means:

$$\mu_{tot}^{Correction} = \frac{\mu_r^{Correction} w^r}{w_r^r}, \tag{7.16}$$

where w_r (given by equation 7.13) is the weight determined from the error on the regressed Møller detector asymmetry. The error bar on the total correction is given by

$$\sigma_{tot}^{Correction} = \frac{\sqrt{(\sigma_{Correction}^2)_r (w^2)^r}}{w_r^r}. \tag{7.17}$$

(with a sum on runs inside the root).

The errors for each correction are dominated by the jitter in the beam parameter associated with the given correction. To calculate the systematic errors on these numbers, it will be necessary to determine the level at which we trust each monitor's measurement, as well as our ability to calculate the sensitivity of the cross-section to beam parameters. For most of the monitors, the experimental asymmetry changes very little (compared to the 21.9 ppb statistical error bar) whether or not the correction is made. For these monitors, an assignment of a 100% error on the correction will be adequate. On the other

hand, the X position correction moves the value of the experimental asymmetry by almost $2\,\sigma$. Consequently, a few concepts must be introduced to determine the sensitivity of the Møller detector to the beam X position. Only then can the systematic error from beam corrections be calculated.

7.7.4 Dipoles

As was stated in section 7.4, the Møller detector rings exhibited large dipoles in their asymmetries throughout the run. A "dipole" in the asymmetry of a Møller detector ring is a large sinusoidal azimuthal variation in the asymmetry (see figure 7.3). The value of an asymmetry X dipole for any Møller detector ring for a single event is given as

$$A_{X\,dipole} = \frac{2}{N_{ring}} \sum_i A_i \sin\left(\frac{2\pi(i - \varphi_{ring})}{N_{ring}}\right), \qquad (7.18)$$

where A_i is the asymmetry of channel i, N_{ring} is the number of channels in the ring, and φ_{ring} is the phase of the top of the ring. The asymmetry dipole for a detector ring for the entire run is computed in the same manner as given in section 7.5 for the Møller detector asymmetry. Table 7.4 lists the magnitude of all X and Y asymmetry dipoles (using the regression analysis).

Detector Ring	X Dipole Value (ppb)	Y Dipole Value (ppb)
Inner	-74.6 ± 39.4	217.5 ± 36.9
Middle	-69.4 ± 32.8	155.8 ± 30.2
Outer	$+99.0 \pm 74.5$	489.2 ± 73.4

Table 7.4: Regressed asymmetry dipoles of the Møller detector rings.

These dipoles can be caused by three very different effects. First, if the incident beam energy is not precisely set to the "magic" energy of 48.37 GeV, the beam acquires

horizontal transverse polarization. Two photon exchange processes will then create an azimuthal asymmetry (a dipole) in the Møller scatters (though the net asymmetry is exactly zero). To study this effect, the beam was run for several hours at 46.6 GeV, exactly halfway between the two experimental energies. At this energy, all the beam polarization is horizontal, so the magnitude and phase of the asymmetry dipoles can be ascertained to a high degree of accuracy. From the 46 GeV data, large dipoles were measured in each ring, which are given in table 7.5. These dipoles were used to set the phase of the vertical axis of each Møller detector ring (as it is not obvious, given the complicated spectrometer and detector geometry, which tube should be considered to be "up").

Detector Ring	Y Dipole, 46 GeV (ppm)	Ring Phase (Tube Number)
Inner	-2.74 ± 0.35	1.169
Middle	-2.99 ± 0.24	2.853
Outer	-2.51 ± 0.43	2.349

Table 7.5: Asymmetry dipoles for the Møller detector rings, 46 GeV data.

The second potential origin of asymmetry dipoles is crosstalk between detector rings, especially from the ep detector. If more ep background (either direct flux, or shower-sharing from the ep detector) hits the outer ring on one side than on the other, an asymmetry dipole would manifest.

Imperfections in the beam corrections are the the third way an asymmetry dipole can manifest. Tubes closer to the horizontal plane are, in general, more sensitive to asymmetries in the beam X position and X angle. If the corrections for the X position BPMs (for example) are being made systematically incorrectly, then the tubes closest to the two sides of the detector will manifest large asymmetries (that will be different in sign, depending on the side of the detector). The magnitude of the correction will diminish for

tubes nearer the horizontal center of the detector. Overall, the detector will manifest an asymmetry X dipole.

7.8 Beam Systematics, Part Two

Now that the asymmetry dipoles are understood, a better assessment of the systematic errors can be made. The methodology of the systematic calculation comes from [38].

From table 7.3, the beam corrections to the experimental asymmetry appear to be dominated by the X position asymmetry. If a monitor existed that was sensitive to the X position measurement, and whose expected asymmetry averaged over the entire run was zero, then this monitor could give an excellent handle on the systematic error from the X correction. With this in mind, table 7.6 gives the corrections and average values for the middle ring's asymmetry dipoles for all of Run I.

Parameter	Run I Asymmetry	Middle Ring X Dipole Correction (ppb)	Middle Ring Y Dipole Correction (ppb)
Q	225 ± 320 ppb	-0.3 ± 6.0	1.0 ± 2.9
E	-0.1 ± 1.4 keV	-7.4 ± 13.5	15.6 ± 16.3
X	$-16.9 \pm 5.6 \mu$m	355.7 ± 128.1	7.7 ± 6.8
Y	$-3.3 \pm 4.0 \mu$m	1.8 ± 9.7	-29.5 ± 98.0
dX	0.41 ± 0.23 nrad	-6.2 ± 16.3	-5.1 ± 9.2
dY	0.12 ± 0.07 nrad	-11.1 ± 11.5	8.6 ± 11.8
total	(undefined)	332.5 ± 130.0	-1.7 ± 96.1
Asymmetry (ppb)	(undefined)	-69.4 ± 32.8	155.8 ± 30.2

Table 7.6: Beam asymmetries and corrections to the middle ring's asymmetry dipoles. Also given are the means of the asymmetry dipoles.

The middle ring's X asymmetry dipole is highly dependent on the X correction and not on other corrections. The magnitude of the X correction to the asymmetry is 355.7 ± 128.1

ppb, while the mean of the asymmetry dipole is -69.4 ± 32.8 ppb. No physical process can give rise to such a dipole. Therefore, the asymmetry X dipole of the middle ring should be consistent with zero. Assuming that the entire value of the asymmetry dipole is due to a faulty measurement in (and correction from) the X position, this indicates that the X position correction can be trusted at the level of $\frac{69.4}{355.7} = 0.195$, or 20%. To be conservative, one sigma will be added to the dipole mean value, changing the confidence level to $\frac{69.4+32.8}{355.7} = 0.29$, or 30%.

This method does not work for the Y correction, primarily because the middle ring's asymmetry Y dipole seems to be only partially sensitive to the Y correction. Also, the middle ring's asymmetry Y dipole is non-zero because of a non-zero horizontal beam polarization. Since this is a real physical effect, the value of this asymmetry dipole cannot be expected to be zero. Thus, this asymmetry dipole cannot be used to determine the systematic error from the Y correction. Therefore, a 100% systematic error will be assigned to the experimental asymmetry from the Y correction (and from all other corrections).

The systematic error from beam corrections is the quadrature sum of the systematic uncertainties on each beam correction. The systematic uncertainty on each beam correction is assumed to be 100% of its value, except for the X position asymmetry, whose uncertainty is 30% of its value. Consequently, the experimental asymmetry beam systematic error is $\sqrt{8.4^2 + 4.6^2 + (0.3 * 36.2)^2 + 3.5^2 + 3.4^2 + 7.5^2} = 17$ ppb. Analysis to reduce the size of this systematic error is ongoing.

7.9 Beam Spotsize Systematic Error

One of the fundamental assumptions of the regression analysis is that the dominant corrections to the experimental asymmetry from the beam are first order. In comparison,

second order beam contributions should be small[15]. A good test of this assumption can be made by analyzing the data from the wire array. If the above assumption is true, the systematic error due to any helicity correlated right-left differences in the beam size (which will be called the spotsize asymmetry) should be small. The analysis presented here comes from [39].

For all of the runs in which the wire array was working, the spotsize asymmetries are defined as

$$A_{PV}^{wirearray} = \frac{\sigma_R - \sigma_L}{\sigma_R + \sigma_L},\tag{7.19}$$

where σ is the width of the spotsize in either x or y. These asymmetries were calculated to be 0.695 ± 1.960 nm for σ_x and -0.416 ± 1.791 nm for σ_y. To calculate the overall correction (or systematic error) due to the spotsize asymmetry, the correlation between the experimental asymmetry and the wire array spotsize (defined as $\pi S_x S_y$, where $S_x = \sigma_x$) was calculated for every run. Each run's correlation was then multiplied by the spotsize asymmetry for that run to achieve an overall correction of -0.05 ± 0.5 ppb. Consequently, a 1 ppb systematic error is assigned to the spotsize asymmetry.

7.10 Ep Results

The ten tubes of the ep detector are analyzed in much the same way as the Møller detector. The per-tube asymmetry formula and the weighting formulae for the ep detector are identical to those for the Møller detector (equations 7.4 and 7.7). However, the optimization of weights is not done for the ep detector; rather, the statistical weights (equation 7.6) discussed in the first part of section 7.4 were used. The reason the weights are not

---

[15]Or, mathematically, in the Taylor series expansion of the dependence of the cross-section on beam parameters, the first derivative terms should dominate.

optimized is that the large asymmetry measured by the ep detector has a very small statistical error (as a percentage of the mean, compared to the Møller detector); consequently, the ep detector's error is bound to be dominated by systematics. A five to ten percent optimization of the statistical error isn't useful, so statistical weights are used.

A plot of the ep detector asymmetry as a function of run number is shown in figure 7.11. A plot of the asymmetry for every slug in Run I, in which the sign of the asymmetry is not corrected for the sign of the halfwave plate state and energy state, is shown in figure 7.12. Although the χ^2 of the first plot is reasonable, it is in fact misleadingly large. The Q^2 of the spectrometer for ep scatters is so different for the two energy states that the ep detector is expected to (and does) manifest two different asymmetries. The two values are -1.430 ± 0.045 ppm for 45 GeV, and -1.735 ± 0.063 for 48.3 GeV, both of which are within the range predicted by theory[13]. These values will be used to determine the corrections to the Møller detector asymmetry from the ep asymmetry.

7.10.1 Ep Systematic Correction to the Møller Detector Asymmetry

The profile monitor was used numerous times during the experiment to map out the distribution of the Møller and ep scatters, both with and without the holey collimator in position. With the holey collimator in position, the Møller and ep scatters must pass through a very small radial acceptance at the collimator, leading to a large separation of the two distributions at the Møller detector. This separation allows the amount of inelastic ep scatters between the two peaks to be accurately measured. Using data from this configuration, the Monte Carlo simulation can be adjusted until it provides a reasonable simulation of the Møller and ep kinematics. The Monte Carlo simulation can then be used to give an accurate determination of the amount of ep flux in the Møller detector.

Figures 7.13 and 7.14 show typical profile detector distributions for runs in which the
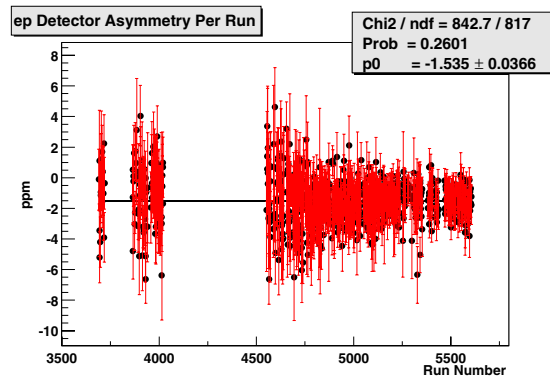
Figure 7.11: ep Detector Asymmetry, All Runs, Run I.

holey collimator was in and out of the beam.[41] These types of scans, taken at several angles (typically every 20 degrees, completely around the azimuth), were made multiple times during the experiment. To create these particular figures, the profile detector tubes, each in its nominal configuration, were scanned radially several times across the face of the Møller detector at the particular angle. Then identical scans were taken with each profile detector tube's shutter inserted, its preradiator inserted, or with both inserted. From these extra scans, the effects of soft photon (and charged particle) backgrounds were subtracted from the data from the original scan.

To estimate the amount of inelastic and elastic ep asymmetry in the Møller detector, these scans need to be compared with a Monte Carlo simulation. The Monte Carlo data pictured was generated by a simulation created specifically for E158[13]. All parameters in the simulation were studied in depth until the simulation agreed very well with the data
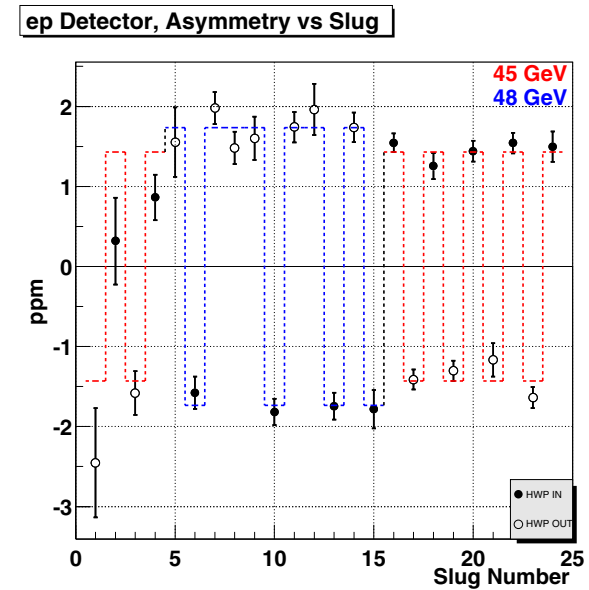
Figure 7.12: ep Detector Asymmetry, All Slugs, Run I. The sign of the ep asymmetry has been left uncorrected with respect to halfwave plate state and energy state. HWP stands for halfwave plate.

45GeV Scan,run 5810data/mc
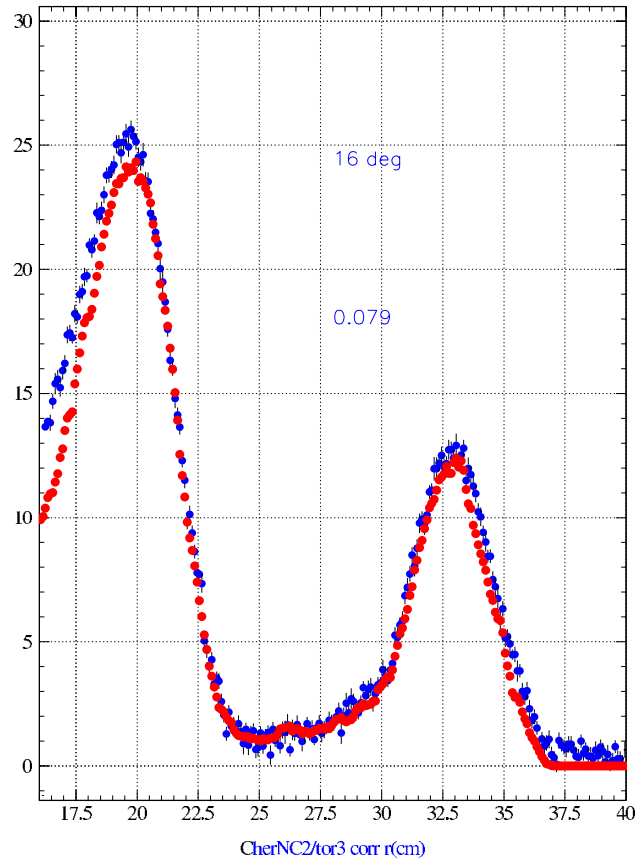
Figure 7.13: Comparison between the Monte Carlo simulation (red) and profile detector data (blue) for a radial profile detector scan at 16 degrees (0 degrees is to the left in this convention) with 3QC1A blocking all but a small radial swath of Møllers and eps. Note the clean separation of the distributions of Møller and ep scatters, and the swath of radiative ep background between the peaks.

45GeV Scan,run 5803data/mc
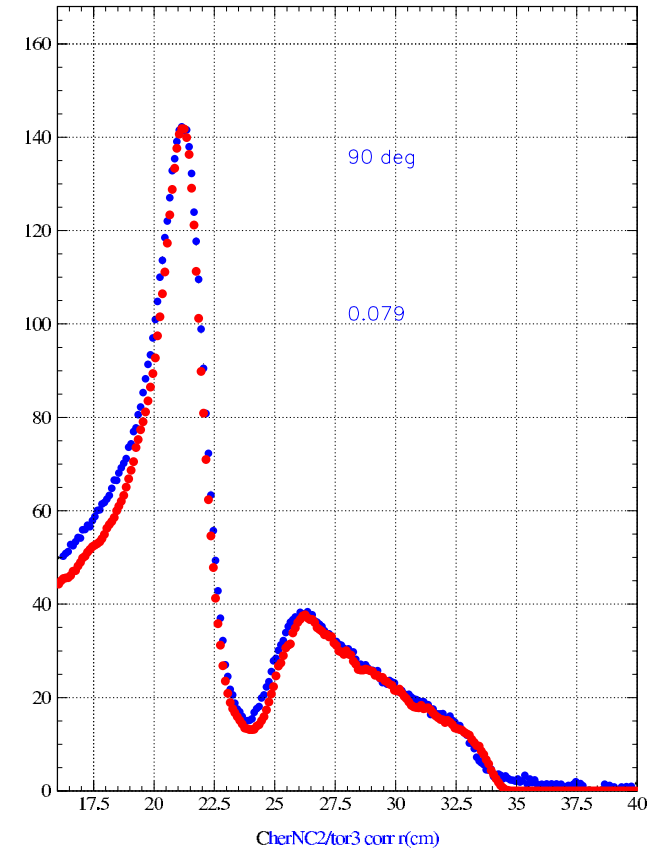
Figure 7.14: Comparison between the Monte Carlo simulation (red) and profile detector data (blue) for a radial profile detector scan at 90 degrees (straight up, in this convention) with nominal spectrometer parameters (3QC1A is in the "out" position).

at all azimuthal angles. As is evident, the agreement between the Monte Carlo data and the experimental data is very good for the radiative eps, so the simulation is believed to be an adequate model of the ep flux[16].

To calculate the amount of inelastic and elastic ep asymmetry contributing to each region of the Møller detector([13],[40],[41]), the simulation first generates an electron at either of the two beam energies, gives it an initial position and angular velocity reflective of the actual beam conditions, and propagates it through the hydrogen target. In the target, "internal" radiative corrections (in which a photon is emitted during the scattering interaction) are approximated by calculating the chance that the electron would radiate from 2.1% r.l. of hydrogen (and doing so, if appropriate). The same process is done as the electron exits the liquid hydrogen target. Next, the electron is stepped through the hydrogen target (20 steps for the entire target). Three other "special" steps are made to simulate the electron propagation through the wire array and the aluminum windows before and after the target. In each step, the angles of the electron momentum are changed slightly to simulate multiple scattering. In addition, once per step, the processes of bremsstrahlung, Møller scattering, ep elastic scattering, and ep inelastic scattering are all considered. In nuclear media, such as the wire array, the elastic and inelastic scattering of electrons off nuclei are also considered. For the Møller, ep, and nuclear processes, the simulation remembers the Q^2 and W from the interaction. Once the electron has been propagated through the target, it is then sent through the appropriate geometrical configuration of magnetic fields and collimators (the spectrometer) until it strikes the detector or is blocked by a collimator. At the detector face, some energy smearing is assumed (to model the detector shower sharing between rings), and the particle asymmetry

---

[16]A second simulation, GEANT (CERN's main simulation package), was also used to model the profile detector data under several sets of conditions. Both simulations agree extremely well.

(determined from the process, the scattering angle, the cross-section, and the Q^2 and W), weighted by the amount of energy deposited by the particle in each ring, is added to the affected rings.

The Monte Carlo calculated contribution to the experimental asymmetry in each ring from the inelastic and elastic ep flux is given in table 7.7. The experimental asymmetry used for these corrections is an estimate based on the Standard Model value of $\sin^2\theta_W$. If this estimate turns out to be inaccurate, a second pass will be made with the Monte Carlo simulation to determine the ep correction to the experimental asymmetry.

ep inelastic correction (ppm)			
	inner ring	middle ring	outer ring
45 GeV	$-.0238 \pm 0.0047$	$-.0201 \pm 0.0048$	$-.0688 \pm 0.0178$
48 GeV	$-.0249 \pm 0.0048$	$-.0224 \pm 0.0055$	$-.1067 \pm 0.0265$
ep elastic correction (ppm)			
	inner ring	middle ring	outer ring
45 GeV	$-.0076 \pm 0.0021$	$-.0062 \pm 0.0017$	$-.0234 \pm 0.0065$
48 GeV	$-.0081 \pm 0.0015$	$-.0070 \pm 0.0017$	$-.0352 \pm 0.0091$

Table 7.7: Corrections to the Møller detector rings' asymmetries (in ppm) from the elastic and inelastic ep flux. Taken from [42].

Besides making a shift to the experimental asymmetry, the ep background also has the effect of "diluting" the experimental asymmetry. The ep background seen by the Møller detector is included in the calculation of the experimental asymmetry, artificially increasing the observed flux of Møller electrons $S_R + S_L$ and consequently the denominator of the asymmetry, $A_{PV} = \frac{S_R - S_L}{S_R + S_L}$[17], leading to a dilution of (decrease in) the asymmetry A_{LR}. The level of this dilution is given in table 7.8.

---

[17]The charge normalization has been removed for clarity.

ep inelastic dilution			
	inner ring	middle ring	outer ring
45 GeV	$.0117 \pm 0.0029$	$.0091 \pm 0.0023$	$.0294 \pm 0.0074$
48 GeV	$.0110 \pm 0.0028$	$.0095 \pm 0.0024$	$.0411 \pm 0.0103$
ep elastic dilution			
	inner ring	middle ring	outer ring
45 GeV	$.0866 \pm 0.0017$	$.0516 \pm 0.0029$	$.1301 \pm 0.0110$
48 GeV	$.0751 \pm 0.0017$	$.0481 \pm 0.0028$	$.1630 \pm 0.0136$

Table 7.8: Dilutions to the Møller detector rings' asymmetries from the elastic and inelastic ep flux. Taken from [42].

7.11 Luminosity Monitor Results

The luminosity monitor was designed to measure the (null) asymmetry in the very forward angle Møller and ep scatters. To calculate the asymmetry of any luminosity monitor channel, the standard formula for the Møller detector is used (equation 7.4). However, the total asymmetry of all eight chambers in either the front or the back monitor is calculated as the unweighted sum of the individual chamber asymmetries. The motivation behind this unweighted sum is straightforward - all chambers have nearly identical gains, and the sum of each opposing pair of chambers (those 180 degrees from one another) sees very close to the same number of incident particles as the sum of any other pair. Also, the luminosity monitor channels, even after regression, give much wider distributions than would be expected from pure statistics. However, if two chambers on opposite sides of the detector are plotted against one another (figure 7.15), a high degree of anti-correlation is evident. If the asymmetries of detectors on opposite sides of the luminosity monitor are summed, the width of the distribution is much closer to what might be expected from

statistics. Thus, the weighting done in summing the Møller detector channel asymmetries is not done for the luminosity monitor.
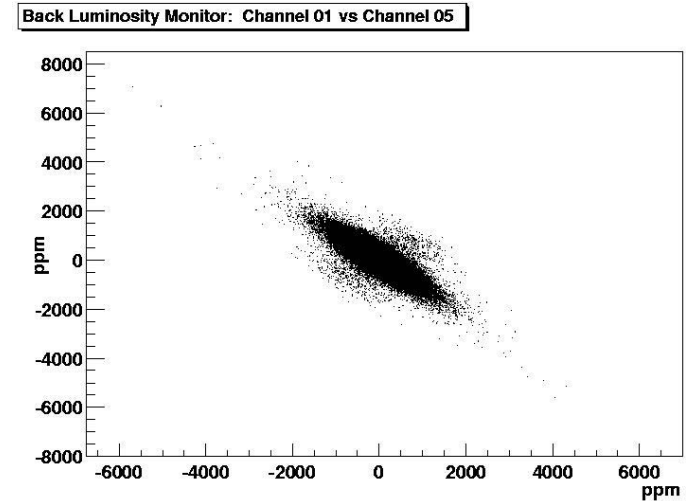
Figure 7.15: A scatter plot of the regressed asymmetries of two opposite channels of the back luminosity monitor. A high degree of anti-correlation is visible.

Figure 7.16 gives, for the front luminosity monitor, a plot of the regressed asymmetry for all slugs in which the monitor was working[18].[33] This plot is a good example of how sign flips like the source halfwave plate and the beam energy change can together

---

[18]The front luminosity monitor was saturated for the first few slugs of run I. For the runs in which it was working, the front luminosity monitor agreed almost perfectly with the back monitor. As the front monitor has the better resolution of the two, it will be the monitor used in the analysis.

suppress systematic errors, even from unknown sources. The χ^2 of the luminosity monitor asymmetry is poor (on a per-slug basis), indicating that unknown systematics are affecting the luminosity monitor. Even so, the mean of the asymmetry is within about one sigma of zero ppb. If the asymmetry is plotted for all combinations of energy and halfwave plate conditions (figure 7.17, taken from [33]), the disagreement between the 45 GeV, halfwave plate out state and the other three states stands out. Studies to find the source of this systematic are ongoing. Still, the luminosity monitor's use as a false asymmetry monitor benefits from the overall cancellation of the systematics by the halfwave plate and energy sign changes. The null result suggests that no large false asymmetries are affecting the Møller detector.

7.12   Pion Results

(Presented here is a summary of the analysis described in [29].) The correction to the experimental asymmetry from pion flux can be calculated as

$$A_{actual} = A_{measured} \times \left(1 - \frac{\epsilon N_\pi}{N_e} \right) + \frac{\epsilon N_\pi}{N_e} A_\pi, \qquad (7.20)$$

where A_{actual} is the real asymmetry, $A_{measured}$ is the measured experimental asymmetry, N_π and N_e are the number of pions and electrons in the Møller detector, and ϵ is the ratio of energy deposited by pions in the Møller detector to that deposited by Møller electrons. In the limit that $\frac{\epsilon N_\pi}{N_e} << 1$, the overall correction is given by

$$A_{Correction} = \frac{\epsilon N_\pi}{N_e} \times (A_{measured} - A_\pi). \qquad (7.21)$$

The overall per-pair resolution of the pion detector is 1.35% at $5.6 \cdot 10^{11}$ electrons per
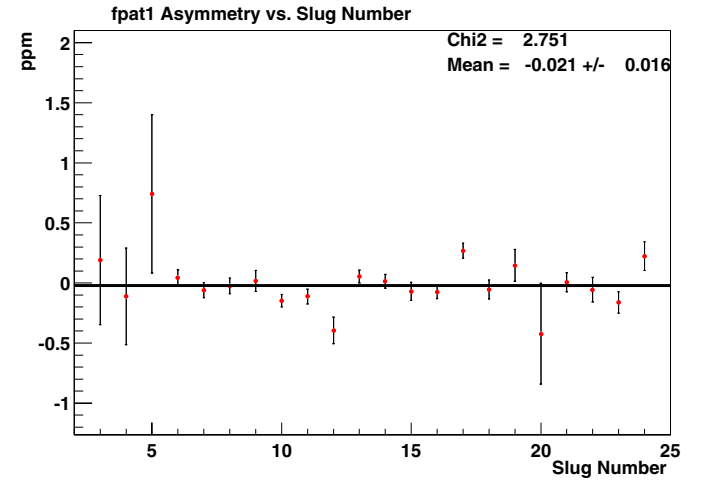
Figure 7.16: The front luminosity monitor asymmetry as a function of slug number. The slugs in this plot are indexed from one instead of zero (as in prior plots). Chi2 stands for χ^2/DOF.

Run I
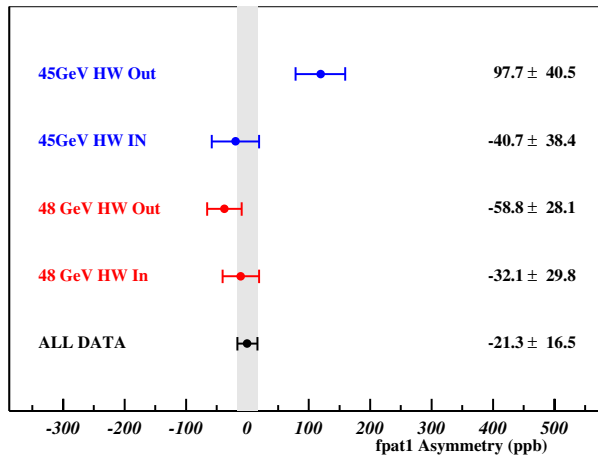
Figure 7.17: The front luminosity monitor asymmetry as a function of halfwave plate and energy state. HW stands for halfwave plate.

spill. Consequently, the measured pion asymmetry is very insensitive to beam motions. In addition, the pion detector is insensitive to charge resolution, so the individual pion PMT signals do not need to be normalized by charge before the PMT asymmetry is calculated (in other words, equation 7.1 is used to calculate the pion asymmetry). This lack of sensitivity allows the cuts applied to the pion detector to be less stringent than those applied to the other detectors. Hence, the pion analysis ignores the timeslot (60 Hz), dithering data, Møller detector ADC saturation, and Møller detector channel asymmetry baseline cuts, as well as all non-baseline cuts except the beam quality cut.

To calculate the number of pions per spill incident on the Møller detector, a GEANT simulation was used to calculate the detection efficiency of the pion detector (as compared to the Møller detector), the pion detector energy resolution, and the percentage of pions counted in multiple pion detector PMTs (multiplicity). The difference in area between the smaller pion detector and the larger Møller detector gives a detection efficiency of 0.24. The pion detector energy resolution is estimated to be 150%. Finally, the multiplicity is estimated to be 28%, due to the large amount of material (lead and copper, in which pions will both scatter and shower) sitting in front of the pion detector. Putting all these terms together, the total pion flux per spill incident on the Møller detector is believed to be 0.62% of the Møller electron flux. This number was also experimentally verified by placing pion PMTs in front and in back of the Møller detector, and by measuring the attenuation of pions by the Møller detector. The overall experimental result was $0.63 \pm 0.21\%$. This same simulation was used to determine the ratio of deposited energy in the Møller detector from pions and electrons; the final number was determined to be $\epsilon = 0.22 \pm 0.15$. Together, these numbers constitute a dilution of the experimental asymmetry of 0.00126. To be conservative, the number that will be used for the dilution from pion flux in the final calculation of the experimental asymmetry is 0.0013 ± 0.002.

The only significant correction to the pion detector asymmetry is the dilution of the asymmetry due to the "background" of Møller and ep scatters on the pion detector. To measure this background, a series of special runs was taken in which both the polarimetry foil and the liquid hydrogen target were placed in the beamline. The polarimetry foil alone creates an asymmetry of around 5% for the Møller electrons. This asymmetry is then diluted by the ratio of Møller scatters from the liquid hydrogen to those from the polarimetry foil. This ratio of thicknesses was measured by comparing the outputs of the channels in the middle ring of the Møller detector for both targets; the ratio was determined to be 115±10. During these runs, the Møller detector measured an asymmetry of 522 ppm, while the pion detector measured an asymmetry of 62 ± 11 ppm. Therefore, the contamination in the pion detector from electron flux is $13.5 \pm 2.7\%$.

Now that the contamination has been calculated, the overall pion detector asymmetry can be normalized. For all runs in Run I, the normalized pion asymmetry is 1.74 ± 0.46 ppm. Plugging this and all other factors into equation 7.21, the correction to the Møller detector asymmetry from the pion asymmetry is believed to be -2.6 ± 1.9 ppb. To be conservative, no correction will be assigned, but the systematic error from the pion flux will be approximated as 5 ppb.

7.13 Dilutions and Corrections from Neutral Backgrounds

The effect of most neutral backgrounds on the experimental asymmetry can be treated as a dilution of the asymmetry. These backgrounds are diverse, and include high-energy photons from spectrometer collimators and the target, low-energy photons from the spectrometer beampipe, synchrotron photons from the dipole chicane, and neutral hadron flux from the ep detector and other sources.

To measure neutral backgrounds, E158 took special runs with the spectrometer in nonstandard conditions. In the first type of run, the liquid hydrogen target was removed from the beamline. In this configuration, only synchrotron radiation should contribute to the Møller detector signal. All of the other background runs were taken with the spectrometer quadrupoles turned off. Without the focusing optics, the Møller flux hits the ep detector instead of the Møller detector. However, the neutral backgrounds hitting the Møller detector are unaffected by this change. In fact, this configuration increases the backgrounds seen by the Møller detector, as low energy charged particles which would ordinarily be swept out of the spectrometer by the quadrupoles will now hit the Møller detector. Also, any background (such as hadron flux) from the ep detector will be increased, due to the larger amount of flux hitting the ep detector with the quadrupoles turned off.

Other quadrupoles-off background runs were taken in which the Møller detector PMTs were "blinded" by putting a piece of aluminum tape over the opening of the PMT. In this configuration, the PMT signals come entirely from neutral hadron background.

Other background runs used these blinded tubes, but also inserted a large lead and tungsten collimator to entirely block the ep detector[19]. By doing so, the contribution of the ep detector to the hadron flux could be calculated more precisely. The effects of this collimator on the ep detector asymmetry will be described in section 7.13.3.

In the final type of run[20], a lead collimator was wrapped around the beampipe immediately downstream of the quadrupoles. This beampipe is struck by a significant number of wide-angle ep scatters, and is now believed to be the primary source of low-energy photon background on the Møller detector for Run I. This collimator has become a permanent fixture of the spectrometer for future runs.

---

[19]These runs were taken during Run II, which ran in the fall of 2002.
[20]These runs also occurred during Run II.

A very thorough analysis of all five types of run was performed [43]; its results will be summarized here. Before estimates of the backgrounds can be calculated, the Møller detector linearity for very small signals must be understood. In normal running conditions, the Møller detector PMTs put out pulses about 0.5 V high, and for such pulses, the Møller detector electronics chain is about 99% linear. For very low signal heights, though, the detector electronics are highly non-linear. This non-linearity can be mostly attributed to the rectifying diodes in the absolute value circuit, which distort small pulses.

To calibrate the detector linearity for small signals, the middle ring's PMTs were run at five different gain settings (four PMTs were run at the nominal setting, another four were run at 1/5 of that setting, and so on), so that the channels spanned a large dynamic range in the Møller detector electronics. Runs were then taken with different targets, including the hydrogen target, the 2 gram and 8 gram carbon targets, the 100 μm polarimetry foil, the wire array, and no target. From all of this data, a very accurate fit was made to the linearity at all signal heights.

Once the linearity was calibrated, the results were used to determine the levels of dilution of the experimental asymmetry from each background source. The no-target runs are dominated by synchrotron radiation, so the dilution factor for synchrotron radiation can be calculated separately from the rest of the backgrounds. The overall synchrotron dilution was measured to be 0.0015 ± 0.0005. The asymmetry present in the synchrotron radiation will be discussed in the next section.

Likewise, the runs in which the Møller detector PMTs were blinded should only be sensitive to neutral hadron background. The overall dilution to the experimental asymmetry from this background is 0.003 ± 0.003. Calculating the asymmetry due to this hadron flux is straightforward. By inserting the lead and tungsten collimator in front of the ep detector, the signals from the blinded PMTs were cut in half. Consequently, it is assumed

that half the hadron flux on these tubes comes from the ep detector. The asymmetry present in the ep detector is approximately 1.5 ppm. Therefore, the correction to the experimental asymmetry from these tubes is believed to be $1.5 \times (0.003 + 0.003) \times 0.5 = -4.5$ ppb (conservatively adding 1 σ to the dilution). The correction which will be used for the determination of the experimental asymmetry is -5 ± 3 ppb.

Calculating the level of soft-photon background involved taking the difference between the Møller detector PMT signals in quadrupoles-off runs with and without the lead beampipe collimator. The calculated dilution is 0.001 ± 0.001. However, like the synchrotron radiation and the neutral hadron background, this background may also possess an asymmetry. The soft-photon asymmetry will be discussed in section 7.13.2.

The final Møller detector background consists of high-energy photons. To calculate the high-energy photon contribution, the levels of all three of the other backgrounds were subtracted from the Møller detector PMT signals in quadrupoles-off runs. The dilution factor from high-energy photons is calculated to be 0.004 ± 0.002.

7.13.1 Synchrotron Asymmetry

Now that the level of synchrotron radiation striking the detector has been calculated, the right-left asymmetry of this radiation can be estimated.[14] Three numbers are needed for this estimation: the amount of synchrotron radiation hitting the detector, the amount of vertical transverse polarization in the beam, and the asymmetry of the synchrotron radiation in the case of 100% vertical beam polarization.

From the data taken at 46 GeV, the horizontal beam polarization was measured to be 85%.[14] At this energy, the asymmetry Y dipole for the Møller detector rings was measured to be approximately -3.0 ppm. On the other hand, for nominal running at 45 and 48 GeV, the asymmetry X dipole for the entire Møller detector is -38.8 ± 26.5 ppb.

Scaling the 46 GeV result, this suggests that the beam was 1.1% horizontally polarized for Run I. A separate analysis of the data from the synchrotron light monitor [14] estimates the transverse polarization at 1.3%. To be very conservative, the value of the horizontal beam polarization used to estimate the synchrotron radiation asymmetry will be 2%.

The asymmetry of synchrotron radiation depends on the energy of the synchrotron photons. Consequently, calculation of the synchrotron asymmetry (for 100% transverse polarization) requires a Monte Carlo estimation of the energy spectrum of synchrotron radiation hitting the Møller detector, as well as an estimation of the cutoff energy below which the Møller detector is insensitive to photon backgrounds. Although the amount of synchrotron power hitting the detector has been calculated, the cutoff energy of the power spectrum is not well-known. Consequently, neither is the absolute fraction of the synchrotron power at any specific energy. If the Møller detector is sensitive to photons at all energies, the synchrotron asymmetry will be 34 ppm for 100% vertical beam polarization. On the other hand, if the Møller detector is only sensitive to particles above 9.5 MeV, the synchrotron asymmetry will be 250 ppm. As the likeliest energy is somewhere in between, the conservative estimate of the synchrotron asymmetry (for a 100% vertically polarized beam) is 150 ppm.

The estimated contribution to the experimental asymmetry from synchrotron radiation is $0.0015 \times 0.02 \times 150 = 4.5$ ppb. This number will be treated as a systematic error rather than as a correction.

7.13.2 Soft-Photon Backgrounds from Aluminum

In the end of Run I, a number of runs were taken in which the spectrometer quadrupoles were turned off and the high voltage on each Møller detector PMT was increased so that the PMT output was roughly equivalent to the signal it gave off in standard running

conditions. Several runs were taken in this configuration, and the asymmetry of the Møller detector was calculated. In this configuration, the measured asymmetry of the inner ring was 1.05 ± 1.91 ppm, of the middle ring was 2.14 ± 1.42 ppm, and of the outer ring was 5.08 ± 1.33 ppm. The asymmetry measured in the ep detector was -0.2 ± 0.2 ppm.

The large asymmetry in the outer ring, as well as the non-zero asymmetry in the other Møller detector rings, are as of yet not entirely explained. The sign of the asymmetry is opposite from the ep asymmetry and from the expected experimental asymmetry. On the other hand, the asymmetry is the same sign as the pion asymmetry, but no mechanism has yet been envisioned which would cause the asymmetry in this configuration to be dominated by pions. On the other hand, it has been proposed that an asymmetry exists in the e^--Aluminum scattering cross section.[44] This possibility is currently the likeliest candidate for explaining the asymmetry seen during these runs.

Due to this result, a correction and systematic error must be assigned to the experimental asymmetry from the low-energy photon flux that scattered from the beampipe downstream of the quadrupoles. Taking the roughly 3 ppm asymmetry from these runs and multiplying it by the 0.001 dilution factor would give an overall correction to the experimental asymmetry of 3 ppb. As this is a very imprecise calculation, no correction will be assigned to the experimental asymmetry; instead, a 6 ppb systematic error will be assigned.

7.13.3 Other Backgrounds

During Run II of E158 (taken in the fall of 2002), the lead and tungsten collimator was left in front of the ep detector, reducing systematic errors associated with leakage of signal from the ep detector into the Møller detector. Although the results are very preliminary, the Run II data shows that the ep detector measured a positive asymmetry of 700 ppb with

this collimator in place. The origin of this asymmetry is unclear, though two hypotheses have been proposed.[45] First, the pion asymmetry is positive, and it is conceivable that the high-Q^2 pions hitting the ep detector have around a 2 ppm asymmetry. The second potential source of this asymmetry is the tails of the showers from Møller scatters. In order to create a signal in the Møller or ep detectors, polarized electrons shower throughout the length of the copper, undergoing many Coulomb interactions. If a very small parity violating asymmetry exists in Coulomb scattering in copper, the far tails of the electron shower could contain an asymmetry in the ppm range.

No matter which process creates the asymmetry in the blocked ep detector, the effects of this background on the experimental asymmetry must be estimated. When the collimator is placed in front of the ep detector, the signal from each ep detector PMT is cut to 2% of its unblocked value. Some of this signal is from energy that has punched through the collimator (which might be pion flux), while the rest of the signal is due to shower-sharing between the Møller detector and the ep detector. For either potential origin of this energy, the estimation of its effects on the Møller detector are straightforward. If a 700 ppb asymmetry is seen in a signal whose magnitude is 2% of the ep flux, then the asymmetry that would be seen in the total ep flux is 700 * 2% = 14 ppb. However, since the ep flux has half the energy of the Møller flux, the total asymmetry that could affect the Møller detector is 7 ppb. This number is very rough (it assumes equal contamination of the Møller detector and the ep detector), and will be assigned as a systematic error on the experimental asymmetry.

7.14   Polarimetry

(All polarimetry results are taken from [46].) Several polarimetry runs were taken during Run I, most lasting around half an hour. These runs were taken with the hydrogen target out, and with one of the polarimetry targets (typically the 50 μm foil) in both the "in" and "out" positions (for background subtraction). For polarimetry runs, the quadrupoles' fields were all changed to vertically focus the peak of the distribution of Møller scatters and bring it closer to the beam axis. This was done both to reduce the background from ep flux and to suppress the Levchuk effect[21], which otherwise might be a considerable source of systematic error. At these settings, the peak of the distribution of Møller scatters, which would ordinarily be centered around 21.5 cm, is brought inward to 18 cm.

Like the Møller detector, the main backgrounds for the polarimetry are ep scatters and low-energy photons. These photons can be measured and their effects removed from the data by taking runs with the polarimetry foil in the beam and runs with the foil out of the beam. To calculate the ep contribution to the polarimetry signal, the polarimetry detector was moved radially inward and outward to map out the profile of the signal, which was then compared to a GEANT Monte Carlo simulation. The radial energy dependence of the background makes the fit more difficult to achieve, but careful analysis of the data gives an overall background of $8 \pm 3\%$.

From the polarimetry data, it appears that the beam polarization was stable throughout the run. On the other hand, the three targets used for polarimetry gave different values for the polarization. Both the 20 μm and the 100 μm foils gave values close to 86.7 %, while the 50 μm foil measured a polarization of 81.2 %. The statistical errors on the numbers are small, and no substantive cause has been given for this discrepancy, as

---

[21] The Levchuk effect is a smearing of the peak of the distribution of Møller scatters due to the transverse momentum of the inner-shell electrons in Fe.[47]

all three targets were tested and found to reproduce target magnetization measurements made before the run. Therefore, the final polarimetry estimate averages all measurements equally to give 84.9%. The statistical error on this number is minute. The systematic errors for this result are much larger, and are dominated by the background subtraction, the difference between the three targets' measurements, and measurement of the target magnetization (which was proportional to a current read off an analog meter each time polarimetry was done). Each systematic error contributes roughly 3%, and the overall polarimetry measurement for Run I is calculated to be $84.9 \pm 4.4(syst)$%.

7.15   False Asymmetries in the Electronics

The magnitude of the high voltage on the source CP Pockels cell is typically around 2700 V. This high voltage is pulsed positively and negatively at 120 Hz; the sign of the high voltage determines the helicity of the beam pulse. If a small portion of this electronic signal were to travel down the two miles of copper cables to the readout electronics in the ESA counting house, it could induce a small amount of charge into the outputs of ADCs. As this charge would be helicity correlated, a false asymmetry could end up being measured on beam monitors or detector channels.

To ensure that no such crosstalk affected the data, a series of 40 million events was taken over a several week period after Run I had ended. For these runs, the source Pockels cells' high voltages were left on (pulsing), and all detectors were left in their "nominal" configurations (although the status of HV supples for the Møller and pion detectors is uncertain). Furthermore, a "battery" (a DC power supply) was connected to a toroid ADC channel in the ESA Counting House, and another was connected to a Møller detector ADC channel in the electronics hut. In addition, the ESA Counting House toroid calibrator was

run through toroids 0 and 1. The toroid calibrator in building 420 was connected to an empty luminosity monitor channel.

Halfway through these runs, it was learned that the triggers being used were not the same as the standard E158 triggers. The triggers were immediately changed to the "nominal" configuration. Ten million events were taken in this "nominal" configuration.

For fast processing of the data, only a small number of ADC channels were analyzed[22]. The only runs processed were those which contained above 400k events, as this is the only way to be certain that these runs did not contain mixed-up spill errors.

A few cuts were made to the data. The diffTrigger cut was required, as was the timeslot cut. Also, a cut was made on a variable called "basetrigger", which can identify pedestal pulses. These pulses needed to be excluded for the analysis of channels using the calibrator pulse. Finally, a few runs were removed from the dataset because they displayed obvious problems in one or more ADC channels, likely caused by DAQ failures.

The final dataset was split into several pieces. Table 7.9 lists the right-left differences for every ADC channel (measured in ADC counts) for the data set with "nominal" triggers. Table 7.10 expands this set to include all of the runs. Finally, table 7.11 lists the asymmetries of all channels with a calibrator or a battery.

As is evident, semi-stringent limits have been set on the potential false asymmetry for all channels, except for the BPMs. The energy and angle BPM channels appear to manifest significant helicity correlated differences. The average difference for all of the angle BPM channels is $-10.3 \pm 3.8 \cdot 10^{-4}$ ADC counts, for both of the energy BPM channels is $-21.8 \pm 7.0 \cdot 10^{-4}$ ADC counts, and for all of the position BPMs is $-4.4 \pm 3.9 \cdot 10^{-4}$ ADC counts, consistent with zero. These values should be compared with the typical signal size from a BPM ADC channel, around 5000 to 20000 ADC counts.

---

[22]All channels were written to tape, so all data are recoverable if necessary.

ADC channel	ADC number	Difference (in 10^{-4} ADC channels)
BPM 12 X	05-0	-18.1 ± 20.7
BPM 24 X	00-0	-8.3 ± 13.0
BPM 31 X	01-0	-21.9 ± 13.3
BPM 31 Y	01-2	-38.5 ± 13.7
BPM 32 X	02-0	-25.1 ± 13.0
BPM 32 Y	02-2	2.5 ± 15.3
BPM 41 X	03-2	-2.8 ± 13.3
BPM 41 Y	03-0	7.1 ± 14.9
BPM 42 X	04-0	-3.1 ± 13.7
BPM 42 Y	04-2	-21.0 ± 14.0
toroid 2	06-4	-4.8 ± 2.0
SLM empty	08-0	-15.1 ± 12.1
SLM empty	08-5	5.7 ± 11.9
SLM0	08-1	-7.1 ± 24.3
SLM2	08-3	-1.6 ± 22.0
blum03	00-3	-19.4 ± 12.6
flum07	02-5	0.4 ± 12.7
Pion 06	04-0	-19.4 ± 25.9
Pion 09	04-4	-1.6 ± 11.3
in01	07-2	-7.8 ± 34.2
mid05	08-5	-30.6 ± 35.8
in04	10-2	0.9 ± 8.1
out10	11-0	-5.0 ± 14.1
ep06	12-3	3.5 ± 18.2
mid14	13-1	1.7 ± 10.7

Table 7.9: All channels and their (right−left) differences, only "nominal" triggers used. Abbreviations: BPM (Beam Position Monitor), SLM (Synchrotron Light Monitor), blum (Back Luminosity Monitor), flum (Front Luminosity Monitor), in (Inner Møller Detector Ring), mid (Middle Møller Detector Ring), out (Outer Møller Detector Ring), ep (EP detector).

ADC channel	ADC number	Difference (in 10^{-4} ADC channels)
BPM 12 X	05-0	-25.4 ± 12.1
BPM 24 X	00-0	-18.1 ± 7.1
BPM 31 X	01-0	-3.7 ± 7.3
BPM 31 Y	01-2	-13.3 ± 7.7
BPM 32 X	02-0	-19.2 ± 7.1
BPM 32 Y	02-2	-5.1 ± 8.4
BPM 41 X	03-2	-9.6 ± 7.2
BPM 41 Y	03-0	-3.9 ± 8.1
BPM 42 X	04-0	2.2 ± 7.7
BPM 42 Y	04-2	-6.4 ± 7.9
toroid 2	06-4	-4.1 ± 1.2
SLM empty	08-0	-7.5 ± 6.3
SLM empty	08-5	4.2 ± 6.1
SLM0	08-1	0.9 ± 11.2
SLM2	08-3	-7.2 ± 10.5
blum03	00-3	2.9 ± 6.5
flum07	02-5	3.0 ± 6.6
Pion 06	04-0	-5.6 ± 16.4
Pion 09	04-4	2.6 ± 5.9
in01	07-2	6.2 ± 20.8
mid05	08-5	-6.7 ± 21.3
in04	10-2	-3.4 ± 4.5
out10	11-0	0.9 ± 8.1
ep06	12-3	-1.6 ± 11.0
mid14	13-1	1.1 ± 6.5

Table 7.10: All channels and their (right−left) differences, all triggers used. Abbreviations: BPM (Beam Position Monitor), SLM (Synchrotron Light Monitor), blum (Back Luminosity Monitor), flum (Front Luminosity Monitor), in (Inner Møller Detector Ring), mid (Middle Møller Detector Ring), out (Outer Møller Detector Ring), ep (EP detector).

ADC channel	ADC number	Asymmetry (ppb)	average signal	(B)attery or (C)alibrator?
toroid 0	06-0	88 ± 48	20450	C
spare toroid channel	06-1	87 ± 61	10k and 20k	C
toroid 01	06-2	-2.7 ± 4.6	23275	B
spare luminosity monitor channel	01-2	131 ± 115	29732	C
spare Møller detector channel	16-1	-2.5 ± 2.9	36833	B

Table 7.11: ADC channels with calibrators/batteries attached, and their overall asymmetries for the dataset with "nominal" triggers.

To determine the systematic correction to the physics data from these helicity correlated differences, the ADC differences must first be calibrated into mm. It turns out that the calibration constants for the two angle BPMs (for x and y) were of opposite sign. In other words, a positive beam deflection caused BPM31 to send a positive voltage into the ADC, and caused BPM32 to send a negative voltage into the ADC. Consequently, the false asymmetries for these BPMs are suppressed. After multiplying the calibration constants for Run I by the asymmetries above, the overall X angle false asymmetry winds up being 4.6 nm, and the false asymmetry for the Y angle is 1.3 nm[23]. BPM24 was used for the energy measurement for the run, so the false energy asymmetry is 0.45 ± 0.18 keV. If these values are multiplied by the average regression slopes for the Møller detector, overall corrections of -3.3 ppb (angle X), 0.8 ppb (angle Y), and -2.4 ppb (energy) are obtained. Note that, due to the difference in sensitivity to beam parameters, individual rings would see these effects far more strongly: the out monopole could see energy deviations on the order of 40 ppb, and the out dipoles could see deviations on the order of 200 ppb.

To find the total contribution to the experimental asymmetry from false asymmetries,

---

[23]All BPMs were calibrated in terms of mm. When angles have been quoted in this document, the angles were calculated as the difference of the target and angle BPMs divided by 40 m.

suppression from sign flips which affect the experimental asymmetry but not the false electronics asymmetry must not be ignored. If the 45 GeV, halfwave plate in state is declared to have a positive sign, then the suppression factor could be defined as the difference in events between this state (and the 48 GeV, halfwave plate out state) and those with the opposite sign, divided by the total number of events. Furthermore, to compare these results to the experimental asymmetry analysis, each run is weighted not by its number of events, but by the weight given by equation 7.6. This creates an overall suppression factor of 0.1, reducing the false asymmetry that could be seen by the Møller detector, $-3.3 + 0.8 - 2.4 = -4.9$ ppb, by a factor of ten. Thus, the total false asymmetry contribution from the BPMs is less than 1 ppb, and can be ignored.

7.16 Calculation of the Experimental Asymmetry

Now that all of the corrections and normalizations have been computed, the asymmetry in Møller scattering can be calculated. First, the data must be unblinded. The blinding value ended up being 186.5 ppb (out of a possible -200 to 200 ppb range). With this correction, the experimental asymmetry measured for Run I is -165.4 ± 21.9 ppb. However, this includes data taken at both 45 and 48 GeV. To calculate the actual experimental asymmetry, the data must be separated by energy state, so that the different ep corrections can be added to each set. The asymmetry for all three rings for each energy state is given in table 7.12. This table also includes the percentage of the experimental asymmetry attributable to each ring's statistics. These percentages will be used as weights in calculating the average ep correction to the detector at each energy.

The average ep correction for the Møller detector at each energy is given by the weighted sum of the corrections for each ring. The systematic errors on the corrections

Detector ring	Asymmetry, 45 GeV	Weight, 45 GeV	Asymmetry, 48 GeV	Weight, 48 GeV
Inner	-0.1755 ± 0.0423	0.2448	-0.1288 ± 0.0539	0.2840
Middle	-0.1915 ± 0.0337	0.5562	-0.1760 ± 0.0429	0.5130
Outer	-0.1189 ± 0.0534	0.1989	-0.1734 ± 0.0638	0.2030

Table 7.12: Unblinded asymmetries for each of the Møller detector rings at each energy. Also included are the statistical weights of each ring.

are added linearly (with weights), as it is assumed that the corrections for different rings are completely correlated. The dilution from the ep flux for each energy state is calculated in an identical manner. This results in the corrections and dilutions given in table 7.13.

	45 GeV	48 GeV
ep elastic correction	-10.0 ± 2.8 ppb	-13.0 ± 3.1 ppb
ep elastic dilution	0.0758 ± 0.0042	0.0791 ± 0.0047
ep inelastic correction	-30.7 ± 7.4 ppb	-40.2 ± 9.6 ppb
ep inelastic dilution	0.0138 ± 0.0034	0.0163 ± 0.0041

Table 7.13: Total corrections and dilutions to the Møller detector asymmetry from the ep elastic and inelastic backgrounds.

The dilutions from ep flux must be added to those dilutions calculated in section 7.13. Summing the dilutions from all photon backgrounds, the pion background, and the ep backgrounds gives overall dilution factors of $10.03 \pm 6.9\%$ for 45 GeV and $10.62 \pm 7.5\%$ at 48 GeV. The errors on these numbers are calculated from the quadrature sum of the errors on each of the dilutions (as none of these backgrounds are expected to be correlated).

The final experimental asymmetry at each energy state is the raw asymmetry, corrected by the pion and ep asymmetry corrections, normalized by the dilution factor, and then normalized by the beam polarization and the linearity. For reference, a list of all dilutions,

corrections, and normalizations is given in table 7.14. The linearity of the Møller detector was given in section 5.1.1 as $99 \pm 1.1\%$. It is simplest to treat the polarimetry and linearity as a single normalization (which will be called the "normalization", to distinguish it from the dilution) of $0.99 \times 0.849 = 0.8406 \pm 0.0446$, where the error is the quadrature sum of the errors on the polarization and the linearity. To summarize the equation,

$$A_{PV}^{M\text{ø}ller} = \frac{A_{measured} - A_{corrections}}{(1 - dilution) \times (normalization)}. \tag{7.22}$$

At 45 GeV, this gives an asymmetry of $-162.4 \pm 37.2(stat) \pm 30.6(syst)$ ppb, and at 48 GeV, $-136.3 \pm 46.5(stat) \pm 31.5(syst)$ ppb. The statistical error on each number is the statistical error on the corresponding raw asymmetry, divided by the dilution and the normalization. The systematic error on each number is the quadrature sum of the systematic errors stemming from the dilutions, the corrections, and the normalization. A plot of the corrected, normalized asymmetry for every slug is shown in figure 7.18.

To arrive at an average asymmetry, the statistical errors are used to weight the two data sets:

$$weight_{45GeV} = \frac{\frac{1}{\sigma_{45GeV}^2}}{\frac{1}{\sigma_{45GeV}^2} + \frac{1}{\sigma_{48GeV}^2}}, \tag{7.23}$$

where σ_{45GeV} is the error on the experimental asymmetry at 45 GeV.

$$A_{total} = \frac{A_{45GeV} \times weight_{45GeV} + A_{48GeV} \times weight_{48GeV}}{weight_{45GeV} + weight_{48GeV}}. \tag{7.24}$$

The statistical error on the final asymmetry is

$$\frac{1}{\sqrt{\frac{1}{\sigma_{45GeV}^2} + \frac{1}{\sigma_{48GeV}^2}}}. \tag{7.25}$$
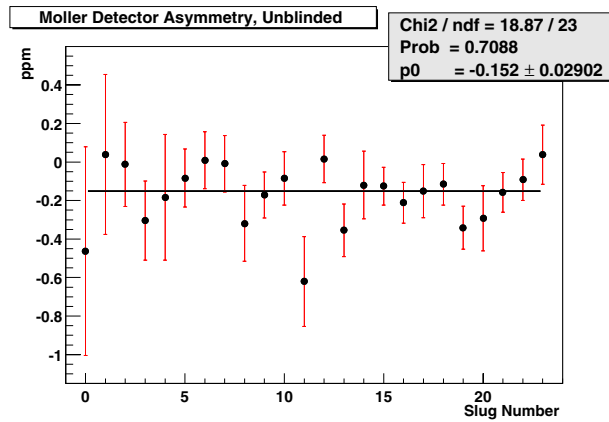
Figure 7.18: Plot of the regressed experimental asymmetry, accounting for all corrections and dilutions.

Raw Experimental Asymmetry		-204.8 ppb
	Dilution	Correction (ppb)
Beam Parameters	0	-39.4 ± 17
Beam Spotsize	0	0 ± 1
ep elastic	0.077 ± 0.0045	-11 ± 3
ep inelastic	0.015 ± 0.004	-34 ± 10
pions	0.0013 ± 0.0020	0 ± 5
synchrotron	0.0015 ± 0.0005	0 ± 4.5
high energy photons	0.004 ± 0.002	0
hadrons	0.003 ± 0.003	-5 ± 3
low energy photons	0.001 ± 0.001	0 ± 6
blocked ep background	0	0 ± 7
	Normalization	
Polarization	$.849 \pm .044$	
Detector Linearity	$.99 \pm .011$	

Table 7.14: Summary of all corrections, dilutions, and normalizations to the Møller detector asymmetry, including the uncorrected asymmetry. Results have been averaged for 45 and 48 GeV for the inelastic and elastic ep values, for clarity.

The systematic error on the final asymmetry is the quadrature sum of the error on the corrections, the dilutions, and the normalization. The error on the corrections for both energies is given by

$$\sigma_{corrections} = \left(\frac{\sigma_{corrections}^{45GeV} \times weight_{45GeV}}{dilution_{45GeV}} + same(48GeV) \right) \times \frac{1}{normalization}, \quad (7.26)$$

the error on the dilutions is given by

$$\sigma_{dilutions} = \left(weight_{45GeV} \times \frac{\sigma_{dilutions}^{45GeV} \times A_{45GeV}^{PV}}{dilution_{45GeV}} \right) + same(48GeV), \quad (7.27)$$

and the error on the normalization is given by

$$\sigma_{normalization} = \left(weight_{45GeV} \times \frac{\sigma_{normalization}^{45GeV} \times A_{45GeV}^{PV}}{normalization_{45GeV}} \right) + same(48GeV). \quad (7.28)$$

The parity violating right-left asymmetry in Møller scattering at a Q^2 of 0.027 is $\boxed{-152.3 \pm 29.0(stat) \pm 30.9(syst) \text{ ppb}}$.

7.17 Calculation of $\sin^2 \theta_W$

To calculate $\sin^2 \theta_W$, equation 2.2 is repeated in a different form:

$$\sin^2 \theta_W = \frac{1}{4} + \frac{A_{PV}}{\frac{m_e E G_F}{\sqrt{2}\pi\alpha} \cdot \frac{16\sin^2 \theta_{CM}}{(4-\sin^2 \theta_{CM})^2}}. \quad (7.29)$$

Obtaining the denominator in the right side of equation 7.29 (this denominator is known as the analyzing power) requires detailed knowledge of the spectrometer acceptance, as the proper range over θ_{CM} must be taken. To calculate the range of scattering angles, the GEANT simulation used to predict profile detector scans was used to calculate the

integral over the acceptance of the Møller detector rings, which then determined the analyzing power as a function of each ring.[49] These analyzing powers were then summed using the weights given in table 7.12 to obtain the analyzing power for the entire detector. All analyzing powers are given in table 7.15.

	analyzing power, 45 GeV	analyzing power, 48 GeV
inner ring	11.487 ± 0.172	11.676 ± 0.175
middle ring	13.190 ± 0.132	13.490 ± 0.135
outer ring	14.010 ± 0.070	14.700 ± 0.074
Møller detector	12.936 ± 0.010	13.221 ± 0.010

Table 7.15: Analyzing power for each ring of the Møller detector and the whole detector at each energy state.

Several schemes exist for reporting the value of $\sin^2 \theta_W$. Each scheme includes or excludes different types of higher-order corrections to $\sin^2 \theta_W$, as some corrections are pertinent to some experiments but not to others. To compare the E158 result to other experiments' values for the weak mixing angle, the data will be presented in the $\overline{MS}$ (modified minimal subtraction) scheme[24][10]. In this scheme, G_F is determined from the muon lifetime. The theoretical corrections to G_F from higher order loop diagrams are well-known, and will not contribute significantly to the theoretical error on $\sin^2 \theta_W$. The value of α is taken at the Z^0 pole ($\alpha = \frac{1}{128}$), instead of at a mass scale of zero ($\alpha = \frac{1}{137}$), a difference of 7%. Using $\alpha(M_Z)$ reduces the effects of 2-loop diagrams, which for $\alpha(0)$ contribute at the level of 7% of the 1-loop diagrams.

The analyzing powers given in table 7.15 need to be corrected for internal bremsstrahlung

---

[24]The numbers in table 7.15 have already been calculated in this scheme.

radiation[25], which the GEANT simulation does not properly handle. The calculation of this correction has only been completed very recently.[50] The overall correction winds up being a scale factor on the analyzing power. The factor is almost exactly the same at both energies, and is 0.9 ± 0.009.

Plugging the bremsstrahlung-corrected analyzing powers into equation 7.29 gives $\sin^2 \theta_W$ at each energy: $0.2360 \pm 0.0032(stat) \pm 0.0026(syst)$ (45 GeV) and $0.2385 \pm 0.0039(stat) \pm 0.0027(syst)$. Again, each statistical error has been calculated by dividing the statistical error on the asymmetry by the analyzing power. Each systematic error is the quadrature sum of the errors on the analyzing power, the bremsstrahlung correction, and the asymmetry.

Calculation of the average value of $\sin^2 \theta_W$ is very similar to the calculation of the overall asymmetry. However, as the statistical errors for each energy have been scaled by the analyzing power, the weight for each dataset is still given by equation 7.23, but σ is now the statistical error on $\sin^2 \theta_W$. The average over both energies is calculated in a manner identical to equation 7.25. The systematic errors for both energies are almost completely correlated, so the systematic error is calculated as the weighted sum of the systematic errors at both energies.

The final value for $\sin^2 \theta_W$ at a Q^2 of 0.027 is $\boxed{0.2370 \pm 0.0025(stat) \pm 0.0026(syst)}$.

---

[25]Internal bremsstrahlung radiation is that radiation which occurs during the e^--e^- interaction and causes interference between the different scattering amplitudes. External bremsstrahlung radiation is defined as radiation which occurs before or after the interaction.

Chapter 8

Conclusions

8.1   Physics Implications

The Standard Model prediction of $\sin^2 \theta_W$ at a Q^2 of 0.027 is 0.2387.[10] The formula for $\sin^2 \theta_W$ expressed in this paper can be summarized as

$$A_{PV} = \frac{1}{Analyzing Power} \times \left\{ 1 - 4\kappa(0)sin^2\theta_W(m_Z)_{\overline{MS}} + O(\alpha) + F_1(y, Q^2) \right\}. \quad (8.1)$$

The factor of κ is the correction which accounts for the diagrams in figure 2.2 (γ-Z mixing and the anapole contribution), reducing the expected value of A_{PV} by around 40%. This factor, according to [10], puts an error of 0.0006 on $\sin^2 \theta_W$[1]. As α is taken at the Z_0 pole, the terms in α do not significantly contribute to the theoretical error. $F_1(y, Q^2)$ contains effects both from $\gamma - Z$ box diagrams, and from the Z-loop contributions to the anapole moment (figure 8.1). This term contributes 0.0003 of additional error to the

---

[1]This error stems from the uncertainty in the sum of $\sum_{quarks}(T_{3f}Q_f - 2s^2Q_f^2)ln\frac{m_f^2}{m_Z^2}$ taken from $e^+e^- \to hadrons$ data.

theoretical value[2]. Consequently, the predicted value is $0.2387 \pm 0.0006 \pm 0.0003$.
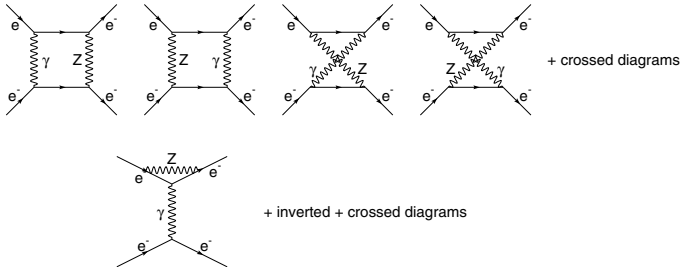

Figure 8.1: One photon box diagrams and the Z-loop contribution to the anapole moment for Møller scattering. Taken from [10].

The difference between the predicted value and the experimental value of $\sin^2 \theta_W$ is (summing errors in quadrature) 0.0017 ± 0.0037, less than one sigma. This difference thus serves as a confirmation of the Standard Model, and also sets limits on several new types of physics.

First, for any arbitrary 4-point contact interaction (see section 2.2), one can express the Lagrangian as

$$\mathcal{L}_{ee} = \frac{4\pi}{2\Lambda_{ee}^2} \left[\eta_{LL}(\bar{\psi}_L \gamma_\mu \psi_L)^2 + \eta_{RR}(\bar{\psi}_R \gamma_\mu \psi_R)^2 + 2\eta_{LR}(\bar{\psi}_L \gamma_\mu \psi_L)(\bar{\psi}_R \gamma_\mu \psi_R) \right], \qquad (8.2)$$

---

[2]This error is large because, in order to calculate $F_1(y, Q^2)$, $\sin^2 \theta_W$ must be known. Whether or not to normalize that $\sin^2 \theta_W$ by $\kappa(0)$ is unclear, so the normalized and raw values are averaged, and assigned an uncertainty equal to the spread of the difference.

with Λ_{ee} as the electron compositeness scale. From [11], Λ_{ee} can be determined from

$$\sin^2 \theta_W (measured) - \sin^2 \theta_W (theory) = \frac{\pi}{G_F \sqrt{2}} \frac{\eta_{RR} - \eta_{LL}}{\Lambda_{ee}^2}. \qquad (8.3)$$

New physics would manifest as a deviation from the Standard Model prediction for $\sin^2 \theta_W$. This deviation could either be positive or negative, depending on the value of $\eta_{RR} - \eta_{LL}$. Defining $\Lambda_{ee}^{\pm}$ to be the electron compositeness scale for $\eta_{RR} - \eta_{LL} = \pm 1$, a 90% confidence level lower bound can be set on $\Lambda_{ee}^{\pm}$ as follows:

$$-0.0017 \pm 1.64 \cdot 0.0037 = \frac{\pi}{G_F \sqrt{2}} \frac{\pm 1}{(\Lambda_{ee}^{\pm})^2}. \qquad (8.4)$$

The corresponding limits are 4.95 TeV (Λ_{ee}^{-}) and 6.60 TeV (Λ_{ee}^{+}).

Also, according to [10], the existence of a massive Z' boson (with a parity violating coupling to the electron) would scale the value of $(\sin^2 \theta_W - 0.25)$ by $1 + 7\frac{m_Z^2}{m_{Z'}^2}$[3]. The expected value of $\sin^2 \theta_W - 0.25$ is -0.0113. Consequently, taking the 90% confidence bound as $\frac{-0.0017 - 1.64 \cdot 0.0037}{-0.0113}$, E158 can set a lower bound on $m_{Z'}$ of 291 GeV. This value has already been ruled out by CDF at Fermilab [51]. Once E158 has achieved its proposed statistical error bar of 0.001 on $\sin^2 \theta_W$, the experimental result will set bounds on the mass of the Z' at the TeV scale (for specific models).

Finally, in certain Higgs models, the existence of a doubly-charged Higgs would allow an s-channel, lepton-flavor violating process involving four electrons.[52, 53] This process could be parameterized as an additional contribution to the coupling for the neutral current cross-section, which is proportional to $G_F(1 - 4\sin^2 \theta_W)$. The E158 result has set 90% confidence limits on this coupling constant of -0.031 G_F (lower) and 0.017 G_F (upper).

---

[3]The scheme used by [10] is an SO(10) GUT. Other schemes may vary by a few hundred GeV.

8.1.1 Summary

E158 has measured the parity violating right-left asymmetry in Møller scattering at a Q^2 of 0.027 GeV^2. The measurement agrees with the Standard Model, setting limits on several extensions of physics beyond the Standard Model. The overall asymmetry of $-152.3 \pm 29.0(stat) \pm 30.9(syst)$ ppb is the smallest asymmetry ever measured in a parity violating electron scattering experiment. By adding the data taken in Run II, as well as the data which will be taken in Run III in the summer of 2003, the statistical error bar on $\sin^2 \theta_W$ is expected to reach 0.001. The systematic error should also be reduced significantly through further study of Runs I and II. The final measurement should eventually constrain four-point contact interactions in electron scattering at the 10 TeV scale.

In addition to measuring the smallest parity violating asymmetry to date, E158 has also made the most precise fractional measurement ever of a parity violating asymmetry with its ep detector. The parity violating asymmetry in ep scattering is consistent with the theoretically predicted value.[13] No further running is planned to improve the error bar on the ep asymmetry, as the goal of the experiment is to measure the asymmetry in Møller scattering, and the systematic error on the Møller detector asymmetry is reduced when the ep detector is entirely blocked.

One final measurement made by E158 is that of the azimuthal dependence of the asymmetry in Møller scattering of a transversely polarized beam off an unpolarized target. As was stated in section 7.7.4, this azimuthal asymmetry occurs due to two-photon exchange diagrams. Analysis of this measurement is ongoing, though it cannot currently be compared to the Standard Model prediction, as no calculation of this process has ever been published. Theoretical work is ongoing to give an accurate prediction of the value of the asymmetry dipole.

8.2 Future Experiments

In the near future, two experiments are slated to run, both of which will use parity violating asymmetries to measure $\sin^2 \theta_W$ at values of Q^2 beneath the Z^0-pole. The first, Q_{weak} [54], intends to make a 4% measurement of the parity violating asymmetry in elastic ep scattering at a Q^2 of 0.03 GeV^2. From that asymmetry, expected to be around -280 ppb, Q_{weak} can derive $\sin^2 \theta_W$ with an overall precision of 0.3%. This experiment, which will run at Jefferson Lab (JLAB) in Hall C, will run a 180 μA continuous-mode electron beam with a polarization of 80% onto a 35 cm liquid hydrogen target. The resulting elastic and inelastic ep scatters will pass through tungsten and concrete collimators before being separated by a toroidal magnet. An integrating quartz Cerenkov calorimeter will be used to measure the elastic ep flux at a scattering angle of 7 to 11 degrees. Q_{weak} is primarily sensitive to lepton-quark couplings, providing a complementary result to E158, which is only sensitive to lepton-lepton couplings.[55] JLAB has scheduled Q_{weak} to begin physics running in 2006.

The second experiment, DIS-Parity [56], has been proposed to run in ESA at SLAC, and would measure the parity violating asymmetry in electron scattering from deuterium at a Q^2 of 20 GeV^2. From this measurement, DIS-Parity would be able to measure $\sin^2 \theta_W$ with a precision of $\pm 0.0006(stat) \pm 0.0006(syst)$. The expected asymmetry in electron-deuterium scattering is on the order of 0.002, making contributions from beam parameters negligible in comparison to E158's sensitivity. On the other hand, DIS-Parity would use the same variety of strained Ga-As photocathode, identical source optics, and the same variety of beam monitors as E158. The former is necessary for DIS-Parity to achieve its statistical error, as it requires a beam luminosity of $9 \cdot 10^{11} e^-$/spill.

A third parity violation experiment, ^{208}Pb [57], has been scheduled to run in Hall A at

JLAB in 2004. This experiment will measure the parity violating asymmetry in electron-Pb scattering in order to make a 1% determination of the radius of the neutron "skin" in Pb. To make this measurement, the overall asymmetry (expected to be on the order of 510 ppb) must be measured to 15 ppb, requiring beam positions to be measured to 0.1 nm. This requirement is an order of magnitude stricter than that for E158. The success of the E158 beam monitors has lent considerable credence to the notion that beam parameters can be measured at the sub-nm level.

8.3   Outlook

E158 has demonstrated for the first time that parity violating asymmetries can be measured at the level of a few ppb. The corrections made to the E158 asymmetry from beam asymmetries were measured by beam intensity and position monitors with approximately an order of magnitude more sensitivity than monitors in prior experiments. The success of these monitors and their electronics paves the way for future experiments intending to measure even smaller asymmetries. The physics of parity violation is a vibrant field, and as current and proposed experiments demonstrate, parity violation is a very useful tool for exploring the fundamental parameters of the known universe.

Appendix A

Dithering

The slopes used to correct the experimental asymmetry for beam asymmetries were determined using the regression analysis. The other method of making corrections for beam asymmetries is known as dithering. The motivation for having a second analysis is that the regression analysis has a flaw, in that it can miscalculate the systematic error from beam parameters. If one beam monitor's asymmetry distribution is narrower than the asymmetry distribution of a redundant monitor, the regression will favor the quieter monitor at the expense of neglecting the monitor more sensitive to beam fluctuations. Since the regression analysis is so monitor-dependent, another method of determining the correlations between Møller detector channel asymmetries and beam asymmetries must be used to crosscheck the regression analysis results.

To obtain the dithering slopes (correlations) between Møller detector channel asymmetries and beam asymmetries, the beam is intentionally mis-steered for some small fraction of the time by upstream corrector magnets. From the regression analysis, the correction to a Møller detector channel's asymmetry is given by $A_{i_{beam}} = m_{ij} b^j$, where $b^j = \Delta B^j$ is a

BPM's[1] measurement of a beam asymmetry[2], and $m_{ij} = \frac{\partial A_i}{\partial B^j}$. If enough magnets (whose strength will be designated as C_k, k being the index of the magnet) exist to move the beam in every direction in beam phase space (including target position, target angle, and beam energy[3]), then the quantity m_{ij} can be determined by taking the following equation:

$$\frac{\partial A_i}{\partial C_k} = \sum_j \frac{\partial A_i}{\partial B^j}\frac{\partial B_j}{\partial C^k} = \sum_j m_{ij}\frac{\partial B_j}{\partial C^k}, \qquad (A.1)$$

and performing a standard χ^2 minimization with respect to m_{ij}.[58]

As is evident from equation A.1, by dithering the beam, the correlations between a Møller detector channel asymmetry and all of the beam asymmetries can be measured independently of beam monitors' resolutions. Likewise, beam correlations which could cause problems with the regression analysis do not affect the dithering analysis, which only concerns itself with the correlation between magnet strengths and beam monitor differences. On the other hand, the dithering suffers from one similar problem as the regression, in that the set of monitors and magnets used in the dithering analysis need to be as "orthogonal" as possible to prevent large errors from creeping up in the determination of m_{ij}[4]. Also, like the regression analysis, the dithering analysis requires the beam jitter to be small, so as not to obscure the derived slopes.

The dithering analysis has one "flaw", in that it does not statistically minimize the width of the experimental asymmetry. Consequently, the width of the asymmetry determined from the dithering analysis might be larger than the width of the regressed

---

[1]Ignore the charge monitors for the moment.
[2]Again, for the BPMs, this is a difference: hence the Δ.
[3]The beam energy is dithered with a klystron instead of a corrector magnet.
[4]To demonstrate this better, equation A.1 could be rewritten using matrices as $AC = AB \cdot BC$, or $AC \cdot BC^{-1} = AB$. If BC is almost singular (due to a redundant set of beam monitor/magnet strength terms), inverting it will cause the errors on AB will blow up.

asymmetry, and might even be somewhat non-gaussian (if noisy monitors are assigned large slopes).

To minimize the error on the dithering slopes, typically the beam will be dithered by several times the amount of its jitter. Consequently, Møller detector channel asymmetries from data taken during the beam dithering can end up being rather large. Therefore, dithering data is only used to determine slopes, and is not used for the physics asymmetry analysis.

To keep the statistical error on the dithering slopes low, several dithering cycles are taken during every run. In each dithering cycle, several corrector magnets (and klystrons for energy) are dithered, producing large correlations between Møller detector channel asymmetries and beam monitor asymmetries. The dithering analysis then uses the dithering data from the magnets which spanned the most orthogonal set of beam parameters (dithering data with other corrector magnets is taken for the sake of redundancy) and calculates the dithering slopes.

A.1 Dithering Analysis

To compare the dither-corrected asymmetry with the regression-corrected asymmetry, the values must be compared on the subset of data in which dithering was working[5]. Figure A.1 shows each Møller detector ring's asymmetry for both types of corrections. One important note about these values: the dithering averages were calculated by using the error bar on the regression analysis to weigh the dithering results on a run-by-run basis (equations 7.13 and 7.14). Consequently, runs in which the dithering wasn't working very well (there may have been only a handful of dithering cycles taken, for instance) are

---

[5]During some runs, the magnets for dithering were off, or the dithering read-back was faulty.

weighted just as strongly as runs in which the dithering was working very well. This has the tendency of inflating the error bars for the dither-corrected asymmetries, especially in the outer ring.

Table A.1 gives the overall corrections from the dithering analysis and from the regression analysis. The two analyses' corrections appear not to agree. The regression makes a very large correction for the beam X position which the dithering ignores, and the dithering makes a large correction for the X angle which the regression ignores. Overall, the two end up disagreeing by 20 ppb, largely due to the X correction difference. The size of the disagreement, though, is within one standard deviation of each of the measurements. Is this a real disagreement? The overall answer to this question is unclear. Systematics studies have revealed that in certain slugs, the dithering analysis makes large (200 ppm) corrections in X, X angle, and energy (see figure A.2 for the Møller detector asymmetry for each slug). The same corrections in these slugs for the regression analysis are smaller. In other slugs, the two analyses appear to agree. As either analysis (or both) could be the cause for the 20 ppb shift, no systematic error has yet been assigned to the final asymmetry due to this disagreement, mostly because the regression analysis appears to agree quite well with the dithering analysis in Run II, in which far more dither cycles were taken on a per-run basis. This agreement suggests the regression has been working throughout the run, and the dithering suffers from a problem in the Run I dataset. Studies of the dithering and regression on the Run I and Run II datasets are ongoing, and it is likely that the data will reveal a problem in one of the two analyses.
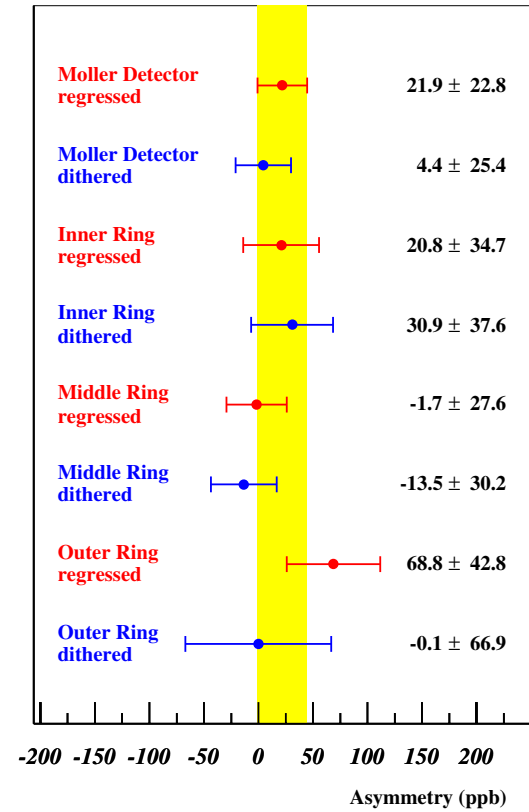
Figure A.1: Asymmetry (blinded), Regression and Dithering, Each Møller Detector Ring

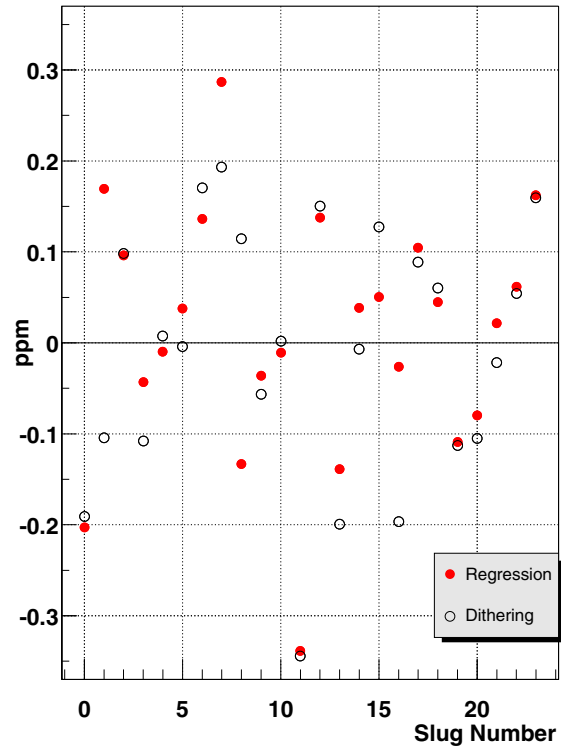**Moller Asymmetry Per Slug, Regression and Dithering**

Figure A.2: Møller Detector Asymmetry (blinded) vs Slug Number, Regression and Dithering Analyses. The error bars (which are dominated by the statistics of the Møller Detector) have been suppressed for clarity.

Parameter	Run I Asymmetry	Regression Correction (ppb)	Dithering Correction (ppb)	Regression Correction, Dithering Subset (ppb)
Q	225 ± 320 ppb	-8.4 ± 5.2	2.0 ± 12.7	-8.3 ± 5.4
E	-0.1 ± 1.4 keV	4.5 ± 13.2	1.8 ± 16.7	4.9 ± 14.0
X	$-16.9 \pm 5.6 \mu$m	-36.2 ± 11.3	-19.7 ± 10.0	-39.4 ± 12.1
Y	$-3.3 \pm 4.0 \mu$m	-3.5 ± 3.2	2.3 ± 3.6	-4.7 ± 3.4
dX	$15.0 \pm 7.5 \mu$m	-3.4 ± 9.7	-14.4 ± 12.5	-1.3 ± 10.2
dY	$2.0 \pm 1.9 \mu$m	7.5 ± 3.8	4.2 ± 4.3	7.6 ± 4.0
total	(undefined)	-39.8 ± 18.2	-23.8 ± 19.7	-41.2 ± 19.2

Table A.1: Corrections from the dithering and regression analyses, on the full dataset and on the dithering subset. Also given are the beam asymmetries, for reference.

References

[1] C.S. Wu *et al.*, *Phys. Rev.* 105 (1957) 1413-1414.

[2] R.L. Garwin, L.M. Lederman, and M. Weinrich, *Phys. Rev.* 105 (1957) 1671-1675.

[3] C.Y. Prescott *et al.*, *Phys. Rev. Lett.* B84 (1979) 524.

[4] The LEP Collaborations, *CERN-EP*/2002-091 (2002).

[5] SLD Collaboration, *Phys. Rev. Lett.* 86 (2001) 1162-1166.

[6] NuTeV Collaboration, *Phys. Rev. Lett.* 88 (2002) 524.

[7] C.S. Wood *et al.*, *Can. J. Phys.* 77 (1999) 7-75.

[8] K. Kumar, E. Hughes, P. Souder, and R. Holmes, *Precision Low-Energy Weak Neutral Current Experiments*, Mod. Phys. Lett A10 (1995) 2979-2992.

[9] E. Derman and W.J. Marciano, *Ann. Phys.* 121 (1979) 147.

[10] A. Czarnecki and W.J. Marciano, *Phys. Rev.* D53 (1996) 1066.

[11] K. Kumar *et al.*, SLAC-Proposal-E158 (1997).

[12] R. Brun *et al.*, *GEANT 3 User's Guide*, CERN/DD/EE84.1.

[13] P. Bosted, *Radiative Corrections for E158*, E158 Technote 23 (2002).

[14] M. Woods *et al.*, *Synchrotron Background Analysis for Run I*, E158 Technote 39 (2003).

[15] B. Humensky *et al.*, *SLAC's Polarized Electron Source Laser System and Minimization of Electron Beam Helicity Correlations for the E158 Parity Violation Experiment*, SLAC-PUB-9381 (2002). Submitted to Nucl. Inst. and Meth. A.

[16] P. Horowitz and W. Hill, *The Art of Electronics*, Cambridge University Press, Cambridge (1980) 437-442.

[17] M. Cooke, *Probing Moller Detector Linearity with the Polarized Iron Foil and Light Filters*, E158 Technote 47 (2003).

[18] D. Whittum and Y. Kolomensky, *Analysis of an Asymmetric Resonant Cavity as a Beam Monitor*, Rev. Sci. Instrum. 70 (1999) 2300-2313.

[19] Raymond Arnold, private communication.

[20] B.Tonguc and M. Woods, *Report on Synchrotron Radiation Analysis*, E158 Technote 17 (2002).

[21] Peter Mastromarino, private communication.

[22] J. Gao *et al.*, *A Liquid Hydrogen Target for the Precision Measurement of the Weak Mixing Angle in Moller Scattering at SLAC*, Nucl. Inst. and Meth. A498 (2003) 90-100.

[23] M. Woods *et al.*, *Spotsize Analysis for Run I*, E158 Technote 40 (2003).

[24] M. Racine, private communication.

[25] P. Bosted, private communication.

[26] Y. Kolomensky, *Precision Measurement of the Neutron Spin Dependent Structure Function*, U. Mass doctoral dissertation (1997).

[27] I. Younus, *E158 Calorimeter*, E158 Technote 47 (2003).

[28] D. Relyea and Y. Kolomensky, private communication overheard by T. Fieguth.

[29] D. Lhuillier, *Pion Detector Analysis*, E158 Technote 42 (2003).

[30] C. Møller, Ann. Phys. 14 (1932) 532;
J. Arrington *et al.*, *Nucl. Inst. and Meth.* A311 (1992) 39.

[31] E. Chudakov, *Polarimetry: New Detector*, http://www.slac.stanford.edu/gen/pol_detector.html (2002).

[32] G.M. Jones, *Luminosity Monitor April-June Run of E158*, E158 Technote 21 (2001).

[33] G.M. Jones, *E158 Run I Luminosity Monitor Asymmetry Analysis*, E158 Technote 38 (2003).

[34] G. Haller, K. Kumar, and P. Anthony, *Integrating ADC VME Module for E158* (2000).

[35] G. Haller, K. Kumar, and P. Anthony, *Fiber-Optics VME Module for E158* (1999).

[36] O. Saxton, private communication.

[37] P. Mastromarino, *Beam Asymmetry Analysis for E158 Run I*, E158 Technote 34 (2003).

[38] M. Woods, P. Mastromarino, and D. Relyea, *Run I Systematic Error for Beam Asymmetry Calculations*, E158 Technote 45 (2003).

[39] M. Woods, *Systematic Errors from (L-R) Asymmetries in Spotsize and Synchrotron Radiation*, E158 March Collaboration Meeting Talk (2003).

[40] P. Souder and K. Kumar, *Systematic Corrections for E158*, E158 Technote 30 (2002).

[41] C.G. Arroyo, *Data/Simulation Comparison of Cherenkov Detector Scans for Run I*, E158 Technote 41 (2003).

[42] C.G. Arroyo, *ep Inelastic Scattering Asymmetry Correction*, E158 Technote 33 (2003).

[43] L. Kaufman and K. Kumar, *Neutral Backgrounds in the Moller Detector*, E158 Technote 44 (2003).

[44] P. Bosted, private communication.

[45] K. Kumar, private communication.

[46] E. Chudakov, *Polarimetry, Run I*, E158 Technote 43 (2003).

[47] L. G. Levchuk, *Nucl. Inst. and Meth.* A345 (1994) 496-499.

[48] D. Relyea, *Null Asymmetry Test Results*, E158 Technote 46 (2003).

[49] B. Tweedie, E158 Technote 50 (2003).

[50] V. A. Zykunov, *Electroweak radiative effects in Moller scattering of polarized particles*, to be published in Sov.J.Nucl.Phys.

[51] F. Abe *et al.* (CDF Collaboration), *Search for New Gauge Bosons Decaying into Dileptons in Anti-P P Collisions at $\sqrt{S} = 1.8-TeV$*, Phys. Rev. Lett. 79 (1997) 2192-2197.

[52] J.F. Gunion *et al.*, *Higgs Bosons in Left-Right-Symmetric Models*, Phys. Rev. D40 (1989) 1546-1561.

[53] M.L. Swartz, *Limits on Doubly Charged Higgs Bosons and Lepton Flavor Violation*, Phys. Rev. D40 (1989) 1521.

[54] Jefferson Lab experiment 02-020, J. Bowman, R. Carlini, J. Finn, S. Kowalski, and S. Page, spokespersons.

[55] A. Kurylov, R. Musolf, and S. Su, *Probing Supersymmetry with Parity Violating Electron Scattering*, CALT-68-2430, MAP-289 (2003). hep-ph/0303026

[56] P. Bosted *et al.*, *DIS-Parity: Search for New Physics through Parity Violation in Deep Inelastic Electron Scattering*, SLAC-LOI (2003).

[57] Jefferson Lab experiment 00-003, R. Michaels, P. Souder, and R. Urciuoli, spokespersons.

[58] W. Emam, *Dithering Analysis*, E158 Technote 32 (2003).